5-1-2007

Evaluation and development of methods for prediction of reaeration in estuaries

Zhiyong Duan

EVALUATION AND DEVELOPMENT OF METHODS FOR PREDICTION OF REAERATION IN ESTUARIES

By

Zhiyong Duan

A Dissertation
Submitted to the Faculty of
Mississippi State University
In Partial Fulfillment of the Requirements
For the Degree of Doctor of Philosophy
in Civil and Environmental Engineering
in the Department of Civil and Environmental Engineering

Mississippi State University

May 2007

EVALUATION AND DEVELOPMENT OF METHODS FOR PREDICTION OF

REAERATION IN ESTUARIES

By

Zhiyong Duan

Approved:

James L. Martin Professor of Civil and Environmental Engineering (Director of Dissertation)	William H. McAnally Associate Professor of Civil and Envir onmental Engineering (Committee member)
Dennis D. Truax Professor of Civil and Environmental Engineering (Committee member)	Richard L. Stockstill Adjunct Professor of Civil and Environmental Engineering (Committee member)
David H. Bridges Associate Professor of Aerospace Engineering (Committee member)	William H. McAnally Associate Professor of Civil and Environmental Engineering Graduate Coordinator in the Department of Civil and Environmental Engineering
Kirk H. Schulz Dean of the College of Engineering	

Name: Zhiyong Duan

Date of Degree: May 4, 2007

Institution: Mississippi State University

Major Field: Civil and Environmental Engineering

Major Professor: Dr. James L. Martin

Title of Study: EVALUATION AND DEVELOPMENT OF METHODS FOR PREDICTION OF REAERATION IN ESTUARIES

Pages in Study: 223

Candidate for Degree of Doctor of Philosophy

The transfer of sparingly soluble gases across the air-water interface has significant effects on the distribution of the constituents in aquatic ecosystems. Gas-liquid transfer rate determines the flux of the sparingly soluble gases driven by the concentration difference. Considerable stream-driven gas-liquid transfer rate formulae have been developed. They have reasonable predictions in one-dimensional uniform flows. However, their applications in more complex cases such as three-dimensional flows are problematic. Furthermore, the wind effects are not incorporated into these formulae. New models need to be developed for gas-liquid transfer rate in three-dimensional flows that incorporate the effects of both wind and streamflow. In this study, first, a model of

gas-liquid transfer rate in non-isotropic turbulent flows is developed. Second, a general stream-driven gas-liquid transfer rate model is developed for the normal ranges of water depth and flow velocity in natural rivers. Third, a wind-stream-driven gas-liquid transfer rate model is developed. Fourth, a model of surface renewal rate caused by turbulence from transition location of shear flows is developed. Fifth, a gas-liquid transfer rate model for wind and dynamic three-dimensional flow systems is developed. A computer program is coded and applied to various cases from simple one-dimensional uniform flow systems to complex wind and dynamic three-dimensional flow systems. A specific model can be selected from the series models for a specific application based on the application requirements and the acceptable computation complexity.

Key words: gas-liquid transfer rate, model, streamflow, wind, dynamic three-dimensional flow

DEDICATION

I would like to dedicate this research to my parents and my wife.

ACKNOWLEDGEMENTS

The author expresses his sincere gratitude to the many people without whose selfless assistance this dissertation could not have materialized. First of all, sincere thanks are due to Dr. James L. Martin, my advisor, for his invaluable guidance and assistance to my studies in the doctoral program. Sincere thanks are also due to all of the other members of my dissertation committee, namely, Dr. Dennis D. Truax, Dr. David H. Bridges, Dr. Richard L. Stockstill, and Dr. William H. McAnally, for the invaluable aid and direction provided by them. Financial support is provided by a research grant from Kelly Gene Cook, Sr. Endowment at Mississippi State University.

TABLE OF CONTENTS

APPENDIX

LIST OF TABLES

LIST OF FIGURES

CHAPTER I

INTRODUCTION

1.1. Introduction of the study

The transfer of sparingly soluble gases across the air-water interface has significant effects on the distribution of the constituents in aquatic ecosystems. For example, dissolved oxygen and carbon dioxide play important roles in biological and chemical processes. Volatile pollutants like polychlorinated biphenyls (PCB) have significant effects on water quality. As Eq.1 shows, gas-liquid transfer rate determines the flux of the sparingly soluble gases driven by the concentration difference (Chapra 1997):

$$N = K_L\left(C_i - C_b\right) \tag{1-1}$$

where N = gas flux, kg/(m^2s); K_L = gas-liquid transfer rate, m/s; C_i = gas concentration at air-water interface, kg/m^3; and C_b = gas concentration in bulk water, kg/m^3. Various factors such as streamflow, wind, wave breaking, etc. influence the gas-liquid transfer rate. In rivers, streamflow is the predominant factor; in wind-driven systems, wind is the predominant factor; in complex water bodies like tidal estuaries, multiple factors are significant and they need to be considered comprehensively.

Two Film Theory and Surface Renewal Theory are two classical theories that have been established to describe the gas-liquid transfer rate. The Two Film Theory (Whitman 1923, Lewis and Whitman 1924) is based on the assumption that an air phase and a water phase are separated by thin boundary layers which control the gas transfer from the bulk air to the bulk water. However, the thickness of the thin boundary layers are difficult to determine. The Surface Renewal Theory (Danckwerts 1951; Danckwerts 1953; Higbie 1935) assumes that water parcels are brought up to the water surface where gas transfer occurs and then taken down to the water column with the entrained gas. The frequency of this movement is described with the surface renewal rate. The gas transfer process varies with the contact time of the water parcels at the water surface, which is difficult to determine.

After these two classical theories, several models were established to overcome the disadvantages of the Two Film Theory and the Surface Renewal Theory. Fortescue and Pearson (1967) developed a Large Eddy Model which established the relationship between the surface renewal time and the underlying waterside turbulence. This model was based on the observation that the water surface in rivers is disturbed mainly by large eddies with low frequency. In this model, eddies are assumed to sweep fresh liquid across the air-water interface where the gas transfer occurs. Then, the eddies are dissipated in the bulk of the absorbing medium. The Small Eddy Model (Banerjee 1968; Lamont and Scott 1970) indicated that the smallest eddies renew the boundary layer at the water surface

most frequently. Thus, the smallest turbulent eddies were considered to control the renewal processes. The Surface Divergence Model (Banerjee 2004) was developed based on the experimental observation of upwelling and attached vortices (Kumar and Banerjee 1998). Using the Blocking Theory (Hunt and Graham 1978), Banerjee related the surface divergence field to the bulk turbulence scales which lead to the Surface Divergence Model expression.

Considerable empirical formulae such as Liss and Merlivat (1986), Wanninkhof (1992), and Wanninkhof and McGillis (1999) have been established for wind-driven gas-liquid transfer rate. A semi-empirical formula of wind-driven gas-liquid transfer rate was developed by O'Connor (1983). When wind shear stress is exerted on water surface, a hydrodynamic roughness is established and its thickness increases with the wind speed, which has significant effects on gas-liquid transfer rate at air-water interface. Asher and Wanninkhof (1998) developed an empirical formula of wave-breaking gas-liquid transfer rate.

The gas-liquid transfer rate could be affected by multiple factors simultaneously. However, most of the existing studies focused on a single factor; while a few studies considered two factors by combining their respective empirical formulae. In the wind-streamflow systems, the total gas-liquid transfer rate was considered as the arithmetic addition of gas-liquid transfer rate caused by streamflow and wind respectively (Chu 2003; Woolf 1995). When wave breaking exists in the water bodies, the area

proportion of the whitecap was used to relate the effects of non-breaking waves and those of breaking waves (Asher et al., 1995).

For stream-driven gas-liquid transfer rate, Covar (1973) indicated that multiple formulae need to be employed for applications in different ranges of water depths and flow velocities in natural rivers. Furthermore, the formulae for the gas-liquid transfer rate (K_L, m/day) due to water column advection is expressed in the form of:

$$K_L = A\frac{U^B}{H^C} \tag{1-2}$$

where U = water flow velocity, m/s; H = water depth, m; and A, B and C = reaeration rate constant coefficients. These formulae work well for one-dimensional uniform riverine reaeration. However, for applications in complex water bodies with three-dimensional flow fields, it is not clear to what extent the existing formulae are applicable to these conditions. And, even if the existing formulae are applicable, what water depth and flow velocity should be used in the formula? For example, in stratified estuaries, the flows in different layers have different magnitudes and directions. Thus, the use of total water depth and average flow velocity in the formula is inherently problematic.

This study will use International System of Units (SI). The exceptions in this study will be specified.

1.2. Objectives of the study

The objectives of the proposed work are first, to evaluate the existing formulae of gas-liquid transfer rate; second, to develop a stream-driven gas-liquid transfer rate model which has general applications for the normal ranges of water depths and flow velocities in natural rivers; third, to develop a gas-liquid transfer rate model with the combined effects of wind and streamflow; and fourth, to develop a gas-liquid transfer rate model for the complex wind and three dimensional flow systems.

1.3. Outline of the study

Chapter 1 presents the application problems and limitations of the existing gas-liquid transfer formulae and the demand for new formulae with more general application ranges. Chapter 2 is the literature review of the past work done on gas-liquid transfer rate. Chapter 3 develops a stream-driven gas-liquid transfer rate model which has general application for the normal ranges of water depths and flow velocities in natural rivers. Chapter 4 develops a gas-liquid transfer rate model with the combined effects of wind and streamflow. Chapter 5 develops a formula of surface renewal rate caused by the turbulence generated at the transition location of shear flows. Chapter 6 develops a gas-liquid transfer rate model in wind and dynamic three-dimensional flow systems. Chapter 7 discusses the conclusions of this study.

CHAPTER II

LITERATURE REVIEW

Gas transfer through an air-water interface is a concern among various research areas such as water resources, environmental engineering, hydraulics, chemical engineering, mechanical engineering, and oceanography. This process could be affected by multiple factors such as streamflow, wind, wave breaking, surfactants, rain, dropletss, buoyancy, etc. Considerable research has been done by focusing on only a single factor with a few researchers focusing on two factors. Mass transfer theories and turbulent theories are the major theoretical bases of the gas-liquid transfer processes.

In this study, only the transfer rate of low soluble gases such as dissolved oxygen, carbon dioxide, and gas phase polychlorinated biphenyls (PCB) will be discussed. When gas is transferred from air to water, both the air phase and the water phase have resistance to the gas transfer. For low solubility gases, the water phase resistance is dominant and the air phase resistance is negligible as it is much smaller than that of the water phase.

2.1. Fick's Law

The flux of chemicals across an air-water interface is determined by Fick's Law (1855) (Weber 2001).

$$N = D\frac{dC}{dx} \tag{2-1}$$

where N = mass flux of chemical per unit surface area, kg/(m^2 s); D = diffusion coefficient, m^2/s; C = gas concentration, kg/m^3; and x = distance perpendicular to air-water interface, m. The gas transfer flux will be zero if the ratio of concentration in air over that in water is equal to the Henry's Law constant:

$$H_e = \frac{C_a}{C_w} \tag{2-2}$$

where H_e = Henry's Law constant; C_a = gas concentration in air, kg/m^3; and C_w = concentration in water, kg/m^3.

2.2. Relationships between the transfer rates of different gases

Different research areas focus on the gas-liquid transfer processes of different gases; e.g. dissolved oxygen is the major concern in environmental engineering and carbon dioxide is the major concern in oceanography. The similarity of the transfer processes of different low solubility gases allows the conversion of transfer rates among different low solubility gases. The related conversion relationships are described with Schmidt number:

$$K_{La} = K_{Lb}\left(\frac{Sc_a}{Sc_b}\right)^x \tag{2-3}$$

where K_{La} = gas-liquid transfer rate of gas a, m/s; K_{Lb} = gas-liquid transfer rate of gas b, m/s; Sc_a = Schmidt number of gas a; Sc_b = Schmidt number of gas b; and x = Schmidt number dependence that is -2/3 for smooth surfaces and -1/2 for rough surfaces (Donelan, et al. 2001). The Schmidt number (Sc) is a dimensionless number which equals to ν/D, with ν as kinematic viscosity, a property of the material. The Schmidt number is used to characterize fluid flows with convection processes caused by simultaneous momentum and mass diffusion (Munson, 1994).

With this relationship, the transfer rates of different gases including oxygen, carbon dioxide, PCBs, etc. are related. With the transfer rate of one gas, the rates of other gases can be calculated by this relationship. In the next sections the existing gas transfer theories, models and formulae will be reviewed. The review will be on not only the reaeration rate of dissolved oxygen but also the transfer rates of general low solubility gases.

2.3. Gas transfer theories and models

2.3.1. Two-film theory

2.3.1.1. Introduction

Two-Film Theory is a classical theory of gas-liquid transfer rate developed by Whitman in 1924. As Figure 2.1 shows, this model assumes that bulk air flow and bulk

water flow are turbulent; while the friction at the air-water interface damps turbulence and two thin layers of stagnant fluids exist in both water side and air side at the air-water interface. As molecular diffusivity is much smaller than turbulent diffusivity, these two thin stagnant layers are dominant in resisting the gas transfer from air to water. Furthermore, for low soluble gases, since the resistance in the thin stagnant layer in the water side is much bigger than that in the air side, the gas-liquid transfer rate is controlled by the water side resistance. Thus, for these sparingly soluble gases, typically only the thin stagnant layer in the water side resistance is considered in developing the gas-liquid transfer rate model and the air side resistance is ignored (Chapra 1997).

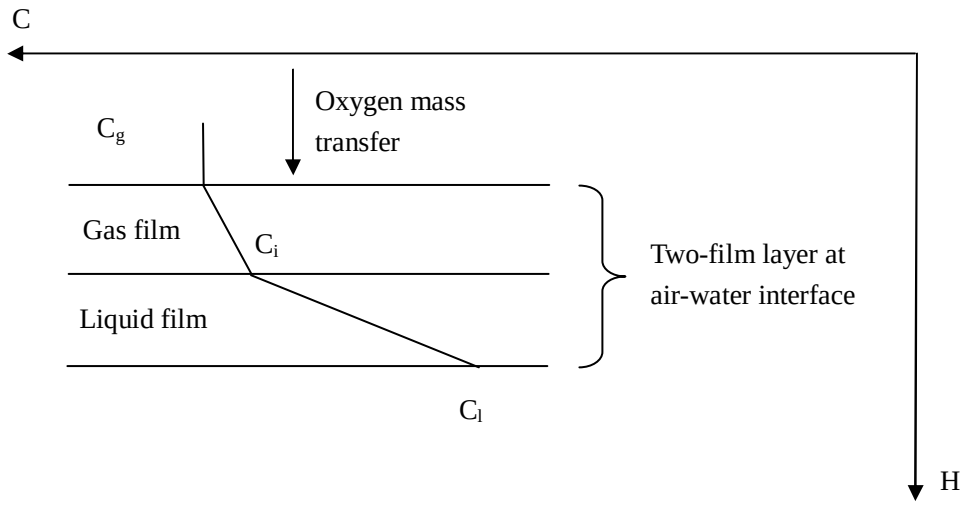

C = Oxygen concentration, kg/m^3; H = water depth, m; C_g = Oxygen concentration in bulk gas, kg/m^3; C_i = Oxygen concentration in two-film layer, kg/m^3; and C_l = Oxygen concentration in bulk liquid, kg/m^3

Figure 2.1 Two-film Theory schematic diagram

2.3.1.2. Formula

The gas flux based on the Two-Film Theory is as (Chapra 1997; Whitman 1924):

$$N = v_v(\frac{P_g}{H_e} - C_l) \tag{2-4}$$

Where P_g = gas pressure in the bulk gas, N/m^2; H_e = Henry's law constant; C_l = liquid concentration in the bulk liquid; v_v = net transfer velocity across the air-water interface, m/day, which can be calculated with:

$$v_v = K_L\left[\frac{H_e}{H_e + RT_a\left(\frac{K_{Ll}}{K_{Lg}}\right)}\right] \tag{2-5}$$

where T_a = temperature in bulk air, K; K_{Ll} = mass transfer velocity in liquid layer, m/day; K_{Lg} = mass transfer velocity in gas layer, m/day; and R = ideal gas constant.

2.3.1.3. Evaluations

The Two-film Theory provides a simple model to describe the process of oxygen mass transfer. But the thin stagnant layers at the air-water interface are assumptions in the Two-film Theory. In actual applications, it is difficult to theoretically determine the thin stagnant layer thickness. It can be obtained experimentally. However, the experimental results are obtained under specific conditions and thus have limitations in general applications.

2.3.2. Surface Renewal Theory

2.3.2.1. Introduction

Surface Renewal Theory is another classical theory of gas-liquid transfer rate which is developed by extending the penetration theory (Danckwerts 1951; Higbie 1935). As Figure 2.2 shows, the water parcel is brought up to the area near the air-water interface for a period when gas transfers from air to water parcels. Then, the parcel is taken down in the water column and another parcel is brought up and repeats this process. Danckwerts (1951) found the gas-liquid transfer rate was rarely affected by the time between renewals which ranged from random to periodic if the mean time between renewals was the same (Chapra 1997).

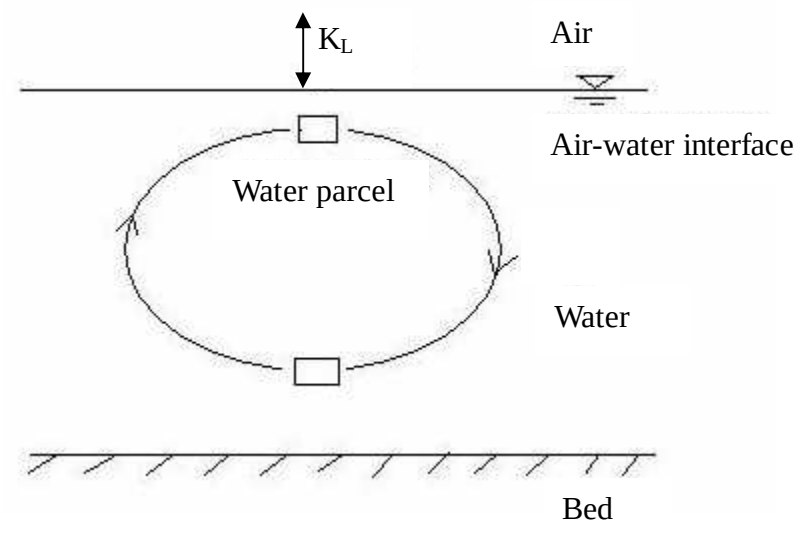

Figure 2.2 Surface Renewal Theory schematic diagram

2.3.2.2. Formula

The surface renewal theory is described as (Chapra, 1997):

$$N = \sqrt{\frac{D}{\pi t}}(C_i - C_l) \tag{2-6}$$

where C_i = concentration at air-water interface, kg/m^3; C_l = concentration in bulk water, kg/m^3; and t = surface renewal time of water parcel at air-water interface, sec. Eq.2.6 shows that the gas-liquid transfer rate through air-water interface is proportional to $D^{1/2}$. This is proved by some experimental results for high Schmidt numbers. High Schmidt numbers often occur when no surface shear exists, which means the wind speed is equal to zero and streamflow turbulence is predominant. Thus, the Surface Renewal Theory is considered to explain the contribution of streamflow turbulence to gas transfer (Chapra, 1997).

2.3.2.3. Evaluations

The importance of this theory is that it shows that the gas-liquid transfer rate is proportional to the square root of the gas molecular diffusivity, which means the resistance to gas transfer is smaller than the pure gas molecular diffusivity. However, the surface renewal time of t is difficult to determine directly.

2.3.3. Eddy diffusivity-type approaches

2.3.3.1. Introduction

Eddy diffusivity-type approaches were introduced by Levich in 1962 and Davies in 1972 in parallel with studies on the Surface Renewal Theory. Many other researchers including Mills and Chang (1973), Lee and Gill (1977), and Kitaigorodskii and Donelan (1984) developed eddy diffusivity-type approaches. It was considered that eddy diffusivity is predominant in gas transfer in these approaches and thus they are similar to the Surface Renewal Theory.

2.3.3.2. Formula

When turbulence is generated only from the water bottom, water column convection, and related motion between air and stream flows, and no other turbulence is generated by wave breaking, the gas-liquid transfer rate K_L is as (Banerjee, 2004):

$$\frac{K_L Sc^{0.5}}{u_*} \propto 0.1 \qquad (2\text{-}7)$$

where u_* = shear velocity which equals to $\sqrt{\frac{\tau}{\rho}}$, m/s (Munson 1994); and Sc = Schmidt number which equals to ν/D, with ν = kinematic viscosity, a property of the material. An expression for the air side is in the similar form (Banerjee, 2004):

$$\frac{K_L Sc_a^{2/3}}{u_*} \propto 0.07 \qquad (2\text{-}8)$$

2.3.3.3. Evaluations

Eq.2.7-2.8 show that gas-liquid transfer rate is a function of the Schmidt number and shear velocity. The turbulence generated from air side and that generated from water side have different effects on gas-liquid transfer rate.

2.3.4. Large Eddy Model (LE)

2.3.4.1. Introduction

The Large Eddy Model is developed to find the connection between the time between renewals and the underlying water side turbulence (Banerjee 1968; Fortescue and Pearson 1967). In this model, the gas transfer is considered to be mainly affected by eddy diffusivity (also referred to as turbulent diffusivity) which is much larger than molecular diffusivity. The magnitude of turbulent diffusivity is of the order of 10^2-10^6 times that of molecular diffusivity (Banerjee 1968; Fortescue and Pearson 1967). Eddies are supposed to sweep fresh water across the air-water interface where gas transfer occurs. Then, eddies dissipate in the absorbing medium column. The surface acts as a constraint on possible motions since no normal velocity is allowed at the surface. The mean mass transfer is modeled as "a regular sequence of steady square roll cells touching the surface, moving as a whole with the local mean surface velocity" (Fortescue, 1967). This model was based on the observation that the air-water surface in rivers is disturbed mainly by large, low frequency eddies and the large eddies are dominant in gas transfer. The large

eddies were considered as two-dimensional eddies since it was verified that shear flows were dominated by two-dimensional roll eddies (Townsend, 1956).

2.3.4.2. Formula

The Large Eddy Model is formed as:

$$K_L = 1.46\left(\frac{D\sqrt{U^2}}{\Lambda}\right)^{\frac{1}{2}} \tag{2-9}$$

where U = streamflow velocity, m/s; and Λ = flow characteristic length, m.

2.3.4.3. Evaluations

The Large Eddy Model provided a connection between gas transfer through air-water interface and bulk turbulent flow characters. The renewal time was calculated by $t \approx \Lambda / U$. It is assumed that there is no normal velocity across the air-water surface. However, this is conflicted by some experimental observations. The eddies are assumed to only obey mass conservation but not momentum conservation. The eddies are supposed to be a sequence of regular and steady eddies, but in actuality the eddies are constantly varying.

2.3.5. Small Eddy Model (SE)

2.3.5.1. Introduction

The Small Eddy Model indicated that the smallest eddies renew the boundary layer most frequently. Thus, the smallest turbulent eddies were considered to control the renewal process (Banerjee 1968; Lamont and Scott 1970) (edited by Moog 1995). The surface renewal rate, r, in Surface Renewal Model is proportional to the inverse of the Kolmogorov time scale:

$$r \propto (\frac{\varepsilon}{\nu})^{0.5} \tag{2-10}$$

$$\varepsilon \propto \frac{u_*^{\ 3}}{H} \tag{2-11}$$

where ε = near-surface turbulent energy dissipation rate, m^2/s^3; u_* = shear velocity which equals to $\sqrt{\frac{\tau}{\rho}}$, m/s (Munson 1994); and H = water depth, m.

2.3.5.2. Formula

The nondimensionalized gas-liquid transfer rate according to the Small Eddy Model is given by:

$$\frac{K_L}{u_*} = K_L^+ \propto R_*^n Sc^{-0.5} \tag{2-12}$$

where Re_* = shear Reynolds number which equals to u_*H/ν; and Sc = Schmidt number which equals to ν/D.

2.3.5.3. Evaluations

The Small Eddy Model provided a connection between gas transfer through air-water interface and bulk turbulent flow characters. The surface renewal time was calculated with:

$$t \approx \left(\frac{\nu}{\varepsilon}\right)^{0.5}.$$

where t = surface renewal time, sec.

2.3.6. Surface Divergence Model (SD)

2.3.6.1. Introduction

Surface Divergence Model was established based on the Blocking theory and the experiment observations of upwelling and attached vortices (Kumar and Banerjee 1998). Blocking theory was proposed to "connect bulk turbulence parameters to those near the interface by superposing an image turbulence field on the other side, which impedes surface normal motions, redistributing the kinetic energy to surface parallel motions, which are enhanced" (Hunt and Graham, 1978). The predictions by this theory have been verified with experiments (Banerjee 1990).

As an approximation, the water-side interface-normal velocity, U_z, can be written as:

$$U_z \sim \frac{\partial U_z}{\partial z}\Big|_{z_{\text{int}}} \tag{2-13}$$

where z = surface-normal coordinate; and z_{int} = surface-normal coordinate value. It can be related to the divergence of the interface-parallel motions at the water surface as:

$$\left.\frac{\partial U_z}{\partial z}\right|_{\text{int}} = \left(\frac{\partial U_x}{\partial x} + \frac{\partial U_y}{\partial y}\right)_{\text{int}} = \gamma \tag{2-14}$$

where the quantity in parentheses is the surface divergence of the surface velocity field fluctuations, U_x = surface velocity at x direction, m/s; U_y = surface velocity at y direction, m/s; γ = velocity gradient, s^{-1}; x = streamwise coordinate tangential to the moving interface; y = spanwise coordinate tangential to the moving interface, and z = normal coordinate.

In the circumstance of free shear air-water interface where the gas transfer with high Sc occurs, the gas-liquid transfer rate, K_L, is given by:

$$\frac{K_L Sc^{1/2}}{U} \approx \mathrm{Re}_t^{-1/2}\left[\left(\frac{\partial U_x}{\partial x} + \frac{\partial U_y}{\partial y}\right)^2\right]_{\text{int}}^{1/4} \tag{2-15}$$

where the subscript "int" denotes the interface, and Re_t = turbulent Reynolds number which equals to $U\Lambda/\nu$.

These introductions were further developed by relating the surface divergence field to the bulk turbulence scales using Hunt and Graham's (1978) blocking theory, which lead to the Surface Divergence Model expression (Banerjee 1990).

2.3.6.2. Formula

The expression of gas-liquid transfer rate, K_L, in Surface Divergence Model is given by:

$$\frac{K_L}{U} \approx Sc^{-\frac{1}{2}} \mathrm{Re}_t^{-\frac{1}{2}} \left[0.3 \left(2.83 \mathrm{Re}_t^{\frac{3}{4}} - 2.14 \mathrm{Re}_t^{\frac{2}{3}} \right) \right]^{\frac{1}{4}} \quad (2\text{-}16)$$

where Re_t = turbulent Reynolds number based on far-field integral length scale Λ and velocity scale U (Banerjee et al. 2004).

2.3.6.3. Evaluations

Surface Divergence Model was developed to provide the relationship between direct measurements of the hydrodynamic parameters and the gas-liquid transfer rate to overcome the disadvantages of Two Film Theory and Surface Renewal Theory. The γ in Surface Diversity Model is easier to measure than the surface renewal time t in the Surface Renewal Model. The method of scattering particles on water surface and measuring their trajectories is used to measure the γ (Kumar and Banerjee 1998).

2.4. Gas-liquid transfer rate formulae

2.4.1. Stream-driven gas-liquid transfer rate formulae

The one-dimensional gas transfer coefficient K_L is generally formulated as (Thorsen, 1999):

$$\frac{K_L}{U} = Sc^a We^b \,\mathrm{Re}^c = \left(\frac{\nu}{D}\right)^a \left(\frac{\sigma}{U^2\Lambda}\right)^b \left(\frac{U\Lambda}{\nu}\right)^c \tag{2-17}$$

where K_L = gas-liquid transfer rate driven by streamflow; ν = kinematic viscosity of the liquid, m^2s^{-1}; D = molecular diffusion coefficient of gas, m^2/s; σ = surface tension, N/m; U = characteristic velocity of flow, m/s; and Λ = characteristic length of flow, m. This equation combined Schmidt number Sc, Weber number We, and Reynolds number Re. A simplified formula obtained from the above formula is as below which can be used in actual applications:

$$K_L = U\left(\frac{\nu}{D}\right)^{-\frac{1}{2}} \left(\frac{U\Lambda}{\nu}\right)^{-\frac{1}{2}} = \left(\frac{UD}{\Lambda}\right)^{\frac{1}{2}} \tag{2-18}$$

Several riverine reaeration formulae such as O'Connor-Dobbins formula, Churchill formula, and Owens and Gibbs formula have been developed (Chapra, 1997).

O'Connor-Dobbins formula is as:

$$K_L = 3.93\frac{U^{0.5}}{H^{0.5}} \tag{2-19}$$

Churchill formula is as:

$$K_L = 5.026\frac{U}{H^{0.67}} \tag{2-20}$$

Owens and Gibbs formula is as:

$$K_L = 5.32\frac{U^{0.67}}{H^{0.85}} \tag{2-21}$$

where K_L = gas-liquid transfer rate, m/day.

2.4.2. Wind-driven gas-liquid transfer rate formulae

Wind is an important factor in affecting gas-liquid transfer rate. There are considerable empirical formulae on wind-driven gas-liquid transfer rate at an air-water interface. Some theoretical formulae explained the effects of wind on gas-liquid transfer rate by introducing the concept of wind-induced roughness. Wind was also considered as a cause of waves which have important effects on gas-liquid transfer rate. The effects of wind-driven waves on gas-liquid transfer rate will be reviewed in the next section.

The wind has significant effects on gas transfer at air-water interface, which is supported by the relationship between wind speed and gas-liquid transfer rate on lake surfaces (MacIntyre et al. 1995; Liss and Merlivat 1986). When wind blows over a water surface, wind stress is exerted at the air-water interface. The shear velocity is determined by the wind speed at a specified height by a drag coefficient:

$$\text{Wind Stress} = \rho_a u_*^2 = \rho_a \frac{C_f}{2} U^2 \qquad (2\text{-}22)$$

where C_f = skin fraction coefficient.

The effects of wind on gas transfer at air-water interface were first discussed by Inhoff and Fair in 1956. As they suggested, the wind on the air-water interface will double the gas-liquid transfer rate; the wind-induced wave will increase gas-liquid transfer rate by ten times; and the whitecaps during wave breaking or caused by dropletss will increase gas-liquid transfer rate by one hundred times. Downing et al. (1955) indicated that wind under 3 m/s will have no significant effects on gas transfer. Eloubaidy

and Plate (1972) noted that the reaeration rate will increase significantly with the wind-induced small waves when wind shear velocity is from 0.7 to 1.1 m/s. Banks (1975) indicated that gas-liquid transfer rate may be proportional to the wind speed.

2.4.2.1. Empirical formulae

Considerable empirical formulae on gas transfer at air-water interface driven by wind have been developed. Kanwisher in 1963 found that gas-liquid transfer rate does not change until the wave speed exceeds 3 m/s, and increases linearly with the square of the wind speed from 3 m/s to 10 m/s. The suggested formula is given by:

$$K_L = \frac{D}{\left(200 - 60\sqrt{W}\right)\times 10^{-6}} \tag{2-23}$$

where K_L = gas-liquid transfer rate, m/s, D = molecular diffusivity, m^2/s, and W = wind speed, m/s.

The research of Thames Survey Committee (1964) on reaeration in Thames River Estuary indicated the gas-liquid transfer rate increases linearly with wind speed at 10 m above the water surface:

$$K_L = \left(10.0 + 3.38W\right)\times 10^{-6} \tag{2-24}$$

Wanninkhof (1992) suggested a wind-driven gas-liquid transfer rate formula as:

$$K_L = \left(\frac{1}{3.6\times 10^5}\right) K W_{10}^2 \left(\frac{Sc}{660}\right)^{-\frac{1}{2}} \tag{2-25}$$

where K_L = gas-liquid transfer rate driven by wind; K = wind-driven gas-liquid transfer rate constant coefficient and equals to 0.31 when short-term wind data are used and 0.39

when long-term climatological wind data are used; W_{10} = wind velocity at 10 m height, m/s; Sc = Schmidt number for dissolved oxygen; and the leading numerical term is a unit conversion factor (cm/hr to m/s).

Broecker and Siems (1984) presented an empirical relationship for a smooth surface:

$$K_L = CSc^{-2/3} \tag{2-26}$$

where C = wind-driven gas-liquid transfer rate constant coefficient. The relationship for a rough surface is:

$$K_L = CSc^{-1/2} \tag{2-27}$$

2.4.2.2. Boundary-layer models

Deacon (1977) presented a relationship to connect gas-liquid transfer rate with Schmidt number and shear velocity in air side:

$$K_L = 0.082Sc^{-\frac{2}{3}}\left(\frac{\rho_a}{\rho_w}\right)^{1/2} u_* \tag{2-28}$$

where ρ_a = density of air, kg/m^3; ρ_w = density of water, kg/m^3; and u_* = shear velocity in air side, m/s.

This formula came from the fact that the gas transfer K_{Lw} is proportional to the shear velocity u_*, the ratio of momentum, the kinematic viscosity ν, and mass m, molecular diffusivity D to the power -2/3. Several assumptions underlie this relationship: e.g., the surface is smooth, and the stress across the air water interface is continuous. The formula

works well only when the surface is smooth, but not well when waves occur (Deacon 1977).

2.4.2.3. Theoretical formulae

By employing the wind-induced roughness at the air-water surface, O'Connor in 1983 and Kerman in 1984 developed the relationships between gas-liquid transfer rate and wind speed for non-smooth air-water interface. For hydrodynamically smooth surface, the liquid film transfer coefficient is (O'Connor 1983):

$$K_{L\delta} = \left(\frac{D}{\nu}\right)^{2/3}\left(C_d \frac{\rho_a}{\rho_w}\right)^{1/2} \frac{\kappa^{\frac{1}{3}}}{\Gamma_0} W \qquad (2\text{-}29)$$

where $K_{L\delta}$ = liquid film transfer coefficient for hydrodynamically smooth surface, m/s; κ = von Karman constant; Γ_0 = equivalent coefficient of viscous layer thickness; and C_d = drag coefficient. At higher wind speeds, the liquid film transfer coefficient for non-smooth surface is (O'Connor 1983):

$$K_{L\tau} = \left(\frac{D}{\kappa z} \cdot \frac{\rho_a \nu_a}{\rho_w \nu_w} \sqrt{C_d} W\right)^{\frac{1}{2}} \qquad (2\text{-}30)$$

where $K_{L\tau}$ = liquid film transfer coefficient for non-smooth surface; z = roughness thickness; ν_a = air kinematic viscosity; and ν_w = water kinematic viscosity.

2.4.3. Non-breaking wave gas-liquid transfer rate formulae

The wind-driven wave at the water surface is generated by the input of energy from the wind and is dissipated by wave breaking. The long and short water waves produce

turbulence and orbital movements which cause continual transport of water from deeper layers to the air-water interface as the Surface Renewal Theory describes. Thus, the water wave substantially increases the gas-liquid transfer rate.

Waves increase gas transfer across air-water interface by about three orders in magnitude (Boettcher 2000). The increase comes from several reasons: increased surface area, bubble-mediated gas transfer, thinned surface boundary layer, and induced transport and mixing in surface and bulk flow. A single model introduced by Woolf in 1997 explicitly separates “breaking” and “non-breaking” contributions with whitecap coverage percentage.

When a non-breaking wave occurs, the water surface remains simply connected, and turbulent transport is the dominant mechanism (Boettcher et al. 2000). On the unbroken wave upwind face, gas transfer is in an upwind direction; on the unbroken wave downwind face, the parasitic capillary wave produces localized vorticity and mixing in the viscous layer as the small gravity wave steepens (Peirson et al. 2003).

The non-breaking wave contribution to the gas transfer is parameterized based on theoretical considerations and experimental observations in wind wave tanks (Jahne et al. 1987):

$$K_L = 1.57 \times 10^{-4} u_* \left(\frac{600}{Sc} \right)^{\frac{1}{2}} K \qquad (2\text{-}31)$$

where u_* = shear velocity of wind, m/s; and K = constant coefficient. This expression is supported by the observations of gas-liquid transfer rate at moderate or high winds.

2.4.4. Wave breaking gas-liquid transfer rate formulae

When wave breaking occurs, the water surface is multiple connected (Boettcher et al. 2000), and it is affected by droplets and spray. “As the gravity wavelets steepen further, they break and the surface ruptures, with surface fluid subducted into an interior region of intense turbulent mixing beneath an intensively-mixed spilling region” (Peirson et al. 2003). As many researchers state, the breaking wave will enhance the gas transfer process significantly. The mechanisms have not been completely conceived. Some researchers have concluded that the gas transfer is determined by the turbulence generated by microscale wave breaking for low and moderate wind speeds (Siddiqui et al. 2004). Some researchers have concluded bubble-mediated gas transfer during wave breaking is dominant (Thorsen, 1999). Some researchers have concluded that the direct transfer of water from air-water surface to turbulent bulk flow by the wind-wave breaking is dominant at moderate wind speeds (Thorsen, 1999).

The gas-liquid transfer rate induced by a breaking wave is about one order higher than that of a non-breaking wave and four orders higher than that of turbulent fluid. Thus, wave breaking significantly enhances the reaeration. For low to moderate wind speeds, near-surface turbulence generated by microscale breaking wave is the dominant factor on gas-liquid transfer rate at air-water interface (Boettcher et al. 2000).

Some researchers used acoustic measurement methods to quantify bubble dynamics and found it dominated the gas transfer across the air-water interface (Boettcher et al.

2000). Some other researchers showed that about 75% of gas transfer is contributed by bubble-mediated gas transfer produced during wave breaking. The whitecap coverage percentage is an indication of the strength of the wave breaking. The bubble size also affects the gas-liquid transfer rate. Thus some studies have focused on measurement of whitecap coverage and some other on bubble size distribution. Breaking waves were found to be produced in a wave-tank at wind speeds exceeding 10 m/s with the concurrent appearance of bubbles. Some experiments have measured the bubble size distribution and their influence on the gas-liquid transfer rate (Thorsen, 1999).

The mean square slope is determined by the roughness feature during microscale wave breaking. Some quantitative experiments investigated the relationship between gas-liquid transfer rate and wave slope when no surfactant exists. These experimental results showed microbreaking significantly contributed to gas transfer for low to moderate wind speeds (Zappa 2001).

Crashing wave envelops pockets of air when wave breaking occurs on water surface. These pockets are then broken up into bubbles within the water body. The bubbles oscillate in the water body because of the dynamic energy coming from the wave breaking (Woolf 1997).

Two factors, wind speed and sea state, determine the wave breaking and whitecap coverage percentage. This has been verified by theories and experimental results. Wave height is often used to describe the sea state. Thus, the gas-liquid transfer rate dominated

by breaking wave is better estimated by satellite retrieval of both wind speed and wave height (Thorsen, 1999).

For developing waves at x direction, the relationship between wave height and wind velocity is as (Thorsen, 1999):

$$H_w = 0.0163x^{0.5}W \tag{2-32}$$

where H_w = wave height, m; and W = wind speed, m/s. For fully developed waves, the relationship is as (Thorsen, 1999):

$$H_w = 0.0246W^2 \tag{2-33}$$

The energy dissipation rate, ε, is proportional to wind speed, W, and wave height, H (Thorsen, 1999):

$$\varepsilon \approx WH \tag{2-34}$$

The gas transfer increases linearly with the increase of whitecap coverage percentage on the water surface. Simple empirical formula on whitecap coverage and wave breaking are generated by considering only wind speed (Thorsen, 1999):

$$Wc = 3.84 \times 10^{-6} W^{3.41} \tag{2-35}$$

$$Wc = 2.98 \times 10^{-7} W^{4.04} \tag{2-36}$$

where Wc = whitecap coverage; and W = wind speed, m/s.

Though "wind speed only" formulations are commonly used, it was realized during early studies that a simple relationship in terms of wind speed or shear velocity is not

expected, and that there is a clear theoretical case to relate whitecapping to the wave field (Cardone 1969; Ross and Cardone 1974).

Two parameters, R_B (a form of Reynolds number for bubble-mediated gas-liquid transfer) and R_H (a form of Reynolds number for wind waves), increase with wave growth. A formula of gas transfer dominated by wave breaking is proposed by using R_B (Zhao et al. 2003). Another formula of gas transfer dominated by wave breaking is proposed by using the non-dimensional parameter Re_H (Woolf 1997):

$$Wc = 4.02 \times 10^{-7} \, \mathrm{Re}_H^{\,0.96} \tag{2-37}$$

$$\mathrm{Re}_H = \frac{u_* H_w}{\nu} \tag{2-38}$$

where H_w = significant wave height of sea, m; and Re_H = a form of Reynolds number for wind waves. The sea state is represented by wave height in these formulae. The whitecap coverage is determined by wave height. For a more developed sea, these formulae indicated that whitecap coverage has more effects than wind speed.

The gas transfer dominated by breaking wave is proportional to fractional whitecap coverage. The coefficient is based on the calculations of bubble-mediated transfer, and therefore depends on the solubility of the gas. A simple formula, appropriate for CO_2 at 20°C, is given by (Woolf 1997):

$$K_L = 850W \tag{2-39}$$

where K_L = gas-liquid transfer rate induced by breaking wave in cm/hr; W = wind speed, m/s.

Furthermore, the total formula of gas-liquid transfer rate induced by non-breaking wave and breaking wave is assumed as the simple sum of the two contributions as below:

$$K_L = K_{Lnw} + K_{Lbw} \tag{2-40}$$

where K_L = total gas-liquid transfer rate induced by non-breaking wave and breaking wave, m/s; K_{Lnw} = gas-liquid transfer rate induced by non-breaking wave, m/s; K_{Lbw} = gas-liquid transfer rate induced by breaking wave, m/s.

2.4.5. Bubble-mediated (whitecap-mediated) gas-liquid transfer rate formulae

Bubble-mediated gas transfer is an important part of the total gas transfer especially during wave breaking, dropletss, etc. It was reported that dissolved oxygen will be supersaturated by deep bubble clouds (Thorpe 1982 and 1986; Woolf and Thorpe 1991). The breaking waves entrain bubbles at high wind speeds, which increase the gas-liquid transfer rate (Memery and Merlivat, 1983; Broecker and Siems, 1984). The bubbles entrained by breaking waves were observed to greatly enhance the gas-liquid transfer rate (Farmer et al. 1993). But some studies indicated that the bubble-mediated gas transfer was at most 7% of the total gas transfer in wind-driven turbulence (Komori and Misumi 2001). Keeling (1993) and Woolf (1993) developed two numerical models to predict the gas-liquid transfer rate with bubbles, but uncertainties in the value for any gas are large. During the generation of bubbles when waves break the turbulence is also enhanced (Monahan and Spillane 1984).

The bubble is generally formed by passing air through an orifice. Bubble volume and radius are empirically given by (Thorsen, 1999):

$$V_B = \frac{2\pi R\sigma}{g\Delta\rho} \tag{2-41}$$

$$d = (\frac{z}{2} \cdot \frac{R\sigma}{\Delta\rho g})^{1/2} \tag{2-42}$$

where V_B = bubble volume, m^3; d = bubble radius, m; R = orifice radius, cm; σ = surface tension, dynes/cm; g = acceleration of gravity, cm/s^2; Δρ = difference between density of liquid, ρ_l, g/cm^3 and the density of the bubble, ρ_B, g/cm^3.

The bubble radius is proportional to the orifice radius and surface tension, and inversely proportional to the density difference between the gas and water. Viscosity and temperature have little effect on bubble diameter. Bubble size is fairly constant at low and moderate wind speeds, but increases dramatically at high wind speeds.

Eckenfelder (1959) described the oxygen transfer in terms of Sherwood number, Reynolds number and Schmidt number:

$$\frac{K_L d_B}{D} = F(\frac{d_B U_B}{\nu})(\frac{\nu}{D}) \tag{2-43}$$

where U_B = bubble velocity, m/s; ν = kinematic viscosity, m^2/s; $K_L d_B/D$ = Sherwood number (Sh); $d_B u/\nu$ = Reynolds number (Re); ν/D = Schmidt number (Sc); and F = bubble-mediated gas-liquid transfer rate constant coefficient.

For greater aeration depths, the end effects were compensated by applying an exponential depth factor:

$$\frac{K_L d_B}{D} H^{1/3} = F(\mathrm{Re})(Sc)^{1/2} \quad (2\text{-}44)$$

where d_B = bubble diameter, m.

2.4.6. Combined effects of breaking wave and bubble

An empirical formula of gas transfer caused by wave breaking including turbulence transfer and whitecap-mediated gas transfer was (Asher and Wanninkhof 1998; edited by Asher et al. 2001):

$$K_L = \left(47U + \left(1.5\times10^5 W - 47U\right)\right)Sc^{-1/2} + W\left(-\frac{37}{\alpha} + 10{,}440\alpha^{-0.41}Sc^{-0.24}\right) \quad (2\text{-}45)$$

where the first term is turbulence transfer caused by wave breaking; the second term is whitecap-mediated gas transfer; α = wind speed constant coefficient; U = streamflow velocity, m/s; and W = wind speed, m/s.

2.4.7. Combined effects of wave, wave breaking and bubble

Woolf (1995) presented a simple model for wave effects on gas transfer. In this model, the gas-liquid transfer rate has two components due to wind stirring (K_{Lw}), surface extension of bubbles (K_{Lb}), and interfacial resistance (R_i):

$$K_{LT} = K_L + K_{Lb} \quad (2\text{-}46)$$

$$1/K_L = 1/K_{Lw} + R_i \quad (2\text{-}47)$$

$$K_{Lw} = au_{*w} \quad (2\text{-}48)$$

$$K_{Lb} = bu_{*w}^{3} \tag{2-49}$$

where K_{LT} = total gas-liquid transfer rate; K_L = gas-liquid transfer rate; u_{*w} = wind shear velocity; a = wind-driven gas-liquid transfer rate constant coefficient; b = bubble-mediated gas-liquid transfer rate constant coefficient; and R_i = resistance constant. Then, a simple "interfacial resistance" model is given by (Woolf 1995):

$$\frac{\left(\frac{600}{Sc}\right)^{0.5}}{K_{LT}} = \frac{1}{K_{L600}} = \frac{1}{0.01u_{*w}} + R_i \tag{2-50}$$

where K_{L600} = gas-liquid transfer rate when Schmidt number equals to 600, m/s.

From a surf pool experiment, Asher et al. (1995) and Wanninkhof et al. (1995) showed that gas-liquid transfer rate K_L could be partitioned into several components: near-surface turbulence generated by currents and nonbreaking wave (K_{Lnw}), turbulence generated by breaking waves (K_{Lbw}), and bubble-mediated transfer (K_{LB}). If the gas concentration grade is large, the total gas-liquid transfer rate is given by:

$$K_L = \left(K_{Lnw} + Wc\left(K_{Lbw} - K_{Lnw}\right)\right) + WcK_{LB} \tag{2-51}$$

where Wc = fractional area of whitecap whitecap coverage.

Asher et al. (1995) indicated that the gas-liquid transfer rate was underestimated by this formula and hypothesized that it was caused by incorrectly parameterizing the dependence of K_{Lnw} and K_{Lbw} on Wc. Ogston et al. (1995) then provided an improved formula:

$$K_L = B\left(\varepsilon_{nw}\nu\right)^{1/4} + Wc\left(\left(\varepsilon_{bw}\nu\right)^{1/4} - \left(\varepsilon_{nw}\nu\right)^{1/4}\right)Sc^{1/2} + b_l Wc\alpha^{-0.043}Sc^{-0.35} \tag{2-52}$$

where K_L = gas-liquid transfer rate, m/s; ε_{nw} = energy dissipation rate due to nonbreaking wave, m^2/s^3; ε_{bw} = energy dissipation rate due to breaking wave, m^2/s^3; b_l = gas-liquid transfer rate coefficient.

2.4.8. Effects of surfactants

The presence of any chemical film at the water surface significantly decreases the gas transfer since it presents a chemical barrier which impedes the gas transfer. The capillary waves generated by wind make an important contribution to the gas transfer. But the existence of the surfactant films damps the capillary waves.

Some experiments found the wave spectra at higher wave numbers were substantially reduced by surfactants at wind shear velocities below 0.2 m s^{-1}. The surface enrichment was suggested to quantify the effects of the surfactants on gas transfer with reasonable accuracy (Hara et al. 2001).

Surfactants have important effects on bubble-mediated gas transfer. When surfactants exist at water surface, bubbles generated during waves breaking may carry surfactants from the sea surface, and will scavenge material from the bulk as the bubbles rise (Scott, 1975).

Bubbles may be covered with material after rising only a few centimeters (Blanchard, 1983). This process was described to change the bubble from hydrodynamically "clean" to "dirty" with the coating of material. The coating has a very great effect on the

gas-liquid transfer rate between the bubbles and the surrounding water, particularly for large bubbles. It was assumed that small bubbles would usually be dirty (Woolf and Thorpe 1991).

Keeling (1993) and Woolf (1993) have argued that formulae for clean bubbles are more appropriate for large near-surface bubbles. It was estimated with models that a contribution of 8.5 cm h^{-1} to the mean global transfer rate of carbon dioxide from bubbles if they were clean, but only 2.6 cm h^{-1} if the bubbles were dirty (Woolf 1993). Thus, the contribution of bubbles to air-sea gas transfer is sensitive to surfactants, and might respond significantly to concentration change of these materials.

2.4.9. Effects of rain and droplets

Wave spectrum is the distribution of wave energy as a function of frequency. The wave spectra are raised at higher wave numbers (above 200 rad m^{-1}) but are not affected at 100 rad m^{-1} during rain. Rain reduces the effects of surfactant films. At higher wave numbers, gas-liquid transfer rate is roughly proportional to the wave spectra; but for the spectra of longer waves, gas transfer has less sensitivity (Hara et al. 2001).

Rain and droplets play a complicated role in gas transfer. The sizes of dropletss are different depending on the type of rain and distribute from 1 mm to 3 mm of diameters. It was found that rain has an abundance of small dropletss and a few large drops from the rain spectra. Since the laminar thin layer is very thin, the rain drops penetrate it, which

increase gas-liquid transfer rate. Furthermore, rain drops strikes the waster surface and produce circular waves propagating outwards and splash drops (Hara et al. 2001).

On the other hand, rain calms the surface, which decreases gas-liquid transfer rate. Though there are no direct effects on gas transfer, it reduces the wave dissipation rate when waves break. And this implies less secondary motions and less surface renewal, which decrease gas-liquid transfer rate. The surface damping affected by rain was described in terms of mean square wave slope. Basically the smaller waves are damped by rain, which produces a smoother surface (Hara et al. 2001).

Some other effects of rain including momentum transfer have no noticeable influence on gas transfer. The primary dynamic effect of rain on the thin layer under water surface is the production of turbulence or secondary motions. The passage of rain drops through the thin layer under surface disturbs the currents and leads to secondary motions that produce turbulence under the water surface. However, the mechanism of turbulence formation has not yet been identified (Thorsen, 1999).

CHAPTER III

STREAM-DRIVEN GAS-LIQUID TRANSFER RATE

3.1. Introduction

Various factors like streamflow, wind, wave breaking, etc. influence the gas-liquid transfer rate. In rivers, the streamflow is the predominant factor. Riverine reaeration rates received the earliest consideration as rivers are the main sources of drinking water and receptors of the wastewater. Considerable empirical formulae have been established based on experiments. Churchill et al. (1962) established an empirical formula for riverine reaeration rates based on the experiments in reservoirs in the Tennessee River valley. Owens et al. (1964) established an empirical formula after they measured the reaeration rate by adding sulfite to reduce the concentration of dissolved oxygen in four shallow streams in the Lake District of Great Britain. Wilcock (1988) carried out a number of gas tracer experiments to measure the reaeration rate at different flow velocities. Efforts have been initiated to develop the semi-empirical models (Langbein and Durum 1967; O'Connor and Dobbins 1956; Wilcock 1984). For example, based on the Surface Renewal Theory, O'Connor and Dobbins (1956) developed a relationship between the reaeration rates and hydraulic parameters including flow velocity and water

depth. Based on the Two Film Theory, Atkinson (1995) proposed a model to calculate the riverine surface reaeration flux.

Both existing empirical and theoretical formulae have limited application ranges. The application ranges of flow velocity and water depth in the existing reaeration rate formulae are listed in Table 3.1. In natural rivers, the flow velocity typically ranges from 0.03 m/s to 1.5 m/s and the water depth ranges from 0.1 to 15 m (Chapra 1997). O'Connor-Dobbins' formula has good predictions for reaeration rates in deep waters with the depth greater than 0.6 m; but it underestimates the rate of reaeration in shallow water or fast flow (Chapra 1997; Covar 1976). Churchill's empirical formula can be used for fast flow (greater than 0.5 m/s); Owens-Gibbs' empirical formula can be used for shallow water (less than 0.6 m) (Chapra 1997; Covar 1976). These empirical formulae were established under specific conditions; thus, their applications are not globally suitable. General theoretical models and related formula for the stream-driven gas-liquid transfer rates are needed for the normal ranges of flow velocity and water depth in the natural rivers. Further, Covar (1976) compared the Owens-Gibbs formula (1964), the Churchill formula (1962) and the O'Connor-Dobbins formula (1956) for the reaeration rate and indicated that the gas-liquid transfer rate in non-isotropic turbulent flows is greater than that in isotropic turbulent flows with the same flow velocity and water depth (Chapra 1997). Isotropic turbulence is the turbulence where the squares, products, and derivatives of the velocity components are independent of direction. Non-isotropic turbulence is the

turbulence where the squares, products, and derivatives of the velocity components are dependent of direction. Isotropic turbulent flows are the flows in which the isotropic turbulence is predominant. Nonisotropic turbulent flows are the flows in which the nonisotropic turbulence is predominant.The difference between gas-liquid transfer rates in isotropic turbulent flows and non-isotropic turbulent flows needs to be explored. Thus, first, a gas-liquid transfer rate model in non-isotropic turbulent flows is developed and compared with the existing empirical formulae; second, a general formula of stream-driven gas-liquid transfer rate is developed for the normal ranges of flow velocity and water depth in natural rivers, namely the flow velocity typically ranges from 0.03 m/s to 1.5 m/s and the water depth ranges from 0.1 to 15 m (Chapra 1997).

Table 3.1. Ranges of water depth and flow velocity of the existing reaeration rate formulae

Formulae	Velocity (m/s)	Depth (m)	References
Churchill	0.5-1.2	0.6-15	Churchill et al. 1962
O'Connor-Dobbins	0.16-1.28	0.52-11.28	O'Connor and Dobbins 1956
Owens-Gibbs	0.04-0.56	0.12-0.74	Owens et al. 1964
Wilcock	0.59-1.12	0.83-2.21	Wilcock 1988

3.2. Gas-liquid Transfer Rate in Non-isotropic turbulent flows

3.2.1. Model development

Surface Renewal Theory (Danckwerts 1951; Danckwerts 1953; Higbie 1935) is a classical theory to describe the gas-liquid transfer process. This theory proposes that the turbulent eddies carry the water parcels up to near the air-water interface for a period when the gas is transferred from air to the water parcel. Then the water parcel is entrained down to the water column. Another parcel is brought up and the gas transfer process is repeated. According to the Surface Renewal Model, gas-liquid transfer rate is determined by the surface renewal rate and molecular diffusion coefficient.

$$K_L = \sqrt{Dr} \tag{3-1}$$

where D = diffusion coefficient, 2.09 x 10^{-9} m^2/s at 20°C; and r = surface renewal rate, s^{-1}. Surface renewal rate r is the frequency at which the water parcels transfer to the air-water interface and entrain gas down to the water column.

For isotropic turbulent flows, two empirical relationships on the vertical fluctuation velocity and the mixing length are (Hamada 1953; Kalinske 1943; Schijf and Schonfeld 1953):

$$\left|\overline{v}\right| = 0.1U \tag{3-2}$$

$$l_\tau = 0.1H \tag{3-3}$$

where l_τ = mixing length, m; $|\overline{v}|$ = vertical fluctuation velocity, m/s; H = water depth, m; and U = free stream velocity, m/s.

It was proposed that the mixing length is the distance the turbulent water parcel can move freely by vertical fluctuation velocity (Rubin and Atkinson 2001). Thus, the surface renewal rate is determined by the mixing length and the vertical fluctuation velocity as:

$$r = \frac{|\overline{v}|}{l_\tau} \tag{3-4}$$

The surface renewal rate in isotropic turbulent flows can be obtained by substituting Eq.3.2 and Eq.3.3 into Eq.3.4 as (O'Connor and Dobbins 1956):

$$r = \frac{|\overline{v}|}{l_\tau} = \frac{U}{H} \tag{3-5}$$

which was substituted into Eq.3.1 to develop the gas-liquid transfer rate formula for isotropic turbulent flows (O'Connor and Dobbins 1956):

$$K_L = \sqrt{D\frac{U}{H}} \tag{3-6}$$

The predictions by the O'Connor and Dobbins formula underestimated the gas-liquid transfer rate in non-isotropic turbulent flows (Chapra 1997; Covar 1976), so these two empirical relationships (Eq.3.2 and Eq.3.3) developed from isotropic turbulent flows are not applicable for non-isotropic turbulent flows.

Surface renewal rate represents how often the surface renewal movements of the water parcels are. It is caused by the turbulence generated from the air-water interface and from the water-bed interface. Either turbulence is a driving force of a surface renewal

movements of the water parcels. Both surface renewal rates have contributions to the gas-liquid transfer rate, though the shear velocity at the water-bed interface is much greater than that at the air-water interface. It is assumed in this study that the total renewal rate is considered as the arithmetic sum of these two surface renewal rates:

$$r = r_1 + r_2 \tag{3-7}$$

where r_1 = surface renewal rate at the air-water interface, s^{-1}; and r_2 = surface renewal rate at the water-bed interface, s^{-1}.

At the water-bed interface or the air-water interface, based on the definition of skin friction coefficient and the definition of shear velocity, the shear velocity as a function of the free flow velocity can be obtained as (Munson 1994):

$$u_{*1} = \sqrt{\frac{C_{f1}}{2}} U \tag{3-8}$$

$$u_{*2} = \sqrt{\frac{C_{f2}}{2}} U \tag{3-9}$$

where u_{*1} = the shear velocity at air-water interface, m/s; u_{*2} = the shear velocity at water-bed interface, m/s; C_{f1} = the skin friction coefficient at air-water interface; and C_{f2} = the skin friction coefficient at water-bed interface. At the air-water interface and the water-bed interface, the vertical fluctuation velocity is assumed to equal the shear velocity (O'Connor and Dobbins 1956; O'Connor 1983):

$$\left|\overline{v_1}\right| = u_{*1} = \sqrt{\frac{C_{f1}}{2}} U \tag{3-10}$$

$$\left|\overline{v_2}\right| = u_{*2} = \sqrt{\frac{C_{f2}}{2}U} \tag{3-11}$$

where $\left|\overline{v_1}\right|$ = the vertical velocity fluctuation in the turbulent boundary layer at the air-water interface, m/s; $\left|\overline{v_2}\right|$ = the vertical velocity fluctuation in the turbulent boundary layer at the water-bed interface, m/s; u_{*1} = the shear velocity at the air-water interface, m/s; and u_{*2} = the shear velocity at the water-bed interface, m/s. In non-isotropic turbulent flows, the water depth is small and only consists of the turbulent boundary layer at the air-water interface and that at the water-bed interface. Though the fluctuating velocity scale in the bulk isotropic turbulent flow is in fact the same order of magnitude as that at the interface, the shear velocity is considered to be approximate zero in the bulk isotropic turbulent flow for convenience. Thus, the equivalent vertical fluctuation velocity can be considered to approximately be arithmetic average of the shear velocity at the friction interface and that in the bulk isotropic turbulent flow, namely $\frac{1}{2}\sqrt{\frac{C_{f1}}{2}U}$ in the turbulent boundary layer at the air-water interface and $\frac{1}{2}\sqrt{\frac{C_{f2}}{2}U}$ in the turbulent boundary layer at the water-bed interface. However, in isotropic turbulent flows, the shear velocity decreases in the water column far from the two-phase interfaces. Thus, the equivalent vertical fluctuation velocity in isotropic turbulent flows is much less than that in non-isotropic turbulent flows.

For non-isotropic turbulent flows, the water depth is the sum of the thickness of the boundary layer at the water-bed interface and that at the air-water interface:

$$H = \delta_1 + \delta_2 \tag{3-12}$$

where δ_1 = thickness of turbulent boundary layer at the air-water interface, m; and δ_2 = thickness of turbulent boundary layer at the water-bed interface, m.

The turbulent boundary layer consists of an inner layer and outer layer. The ratio of the spaces covered by the inner layer and the outer layer is about 0.15:1 (Richardson 1989). The inner layer consists of viscous layer and overlap layer. The ratio of the spaces covered by the viscous layer and the overlap layer is about 35:135 (Richardson 1989). Thus, the ratio of the viscous layer and the turbulent boundary layer is as:

$$\frac{\delta_v}{\delta} = \frac{35}{135} \times \frac{0.15}{1} = 0.039 \tag{3-13}$$

where δ_v = thickness of viscous layer in turbulent boundary layer, m, which is as (White 2006):

$$\delta_v = \frac{\Gamma_0 \nu}{u_*} \tag{3-14}$$

where Γ_0 = coefficient of viscous layer; ν = kinematic viscosity, 1 x 10^{-6} m^2/s at 20°C; and u_* = shear velocity, m/s. Substitution of Eq.3.8 or Eq.3.9, and Eq.3.14 into Eq.3.13 yields the thickness of turbulent boundary layer as:

$$\delta = \frac{\Gamma_0 \nu}{0.039\sqrt{\frac{C_f}{2}}U} \tag{3-15}$$

where C_f = skin friction coefficient at two-phase interface.

The outer layer covers much more space of the turbulent boundary layer than the viscous layer (Richardson 1989). Thus, the mixing length in the outer layer can be

considered to approximately represent the equivalent mixing length in the turbulent boundary layer:

$$l_1 = 0.09\delta_1 \tag{3-16}$$

where l_1 = mixing length in turbulent boundary layer at the air-water interface, m (White 2006). The mixing length can be expressed as a function of water depth by substituting Eq.3.12 into Eq.3.16 as:

$$l_1 = 0.09H\left(\frac{\delta_1}{\delta_1 + \delta_2}\right) \tag{3-17}$$

Substitution of Eq.3.15 into Eq.3.17 yields:

$$l_1 = 0.09H\left(\frac{\dfrac{\Gamma_0 \nu}{0.039\sqrt{\dfrac{C_{f1}}{2}}U}}{\dfrac{\Gamma_0 \nu}{0.039\sqrt{\dfrac{C_{f1}}{2}}U} + \dfrac{\Gamma_0 \nu}{0.039\sqrt{\dfrac{C_{f2}}{2}}U}}\right) = 0.09H\left(\frac{1}{1+\sqrt{\dfrac{C_{f1}}{C_{f2}}}}\right) \tag{3-18}$$

Substitution of Eq.3.10 and Eq.3.18 into Eq.3.5 yields the surface renewal rate caused by the turbulence at the air-water interface as:

$$r_1 = \frac{\left|\overline{v_1}\right|}{l_1} = \frac{\dfrac{1}{2}\sqrt{\dfrac{C_{f1}}{2}}U}{0.09H\left(\dfrac{1}{1+\sqrt{\dfrac{C_{f1}}{C_{f2}}}}\right)} \tag{3-19}$$

where r_1 = surface renewal rate caused by the turbulence generated from the air-water interface, s^{-1}. Similarly, in the turbulent boundary layer at the water-bed interface, the surface renewal rate is formulated as:

$$r_2 = \frac{|\overline{v_2}|}{l_2} = \frac{\frac{1}{2}\sqrt{\frac{C_{f2}}{2}}U}{0.09H\left(\frac{1}{1+\sqrt{\frac{C_{f2}}{C_{f1}}}}\right)} \tag{3-20}$$

where r_2 = surface renewal rate caused by the turbulence generated from the air-water interface, s^{-1}; and l_2 = mixing length in turbulent boundary layer at the air-water interface, m. Apparently, an important effect of the friction at the air-water interface was that the proportional coefficient in the linear relationship between the mixing length (l) and the water depth (H) was changed and was less than the proportional coefficient value in Eq.3.3 of 0.1. Substitution of Eq.3.19 and Eq.3.20 into Eq.3.7 yields the total renewal rate:

(3-21)

$$r = \frac{\frac{1}{2}\sqrt{\frac{C_{f1}}{2}}U}{0.09H\left(\frac{1}{1+\sqrt{\frac{C_{f1}}{C_{f2}}}}\right)} + \frac{\frac{1}{2}\sqrt{\frac{C_{f2}}{2}}U}{0.09H\left(\frac{1}{1+\sqrt{\frac{C_{f2}}{C_{f1}}}}\right)} = \left[\frac{\frac{1}{2}\sqrt{\frac{C_{f1}}{2}}}{0.09\left(\frac{1}{1+\sqrt{\frac{C_{f1}}{C_{f2}}}}\right)} + \frac{\frac{1}{2}\sqrt{\frac{C_{f2}}{2}}}{0.09\left(\frac{1}{1+\sqrt{\frac{C_{f2}}{C_{f1}}}}\right)}\right]\frac{U}{H}$$

The comparison between Eq.3.5 and the mixing length in Eq.3.21 shows that the coefficient in non-isotropic turbulent flows is different from that in isotropic turbulent flows.

Substitution of Eq.3.21 into Eq.3.2 yields the gas-liquid transfer rate:

$$K_L = \sqrt{Dr} = \sqrt{\left[\frac{\frac{1}{2}\sqrt{\frac{C_{f1}}{2}}}{0.09\left(\frac{1}{1+\sqrt{\frac{C_{f1}}{C_{f2}}}}\right)} + \frac{\frac{1}{2}\sqrt{\frac{C_{f2}}{2}}}{0.09\left(\frac{1}{1+\sqrt{\frac{C_{f2}}{C_{f1}}}}\right)}\right]\frac{DU}{H}} \qquad (3\text{-}22)$$

where K_L = gas-liquid transfer rate, m/s; D = diffusion coefficient, m^2/s; r = surface renewal rate, s^{-1}; C_{f1} = skin-friction coefficient at air-water interface; C_{f2} = skin-friction coefficient at water-bed interface; U = free stream velocity, m/s; and H = water depth, m. Eq.3.22 is the formula of gas-liquid transfer rate in non-isotropic turbulent flows developed in this study.

The skin friction coefficient at air-water interface C_{f1} is much smaller than the skin friction coefficient at air-water interface C_{f2} since the air flow or water flow drags each other to move at the air-water interface but the bed keeps rest no matter how water flow is at the water-bed interface. The skin friction coefficient is a function of the Reynolds number. Since it is difficult to determine the Reynolds number here, the empirical values 4.0×10^{-3} was selected for the skin friction coefficient C_{f1} to calculate gas-liquid transfer

rate under the normal wind speed (O'Connor-Dobbins 1983). Similarly, the empirical value 4.16 x 10^{-2} was used for C_{f2} (O'Connor-Dobbins 1956). Substitution of the values of C_{f1} and C_{f2} into Eq.3.16 yields:

$$r = 3.71\frac{U}{H} \tag{3-23}$$

Compared with Eq.3.6, the total renewal rate in non-isotropic turbulent flows is much greater than that in isotropic turbulent flows. Under the same flow velocity and water depth, non-isotropic turbulent flows have a greater surface renewal rate than isotropic turbulent flows.

Substitution of Eq.3.23 into Eq.3.1 yields the gas-liquid transfer rate as:

$$K_L = 1.93\sqrt{D\frac{U}{H}} \tag{3-24}$$

3.2.2. Discussion

Comparisons of Eq.3.24 and Eq.3.6 showed that the gas-liquid transfer rate in non-isotropic turbulent flows and that in isotropic turbulent flows are both proportional to $\sqrt{D\frac{U}{H}}$; but the coefficient in Eq.3.24 is 2.06 which is greater than that of Eq.3.6. Thus, the gas-liquid transfer rate in non-isotropic turbulent flows is greater than that in isotropic turbulent flows.

Covar (1976) suggested that Owens-Gibbs empirical formula (Eq.3-30) can be applied in non-isotropic turbulent flows (water depth < 0.6 m) and O'Connor-Dobbins

formula (Eq.3-28) can be applied in isotropic turbulent flows (deep water or fast flow). The predictions of these two formulae and Eq.3.24 are displayed in Figure 3.1. The predicted values with Eq.3.24 are close to those calculated by the Owens-Gibbs empirical formula and much greater than those calculated by the O'Connor-Dobbins formula. Furthermore, the Owens-Gibbs empirical formula reflects the experimental data. Thus, Eq.3.24 was verified to be reasonable. The change of the proportional coefficient of the linear relationship between the mixing length and the water depth and the accumulation of the surface renewal rates at the air-water interface and the water-bed interface are the main reasons why the values of the gas-liquid transfer rate in non-isotropic turbulent flows are greater than the values predicted by the O'Connor-Dobbins formula. In isotropic turbulent flows, the empirical relationships shown in Eq.3.2 and Eq.3.3 inherently incorporate the effects of both the surface renewal rate caused by both the turbulence generated at the air-water interface and at the water-bed interface. In non-isotropic turbulent flows, when the existing empirical relationships are not applicable, contributions from these two surface renewal rates to the total surface renewal rate need to be considered. The surface renewal rate caused by the turbulence at the air-water interface cannot be ignored in non-isotropic turbulent flows.

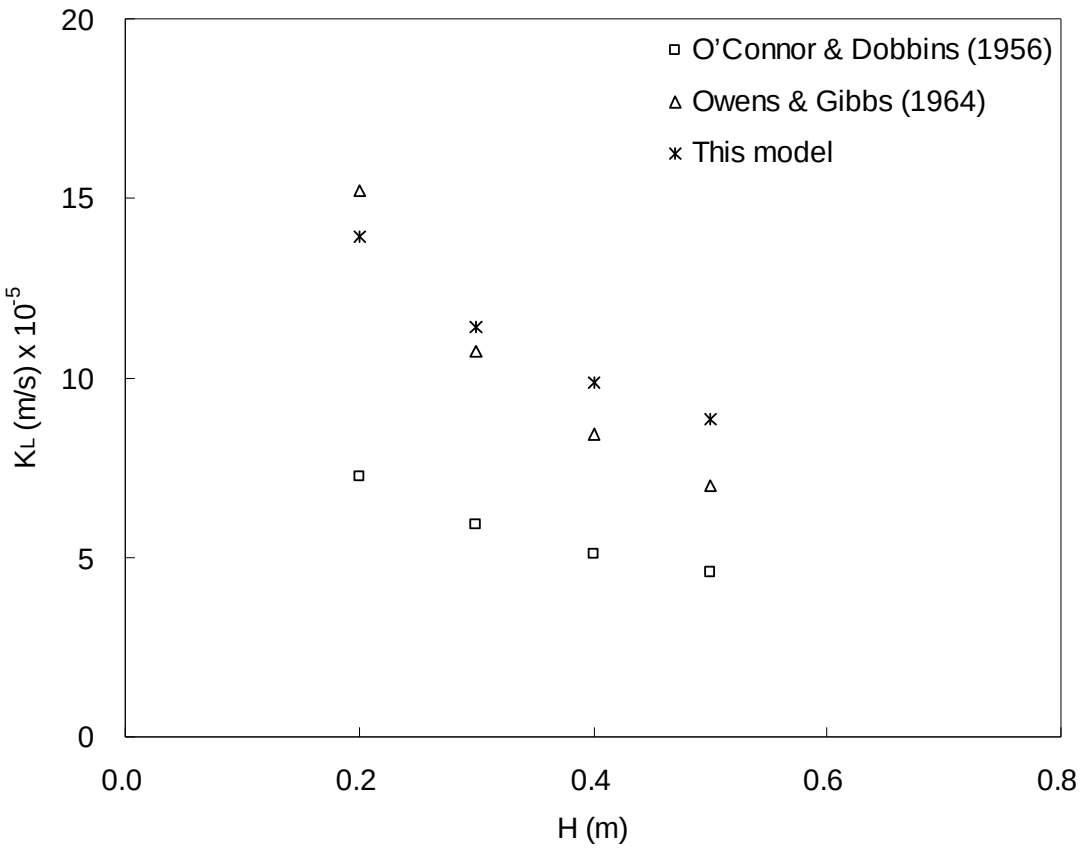

Figure 3.1 Comparisons of predicted values by this model, Owens-Gibbs empirical formula and O'Connor-Dobbins semi-empirical formula on stream-driven gas-liquid transfer rate (U = 0.5 m/s)

3.2.3. Conclusions

In non-isotropic turbulent flows, the surface renewal rate caused by the turbulence from both the air-water interface and the water-bed interface contribute to the gas-liquid transfer. In this study, the total renewal rate is assumed to be the arithmetic sum of these two surface renewal rates. New relationships between the mixing length and water depth in non-isotropic turbulent flows showed that the linear coefficient is less than that in

isotropic turbulent flows. The model developed in section 3.2 explained the reasons why the gas-liquid transfer rate in non-isotropic turbulent flows is greater than that in isotropic turbulent flows under the same flow velocity and water depth. The predicted values with this new model have reasonable agreements with the Owens-Gibbs empirical formula in non-isotropic turbulent flows. The comparisons of the predicted values of the new model with the calculated values with O'Connor-Dobbins semi-empirical formula showed the former are greater than the latter, which was the same as Covar indicated.

3.3. Stream-driven Gas-liquid Transfer Rate

3.3.1. Model development

In section 3.2, both the water-bed interface and the air-water interface were found to have significant effects on the gas-liquid transfer rate in non-isotropic turbulent flows. Based on this, a theoretical stream-driven gas-liquid transfer rate model can be developed for the normal ranges of water depth and flow velocity in the natural rivers which can be applied for both non-isotropic turbulent flows and isotropic turbulent flows.

3.3.1.1. Vertical fluctuation velocity and mixing length

Surface renewal rate is the frequency with which the water parcels transfer to the air-water interface and entrain the gas down to the water column. Prandtl (1925) indicated the mixing length is the distance the turbulent water parcel can move freely with the vertical fluctuation velocity. Thus, the surface renewal rate is determined by the mixing length and the vertical fluctuation velocity as Eq.3.4 shows. For isotropic turbulent flows, two empirical relationships (Hamada 1953; Kalinske 1943; Schijf and Schonfeld 1953) as Eq.3.2 and Eq.3.3 show can be employed to determine the surface renewal rate as Eq.3.5 shows. Thus, the surface renewal rate can be calculated with the hydraulic parameters of the flow velocity and water depth. This is the basis for

development of the classic O'Connor-Dobbins formula (1956) for stream-driven gas-liquid transfer rate in isotropic turbulent flows.

These two empirical relationships were obtained in the deep rivers and estuaries where the isotropic turbulence is the predominant driving force of reaeration. As they are empirical relationships, Eq.3.3 and Eq.3.4 inherently incorporate the combined effects of both the turbulence from the air-water interface and that from the water-bed interface. However, for shallow water or fast flow, isotropic turbulence is not predominant and these two empirical relationships are not suitable to use for the calculation of the surface renewal rate. Thus, as section 3.2 discussed, O'Connor-Dobbins' formula underestimates the reaeration rate when it is applied to shallow water or fast flow. More general formulae on the mixing length and the vertical fluctuation velocity in terms of hydraulic parameters need to be developed for the normal ranges of flow velocity and water depth.

In the theory of turbulent flows, the mixing length does not have a general formula. Formulae have been developed for several specific cases. Eq.3.3 is the empirical relationship between the mixing length and water depth in deep rivers when isotropic turbulent flow is predominant. Further, Prandtl and von Karman gave the estimates of the mixing length for the overlap layer and the outer layer in the turbulent boundary layer (White 2006):

In the overlap layer:

$$l = \kappa H \tag{3-25}$$

In the outer layer:

$$l = 0.09\delta \tag{3-26}$$

where κ = von Karman constant; and δ = thickness of turbulent boundary layer, m. The thickness of the viscous layer in the turbulent boundary layer is as Eq.3.14 shows.

The viscous layer in this study refers to the combination of linear layer and buffer layer in turbulent boundary layer. At the water-bed interface, the equivalent coefficient of viscous layer thickness Γ_0 has a constant value of 35 (White 2006). At the air-water interface, O'Connor (1983) employed Eq.3.14 with a variable value of Γ_0 to develop a formula of wind-driven gas-liquid transfer rate. Thus, Eq.3.14 is also considered to be applicable to air-water interface. According to Eq.3.25, if turbulence is considered to start from the edge of the viscous layer, the smallest mixing length is at the edge of the viscous layer and is proportional to the thickness of the viscous layer, δ_v:

$$l_v = \kappa\delta_v = \frac{\kappa\Gamma_0\nu}{u_*} \tag{3-27}$$

where l_v = mixing length at the edge of viscous layer, m.

If the general formula of the stream-driven gas-liquid transfer rate is developed based on the formulae of the mixing length including Eq.3.3, Eq.3.25 and Eq.3.26, multiple formula formats will be obtained for the overlap layer, outer layer, isotropic turbulent flows, etc. Further, because there is not a mixing length formula for the transitional range of water depth from the turbulent boundary layer to the isotropic turbulent flow, the general formula of gas-liquid transfer rate based on the existing mixing length formulae

cannot cover the transitional range. In order to solve these problems and simplify the general formula, a new mixing length formula will be constructed to cover the normal ranges of water depth

Figure 3.2 shows the reaeration rate values predicted by the O'Connor and Dobbins' formulae (Eq.3.28), Churchill's formulae (Eq.3.29), Owens-Gibbs' formulae (Eq.3.30) (Chapra 1997) at a fixed flow velocity of 0.8 m/s:

$$K_L = 4.55 \times 10^{-5} \times \frac{U^{0.5}}{H^{0.5}} \tag{3-28}$$

$$K_L = 5.82 \times 10^{-5} \times \frac{U}{H^{0.67}} \tag{3-29}$$

$$K_L = 6.16 \times 10^{-5} \times \frac{U^{0.67}}{H^{0.85}} \tag{3-30}$$

The trend of the reaeration rate values indicates that the gas-liquid transfer rate increases on a scale larger than an exponential rate as the water depth decreases especially when it is less than 0.6 m. Thus, a powered exponential function is developed to describe the relationship between the mixing length and the water depth through all of the ranges of the water depth at a fixed flow velocity:

$$l = l_\tau \left(\frac{l_v}{l_\tau} \right)^{\left(\frac{\delta_{v1} + \delta_{v2}}{H} \right)^n} \tag{3-31}$$

where δ_{v1} = thickness of viscous layer at the air-water interface, m; δ_{v2} = thickness of viscous layer at the water-bed interface, m; and n = exponential coefficient. Eq.3.31 shows that when the water depth of H is very small and close to the sum of the thickness

of the viscous layers $(\delta_{v1} + \delta_{v2})$, the mixing length of l will be close to l_v. When the water depth of H is much larger than $(\delta_{v1} + \delta_{v2})$, $\frac{(\delta_{v1} + \delta_{v2})}{H}$ will be close to zero and l will be close to l_τ.

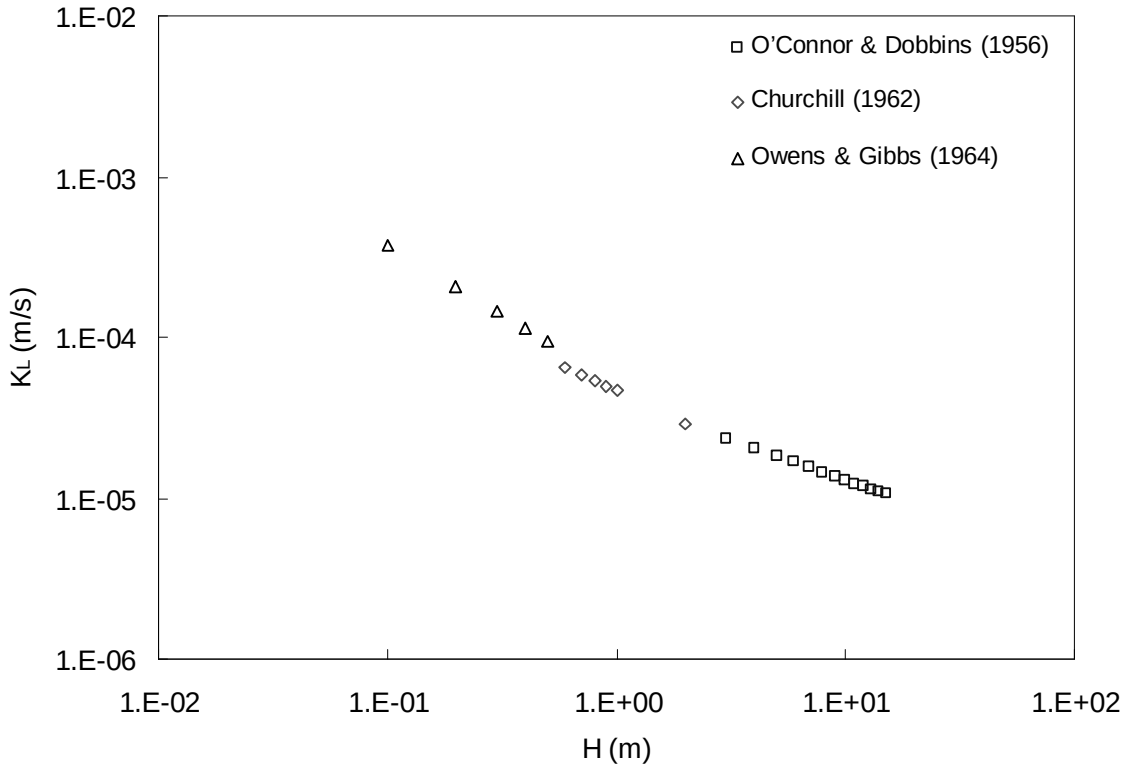

Figure 3.2 Reaeration rates predicted with the existing reaeration rate formulae

The vertical fluctuation velocity decreases across the space from the friction interface to the isotropic bulk flow. At the friction interface where the turbulence is generated, the vertical fluctuation velocity is a maximum and is equal to the shear velocity $\sqrt{\frac{C_f}{2}}U$:

$$\left|\overline{v}\right| = u_{*i} = \sqrt{\frac{C_f}{2}}U \tag{3-32}$$

where u_{*i} = shear velocity at friction interface, m/s; and C_f = skin-friction coefficient. Though the fluctuating velocity scale in the bulk isotropic turbulent flow is in fact the same order of magnitude as that at the interface, the shear velocity is considered to be approximate zero in the bulk isotropic turbulent flow for convenience:

$$\left|\overline{v}\right| = u_{*b} \approx 0 \tag{3-33}$$

where u_{*b} = shear velocity in isotropic turbulent flow bulk far away from the friction interface.

It is difficult to get a general formula to describe the vertical fluctuation velocity across the space from the friction interface to the isotropic turbulent flow bulk for all of the normal ranges of flow velocity and water depth in natural rivers. Thus, in order to generalize and simplify the formula for the stream-driven gas-liquid transfer rate, the arithmetic average of u_{*i} and u_{*b} will be considered as the equivalent vertical fluctuation velocity for convenience:

$$\left|\overline{v}\right| = \frac{u_{*i} + u_{*b}}{2} = \frac{U}{2}\sqrt{\frac{C_f}{2}} \tag{3-34}$$

The effect of the variety of equivalent vertical fluctuation velocity on the gas-liquid transfer rate will be incorporated into the formula of the mixing length by introducing an empirical constant, δ_0, to replace $(\delta_1+\delta_2)$ in Eq.3.31:

$$l = l_\tau \left(\frac{l_v}{l_\tau} \right)^{\left(\frac{\delta_0}{H} \right)^n} \tag{3-35}$$

The values of δ_0 and n are adjusted to tally with combined predictions of O'Connor-Dobbins formulae, Churchill formula, and Owens-Gibbs formula showed as Figure 3.2. Normally δ_0 has the same order of magnitude as that of (δ_{v1}+δ_{v2}) which order is normally from 10^{-3} to 10^{-1} m in the natural rivers.

In order to simplify the stream-driven gas-liquid transfer rate formula that will be developed in this section, the constant value of 35 will also be used for Γ_0 at the air-water interface. The effect of the variety of Γ_0 on the gas-liquid transfer rate will also be incorporated into the formula of the mixing length by employing δ_0.

For water-bed interface, Eq.3.32 is applicable based on wall turbulence theory (White 2006); for the air-water interface, O'Connor (1983) considered it was also applicable when a different skin-friction coefficient was used and developed a formula of wind-driven gas-liquid transfer rate. The skin-friction coefficient is noted to be Reynolds number dependent. In order to simplify the formula developed in this study, an equivalent value is selected for C_{f1} and C_{f2} respectively. A skin-friction coefficient at air-water interface (C_{f1}) of 4.00 x 10^{-3} was obtained using Eq.3.32 with the known wind speed and shear velocity in O'Connor's (1983) research. A value of 4.16 x 10^{-2} for the skin-friction coefficient at the water-bed interface (C_{f2}) was obtained using the relationship between skin-friction coefficient at water-bed interface and Chezy coefficient and the

experimental data of Chezy coefficient from O'Connor and Dobbins' research (1956). Similarly, the effect of the variety of C_{f1} and C_{f2} on the gas-liquid transfer rate will be incorporated into the formula of the mixing length by adjusting δ_0.

3.3.1.2. Accumulation of surface renewal rates

The stream flow not only experiences friction with the bed but also with the air above the stream. As a result, turbulence is produced at both the water-bed interface and the air-water interface. Both kinds of turbulence cause water parcels to move from the water bulk toward the air-water interface for reaeration with a surface renewal frequency (surface renewal rate) respectively. It is assumed in this study that the total surface renewal frequency of dissolved oxygen is the addition of the two surface renewal frequencies caused by the two sources of turbulence. Thus, the total renewal rate equals to the sum of the renewal rate caused by the turbulence from the water-bed interface and that caused by the turbulence from the air-water interface:

$$r = r_1 + r_2 \tag{3-36}$$

where r_1 = surface renewal rate at the air-water interface, s^{-1}; r_2 = surface renewal rate at the water-bed interface, s^{-1}.

3.3.1.3. Formulae of stream-driven gas-liquid transfer rate

This study is to develop a semi-empirical formula which has general applications for the normal ranges of water depth and flow velocity in natural rivers. When the expressions on vertical fluctuation velocity (Eq.3.34) and mixing length (Eq.3.35) are used for the development of the new formula, it will be applicable for both non-isotropic turbulent flows and isotropic turbulent flows.

In the following, variables with the subscript 1 refer to the air-water interface; while subscript 2 refers to the water-bed interface. Eq.3.3, Eq.3.27, Eq.3.34 and Eq.3.35 can be applied at both air-water interface and water-bed interface; but the skin-friction coefficients at these two interfaces are different. Substitution of Eq.3.34 and Eq.3.35 into Eq.3.1 yields the surface renewal rate at the air-water interface, r_1, and that at the water-bed interface, r_2:

$$r_1 = \frac{0.5u_{*1}}{l_{\tau 1}\left(\frac{l_{v1}}{l_{\tau 1}}\right)^{\left(\frac{\delta_0}{H}\right)^n}} \tag{3-37}$$

where u_{*1} = shear velocity at the air-water interface, m/s; $l_{\tau 1}$ = mixing length in isotropic turbulent flow at the air-water interface, m; l_{v1} = mixing length at the edge of viscous layer at the air-water interface, m.

$$r_2 = \frac{0.5u_{*2}}{l_{\tau 2}\left(\frac{l_{v2}}{l_{\tau 2}}\right)^{\left(\frac{\delta_0}{H}\right)^n}} \tag{3-38}$$

where u_{*2} = shear velocity at the water-bed interface, m/s; $l_{\tau 2}$ = mixing length in isotropic turbulent flow at the water-bed interface, m; l_{v2} = mixing length at the edge of viscous layer at the water-bed interface, m. Substitution of Eq.3.37 and Eq.3.38 into Eq.3.36 yields the total surface renewal rate:

$$r = \frac{0.5u_{*1}}{l_{\tau 1}\left(\frac{l_{v1}}{l_{\tau 1}}\right)^{\left(\frac{\delta_0}{H}\right)^n}} + \frac{0.5u_{*2}}{l_{\tau 2}\left(\frac{l_{v2}}{l_{\tau 2}}\right)^{\left(\frac{\delta_0}{H}\right)^n}} \tag{3-39}$$

Substitution of Eq.3.39 into Eq.3.1 yields the general formula of stream-driven gas-liquid transfer rate:

$$K_L = \sqrt{Dr} = \sqrt{D(r_1 + r_2)} = \sqrt{D\left[\frac{0.5u_{*1}}{l_{\tau 1}\left(\frac{l_{v1}}{l_{\tau 1}}\right)^{\left(\frac{\delta_0}{H}\right)^n}} + \frac{0.5u_{*2}}{l_{\tau 2}\left(\frac{l_{v2}}{l_{\tau 2}}\right)^{\left(\frac{\delta_0}{H}\right)^n}}\right]} \tag{3-40}$$

In Eq.3.40 u_{*1} and u_{*2} can be calculated with Eq.3.32 with specific values of skin-friction coefficient for these two interfaces; l_{v1} and l_{v2} can be calculated with Eq.3.27; $l_{\tau 1}$ and $l_{\tau 2}$ can be calculated with Eq.3.3. Substitution of Eq.3.3, Eq.3.27 and Eq.3.32 into Eq.3.40 yields the general formula of stream-driven gas-liquid transfer rate in terms of hydraulic parameters:

$$K_L = \sqrt{D\left[\frac{0.5\sqrt{\frac{C_{f1}}{2}}U}{0.1H\left(\frac{\frac{\kappa\Gamma_0\nu}{\sqrt{\frac{C_{f1}}{2}}U}}{0.1H}\right)^{\left(\frac{\delta_0}{H}\right)^n}} + \frac{0.5\sqrt{\frac{C_{f2}}{2}}U}{0.1H\left(\frac{\frac{\kappa\Gamma_0\nu}{\sqrt{\frac{C_{f2}}{2}}U}}{0.1H}\right)^{\left(\frac{\delta_0}{H}\right)^n}}\right]} \quad (3\text{-}41)$$

where K_L = gas-liquid transfer rate, m/s; D = diffusion coefficient, m^2/s; C_{f1} = skin-friction coefficient at air-water interface; C_{f2} = skin-friction coefficient at water-bed interface; U = free stream velocity, m/s; H = water depth, m; κ = von Karman constant; Γ_0 = coefficient of viscous layer; and ν = kinematic viscosity, m^2/s. The model formulated as Eq.3.41 is named as "Stream-driven KL Model" in this study.

Testing of Eq.3.41 required specification of coefficient values. Both the diffusion coefficient and the viscosity depend on temperature. As some relationships have been established for the conversions of diffusion coefficient and viscosity between different temperatures, many gas-liquid transfer rate models were developed under a certain temperature like 20°C. Thus, the tests in this study were conducted assuming 20°C, the temperature used in developing Churchill's, O'Connor-Dobbins, and Owens-Gibbs formulae. The diffusion coefficient at 20°C is 2.09 x 10^{-9} m^2/s (Lide 2000) and the

viscosity at 20°C is 1.00 x 10^{-6} m^2/s (Yaws 1999). The value of 5.5 x 10^{-2} m for δ_0 and the value of 0.9 for n are obtained by adjusting δ_0 and n to have Eq.3.41 to tally with Eq.3.28-3.30 for the normal ranges of flow velocity and water depth in natural rivers.

3.3.2. Model testing

3.3.2.1. Comparison with existing formulae

Table 3.1 shows that each existing formula is applicable for specific ranges of flow velocity and water depth. O'Connor-Dobbins' formula, Churchill's formula and Owens-Gibbs' formula have successfully reproduced observed data (Chapra 1997; Covar 1976). Thus, the predictions of three existing formulae were combined to compare with the predictions of Eq.3.41, the general formula of the stream-driven gas-liquid transfer rate for the normal ranges of flow velocity and water depth in the natural rivers. As section 3.1 states, in natural rivers, the flow velocity typically ranges from 0.03 m/s to 1.5 m/s and the water depth ranges from 0.1 to 15 m (Chapra 1997). For the streams whose water depth and flow velocity are outside of these normal ranges, only δ_0 needs to be adjusted and Eq.3.41 is still applicable. The comparisons are plotted at the flow velocity of 0.03, 0.06, 0.1, 0.4, 0.8, 1 and 1.5 m/s in Figure 3.3-3.5 and for each fixed flow velocity the water depth is from 0.1 to 15 m. Figure 3.3-3.5 show that this model has a close agreement with these existing formulae.

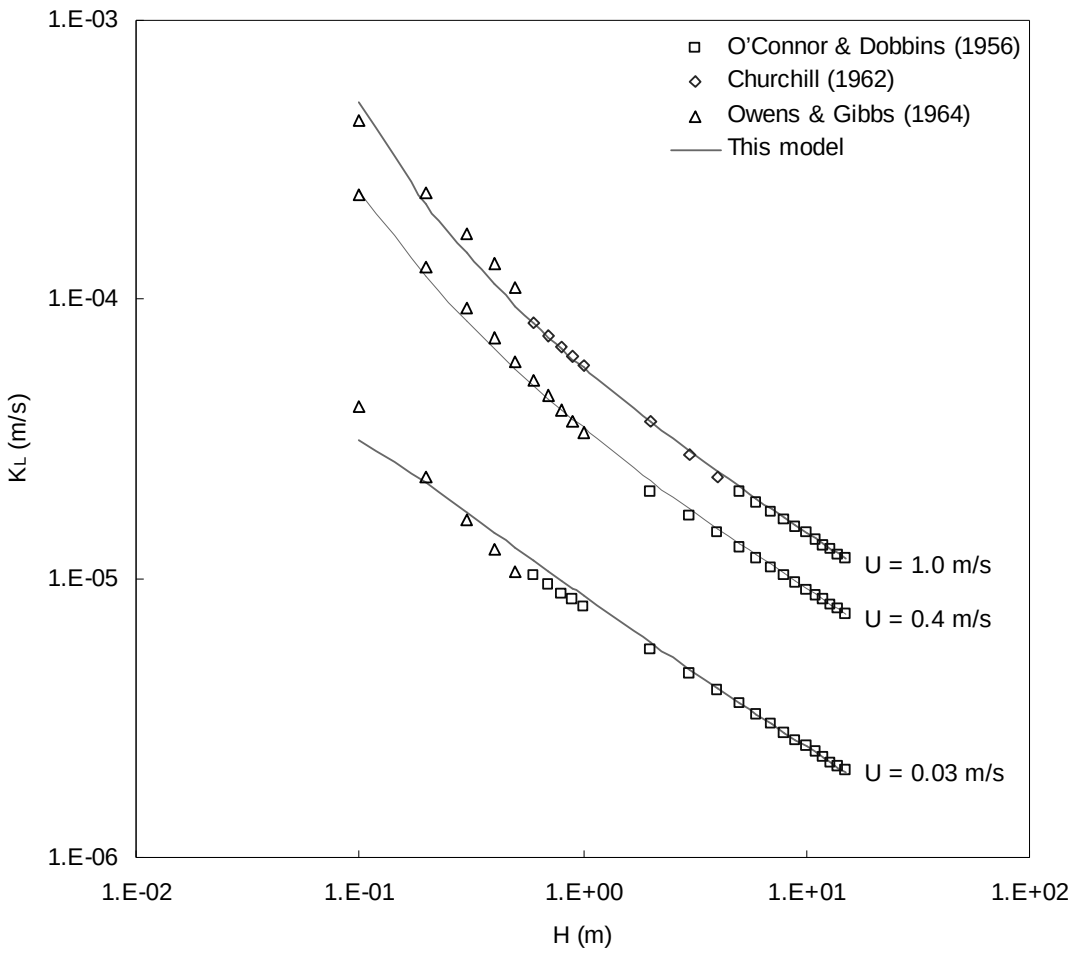

Figure 3.3. Gas-liquid transfer rate at the stream velocity of 0.03, 0.4 and 1.0 m/s

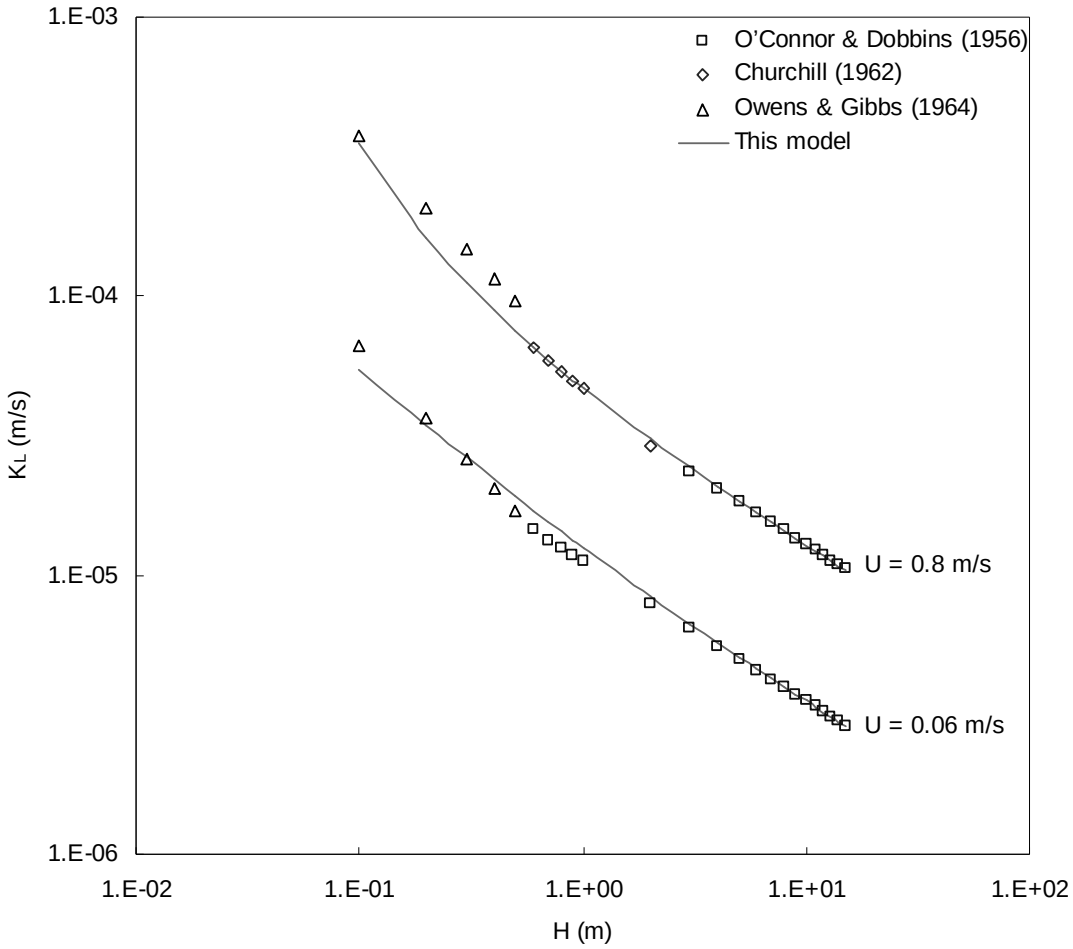

Figure 3.4. Gas-liquid transfer rate at the stream velocity of 0.06 and 0.8 m/s

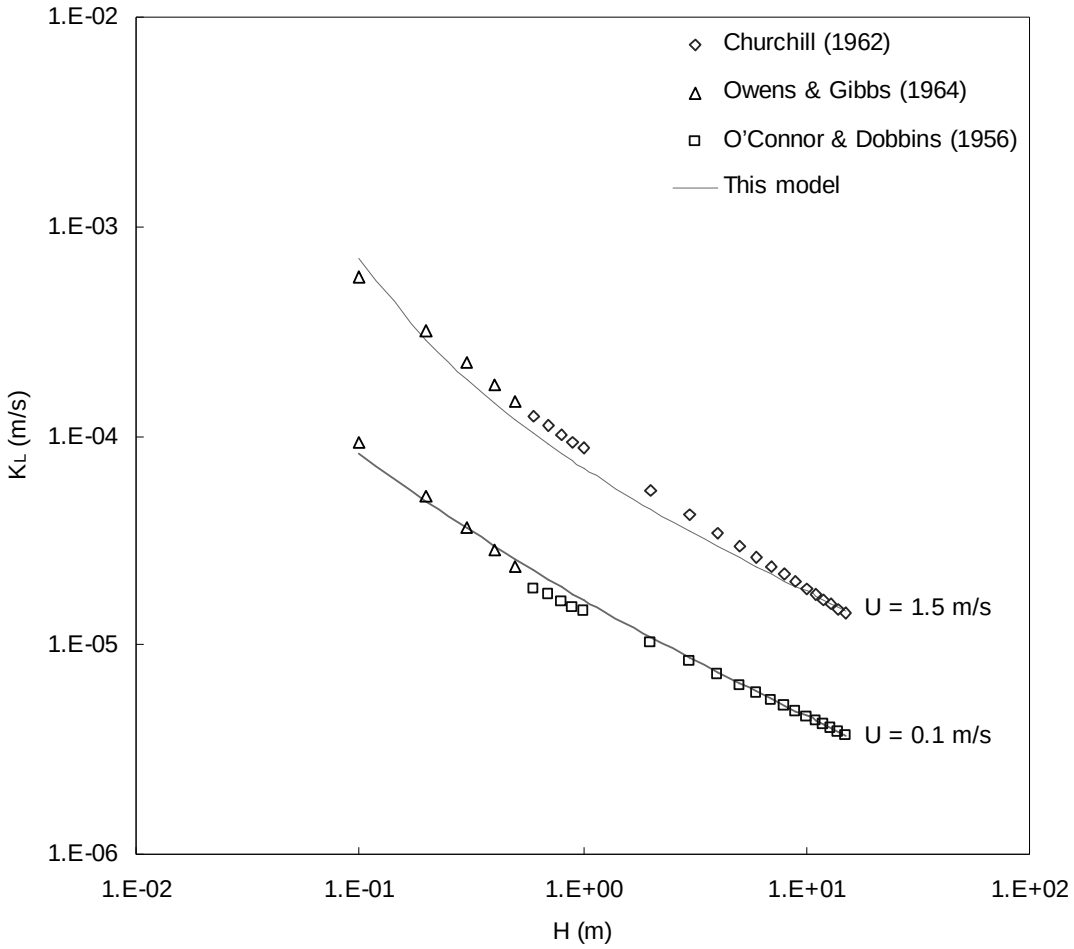

Figure 3.5. Gas-liquid transfer rate at the stream velocity of 0.1 and 1.5 m/s

3.3.2.2. Comparison with experimental data

The predictions of Eq.3.41, the general formula of the stream-driven gas-liquid transfer rate for the normal ranges of flow velocity and water depth in the natural rivers were compared with the experimental data reported in O'Connor and Dobbins' research (1956) and Owens and Gibbs' research (1964). Figure 3.6 shows the predictions tally the experimental data well.

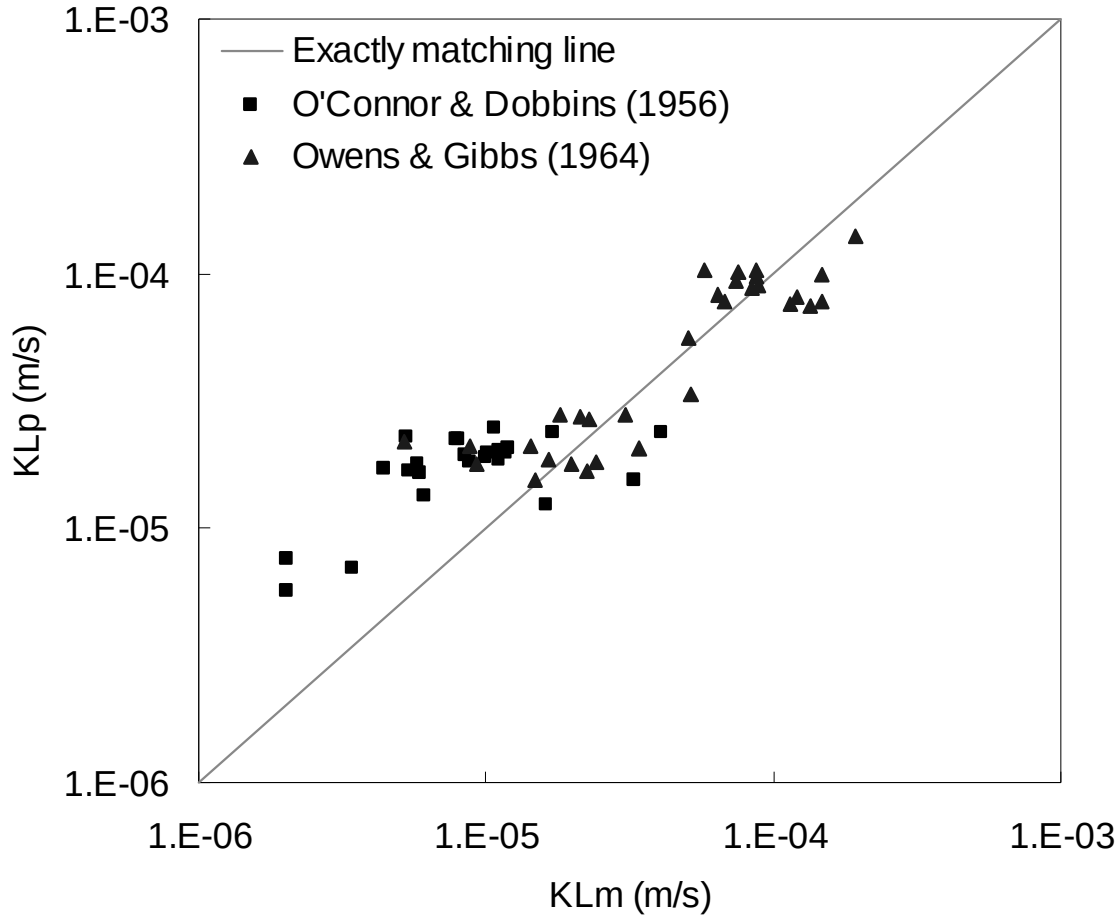

Figure 3.6. Comparison of predicted and measured gas-liquid transfer rate

3.4. Conclusions

The construction of the formulae of the mixing length and the vertical fluctuation velocity leads to the establishment of a general formula of the surface renewal rate. The arithmetic sum of these surface renewal rates caused by the turbulence from the water-bed interface and that caused by the turbulence from the air-water interface was considered as the total surface renewal rate. Then, based on the Surface Renewal Theory,

the total surface renewal rate was used to obtain a general model and formula of the stream-driven gas-liquid transfer rate. This model is applicable for the normal ranges of flow velocity and water depth in natural rivers. The predictions of this model have reasonable agreement with the existing formulae and observed data.

CHAPTER IV

WIND-STREAM-DRIVEN GAS-LIQUID TRANSFER RATE

4.1. Introduction

In wind-driven gas-liquid transfer systems, wind is the predominant factor for the gas transfer process. When wind blows over water, turbulence is generated at the air-water interface, which is the driving force of the surface renewal movement of the water parcels. Considerable empirical relationships have been established for the wind-driven gas-liquid transfer rate (Broecker et al. 1978; Jahne et al. 1979; Liss and Merlivat 1986; Wanninkhof 1992; Wanninkhof and McGillis 1999). A theoretical model on wind reaeration rate has also been developed (O'Connor 1983).

In stream-driven gas-liquid transfer systems, when wind impacts are negligible, streamflow is the predominant factor for the gas transfer process. When stream flows over bed, turbulence is generated at the water-bed interface and the air-water interface. Both kinds of turbulence are driving forces of the water parcels' surface renewal movement. Efforts have been exerted to build the empirical formulae (Churchill 1962; Owens and Gibbs 1964). Some theoretical models have been developed (O'Connor and Dobbins 1956; Langbein and Durum 1967; Wilcock 1984).

In many cases in the natural environment, both wind and stream have important effects on the gas transfer across the air-water interface. A model on the combined effects of wind and stream on gas-liquid transfer rate needs to be developed. In this study, the vector sum of shear velocities at the air-water interface comprised the contributions of both wind and stream. The concept of effective viscous layer was used to represent the erosion of the roughness on the viscous layer thickness and the decrease of the resistance to the gas transfer through the viscous layer. A sequential resistance model was developed to describe the gas transfer through the viscous layer and the outer layer serially in the turbulent boundary layer at the air-water interface. The total surface renewal rate is considered as the arithmetic sum of the surface renewal rates caused by the turbulence from the air-water interface and the turbulence from the water-bed interface. Then the gas-liquid transfer rate model and its related formulae were developed for the combined effects of wind and stream.

Further, though considerable empirical formulae have been developed for wind-driven gas-liquid transfer rate, they are normally limited in their applicability due to the specific experimental conditions under which they were developed. A more generally applicable relationship on wind-driven gas-liquid transfer rate needs to be derived from the formula of wind-stream-driven gas-liquid transfer rate.

4.2. Combined effects of Wind and Stream on Gas-liquid Transfer Rate

4.2.1. Model development

4.2.1.1. Serial resistance model

Both wind and stream exert shear forces at the air-water interface, which establish a turbulent boundary layer in both air phase and water phase. For sparingly soluble gases, the turbulent boundary layer in the water phase is considered to be much more significant because the stagnant liquid film in water phase is predominant in the gas transfer process in comparison to the stagnant gas film in the air phase. The turbulent boundary layer includes an inner layer and an outer layer. The inner layer and the outer layer have a common region, which is called the overlap layer. Inside the inner layer, starting from the air-water interface, there is a linear layer and a buffer layer underlain by the overlap layer. The first two layers are named as the viscous layer here. At the air-water interface, the friction between air flow and water flow damps the turbulence and thus a viscous layer exists next to the friction interface based on the Two-film Theory. At the distance far from the friction interface, the flow becomes turbulent. Thus, the turbulent boundary layer at the air-water interface is assumed to be composed of a viscous layer and a turbulent layer (similar to outer layer). Gas transferring from air to water bulk goes through the viscous

layer and the turbulent layer serially. Thus, a serial resistance model is established to describe the total resistance that the gas encounters in the turbulent boundary layer:

$$\frac{1}{K_L} = \frac{1}{K_{Lv}} + \frac{1}{K_{L\tau}} \tag{4-1}$$

where K_L = gas-liquid transfer rate, m/s; K_{Lv} = gas-liquid transfer rate controlled by molecular diffusion, m/s; $K_{L\tau}$ = gas-liquid transfer rate controlled by turbulent diffusion, m/s. Since resistance due to viscosity is predominant in the viscous layer, this layer can be considered as a stagnant liquid film. In this film, molecular diffusion is the driving force of gas transfer. Thus, K_{Lv} can be formulated based on the Two-film Theory (Whitman 1923) as:

$$K_{Lv} = \frac{D}{\delta_v} \tag{4-2}$$

where D = diffusion coefficient, m^2/s; δ_v = effective thickness of viscous layer, m. Turbulent diffusion is the main driving force of gas transfer in the outer layer, turbulent eddies carry gas to transfer through the outer layer to the water bulk with a renewal rate of r. Thus, gas-liquid transfer rate in the outer layer, $K_{L\tau}$, can be formulated according to the Surface Renewal Theory (Danckwerts 1951; Danckwerts 1953; Higbie 1935) as:

$$K_{L\tau} = \sqrt{Dr} \tag{4-3}$$

where r = surface renewal rate, s^{-1}. Substitution Eq.4.2 and Eq.4.3 in Eq.4.1 yields:

$$\frac{1}{K_L} = \frac{1}{\frac{D}{\delta_v}} + \frac{1}{\sqrt{Dr}} \tag{4-4}$$

where δ_v = thickness of viscous layer in turbulent boundary layer, m. The thickness of the viscous layer is proportional to the ratio of kinetic viscosity and shear velocity (White 2006). Similarly, the effective thickness of the viscous layer δ_v is also proportional to the ratio of kinetic viscosity and shear velocity:

$$\delta_v = \Gamma \frac{\nu}{u_*} \tag{4-5}$$

where Γ = equivalent coefficient of viscous layer thickness, m; ν = kinematic viscosity, m^2/s; u_* = shear velocity, m/s. The viscous layer in this study refers to the combination of the linear layer and the buffer layer in turbulent boundary layer. For the water-bed interface, Γ has a constant value of 35 (White 2006); for air-water interface, O'Connor (1983) employed Eq.4.5 with a variable value of Γ to develop a formula of wind-driven gas-liquid transfer rate. Thus, Eq.4.5 is also considered to be applicable to air-water interface. Substitution of Eq.4.5 into Eq.4.2 yields:

$$K_{Lv} = \frac{D}{\Gamma \frac{\upsilon}{u_*}} \tag{4-6}$$

The mixing length is the distance that the turbulent water parcel can move freely with the vertical fluctuation velocity (Rubin and Atkinson 2001). Thus, the surface renewal rate is determined by the mixing length and the vertical fluctuation velocity as:

$$r = \frac{\left|\overline{v}\right|}{l} \tag{4-7}$$

where $\left|\overline{v}\right|$ = vertical velocity fluctuation, m/s; and l = mixing length, m. In the overlap layer, the vertical velocity fluctuation is considered to be equal to the shear velocity (O'Connor and Dobbins 1956):

$$\left|\overline{v}\right| = u_* \tag{4-8}$$

Based on the Prandtl-von Karman mixing length hypothesis, the mixing length in the outer layer of the turbulent boundary layer is proportional to the turbulent boundary layer thickness (White 2006):

$$l = 0.09\delta \tag{4-9}$$

where δ = turbulent boundary layer thickness, m.

The thickness ratio of the viscous layer of δ_v over the inner layer is about 35 to 135. The thickness ratio of the inner layer over the turbulent boundary layer of δ is about 0.1 to 1 (Reynolds 1974). Thus, the thickness of turbulent boundary layer of δ is proportional to the thickness of the viscous layer of δ_v (m):

$$\delta = \frac{\frac{135}{\Gamma}\delta_v}{0.1} = \frac{1350}{\Gamma}\delta_v \tag{4-10}$$

where δ = turbulent boundary layer thickness, m; and Γ = equivalent coefficient of viscous layer thickness. Substitution of Eq.4.5, Eq.4.7, Eq.4.8, Eq.4.9 and Eq.4.10 into Eq.4.6 yields:

$$r = \frac{u_*}{0.09\delta} = \frac{u_*\Gamma}{121.5\delta_v} = \frac{u_*^{\,2}}{121.5\nu} \tag{4-11}$$

Substitution of Eq.4.11 into Eq.4.3 yields:

$$K_{L\tau} = \sqrt{\frac{Du_*^{\,2}}{121.5\nu}} \tag{4-12}$$

and substitution of Eq.4.6 and Eq.4.12 into Eq.4.1 yields:

$$\frac{1}{K_L} = \frac{1}{\frac{D}{\Gamma\frac{\nu}{u_*}}} + \frac{1}{\sqrt{\frac{Du_*^{\,2}}{121.5\nu}}} \tag{4-13}$$

which is the formulae of gas-liquid transfer rate in the turbulent boundary layer at the air-water interface.

4.2.1.2. Multiple turbulence sources

There are two turbulence sources in the gas transfer system caused by both wind and stream. One is at the air-water interface where a turbulent boundary layer is established by the shear forces of both wind and stream. The other is at the water-bed interface where a turbulence boundary layer is established by the shear forces of the stream flowing over the bed. The former turbulence drives the gas to transfer from the air-water interface to the water bulk with a surface renewal rate r_{1e}. The latter turbulence drives the same surface renewal movement with a surface renewal rate r_2. In this study it is assumed that the total surface renewal rate of dissolved oxygen is the arithmetic addition of these two surface renewal rates caused by the two kinds of turbulence respectively:

$$r = r_{1e} + C_r r_2 \tag{4-14}$$

where r_{1e} = equivalent surface renewal rate at air-water interface, s^{-1}; r_2 = surface renewal rate at water-bed interface, s^{-1}; and C_r = effective coefficient of the surface renewal rate at water-bed interface, which is determined by the effects of the wind on the surface renewal rate at water-bed interface.

The gas-liquid transfer rate caused by the turbulence at the air-water interface can be obtained by substituting r_1 into Eq.4.4, which equals to the gas-liquid transfer rate obtained by substituting r_{1e} into Eq.4.3. Thus, the equivalent surface renewal rate that is caused by the turbulence at the air-water interface (r_{1e}) can be formulated as:

$$r_{1e} = \frac{1}{D}\left(\frac{1}{\frac{1}{\frac{D}{\delta_1}} + \frac{1}{\sqrt{Dr_1}}}\right)^2 \quad (4\text{-}15)$$

where δ_1 = thickness of viscous layer in turbulent boundary layer at the air-water interface, m; and r_1 = surface renewal rate at air-water interface, s^{-1}. Substitution of Eq.4.14 into Eq.4.3 yields the total gas-liquid transfer rate:

$$K_L = \sqrt{D\left(r_{1e} + C_r r_2\right)} \quad (4\text{-}16)$$

4.2.1.3. Formulation with shear velocity

At the water-bed interface, the shear velocity, u_{*2}, is caused only by the stream and is formulated as (White 2006):

$$u_{*2} = \sqrt{\frac{C_{f2}}{2}U} \quad (4\text{-}17)$$

where u_{*2} = shear velocity at water-bed interface, m/s; and C_{f2} = skin-friction coefficient at water-bed interface. In O'Connor's research in 1983 on wind-driven gas-liquid transfer

rate, Eq.4.17 was considered to be also applicable for the shear velocity at air-water interface with a different value for the skin-friction coefficient:

$$u_{*1} = \sqrt{\frac{C_{f1}}{2}} U \tag{4-18}$$

where u_{*1} = shear velocity at water-bed interface, m/s; and C_{f1} = skin-friction coefficient at air-water interface.

Normally the previous studies on wind-driven gas-liquid transfer rate considered wind speed as a one-dimensional variable. However, in wind-stream-driven systems, the wind and stream directions may not be parallel. Thus, in this study, the wind speed and streamflow velocity are considered as a two-dimensional system. At the air-water interface, as Figure 4.1 shows, the effective wind speed is the vector difference of the wind speed and the flow velocity:

$$\vec{W}_e = \vec{W} - \vec{U} \tag{4-19}$$

where W_e = effective wind speed, m/s.

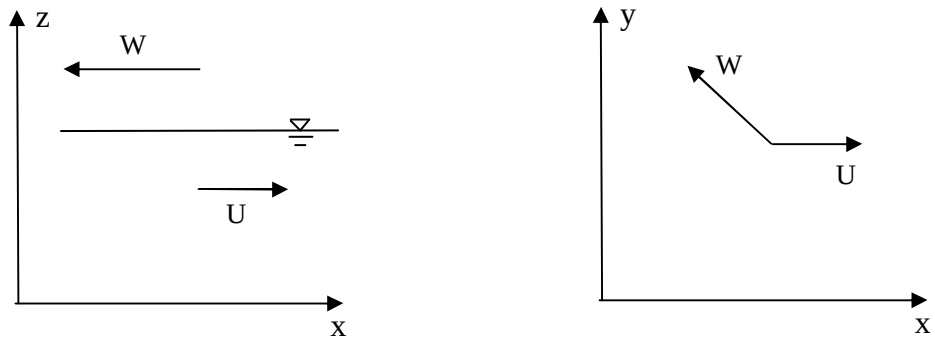

Figure 4.1. Vectors of wind speed and stream velocity on the flat plane of air-water interface

The relationship between the shear velocity in water phase and that in air phase is as (O'Connor 1983):

$$u_{*w} = \sqrt{\frac{\rho_a}{\rho_w}} u_{*a} \tag{4-20}$$

where u_{*a} = shear velocity at the air-water interface in air phase, m/s; u_{*w} = shear velocity at the air-water interface in water phase, m/s; ρ_a = density of air, 1.2 kg/m^3; and ρ_w = density of water, 998.2 kg/m^3. As the air-water interface is considered as a two-dimensional system, the magnitude of the shear velocity sum at the air-water interface, u_{*1}, is formulated from Eq.4.19 as:

$$u_{*1} = \sqrt{u_{*1,x}{}^2 + u_{*1,y}{}^2} \tag{4-21}$$

Substitution of Eq.4.18 and Eq.4.20 into Eq.4.21 yields:

$$u_{*1} = \sqrt{\left[\sqrt{\frac{\rho_a}{\rho_w}}\sqrt{\frac{C_{f1}}{2}}\left(W_x - U_x\right)\right]^2 + \left[\sqrt{\frac{\rho_a}{\rho_w}}\sqrt{\frac{C_{f1}}{2}}\left(W_y - U_y\right)\right]^2} \quad (4\text{-}22)$$

where C_{f1} = skin-friction coefficient at air-water interface; W_x = *x*-direction wind speed, m/s; W_y = *y*-direction wind speed, m/s; U_x = *x*-direction streamflow velocity, m/s; and U_y = *y*-direction streamflow velocity, m/s. In this study, wind speed is at the position of 10 m above the water surface. With Eq.4.18 and Eq.4.22 the gas-liquid transfer rate in Eq.4.16 can be formulated in terms of hydraulic parameters such as wind speed, free flow velocity, air density, water density, skin friction coefficients, etc.

4.2.1.4. Effective viscous layer

When wind blows over a water surface, a shear stress is exerted at the air-water interface which establishes a surface roughness. Thus, the roughness thickness is a function of the shear velocity. As Figure 4.2 shows, the curve of roughness thickness has three segments. From left to right, the roughness thickness decreases with shear velocity until point A; then it increases from point A to point B. When the roughness thickness is equal to the thickness of viscous layer, the roughness thickness will remain constant as the shear velocity increases, which is shown as the line after point B (O'Connor 1983).

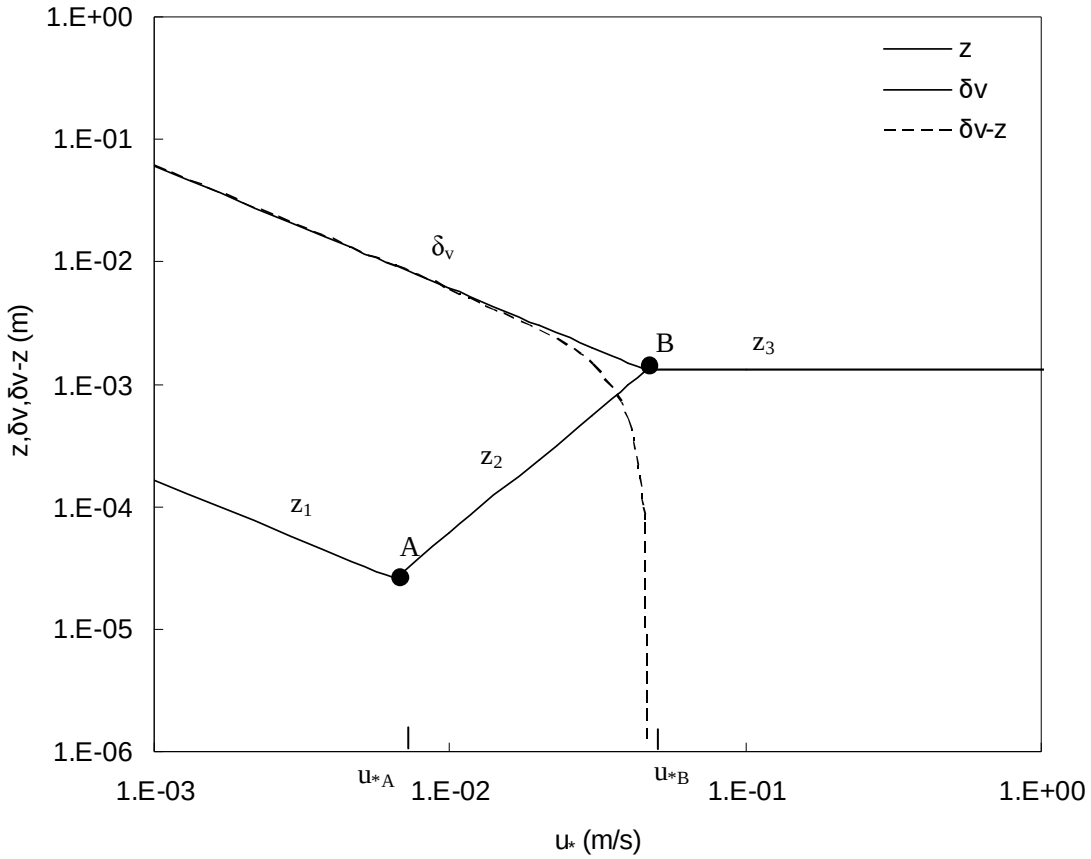

z = roughness thickness, m; δ_v = thickness of viscous layer in turbulent boundary layer, m; δ-z = effective thickness of viscous layer, m; and u_* = shear velocity, m/s

Figure 4.2. Effective thickness of viscous layer (δ-z) (modified from O'Connor 1983)

In the first segment which is from zero to point A, the roughness thickness is proportional to the ratio of kinetic viscosity over shear velocity (O'Connor 1983):

$$z_1 = \frac{1}{\lambda_l}\frac{\nu}{u_*} \tag{4-23}$$

where z_1 = roughness thickness in the first segment, m; and λ_1 = roughness coefficient. In the second segment which is from point A to point B, the roughness thickness is proportional to the square of the shear velocity (O'Connor 1983):

$$z_2 = \frac{\alpha u_*^2}{g} \tag{4-24}$$

where z_2 = roughness thickness in the second segment, m; α = roughness coefficient; and g = acceleration of gravity, 9.8 m/s^2. In the third segment which is after point B, the roughness thickness pierces the viscous layer completely and then remains constant:

$$z_3 = z_e \tag{4-25}$$

where z_3 = roughness thickness in the third segment, m; and z_e = roughness thickness when viscous layer is completely pierced, m. Because the roughness pierces into the viscous layer, the effective thickness of viscous layer is less than the viscous layer thickness and equals the viscous layer thickness minus the roughness thickness:

$$\delta_{ve} = \delta_v - z \tag{4-26}$$

where δ_{ve} = effective thickness of viscous layer in the turbulent boundary layer, m; and z = roughness thickness, m. This is displayed as the dashed line in Figure 4.2. The effective viscous layer thickness represents the actual distance where the gas encounters the viscosity resistance during the transfer process. Since the roughness thickness has three

segments, the effective viscous layer thickness also includes three segments as Table 4.1 shows.

Table 4.1. Effective viscous layer thickness in different ranges of shear velocity at the air-water interface

Ranges of shear velocity	Effective viscous layer thickness
$0 \le u_* \le u_{*A}$	$\delta_{ve} = \Gamma_0 \frac{\upsilon}{u_*} - \frac{1}{\lambda_l}\frac{\upsilon}{u_*}$
$u_{*A} \le u_* \le u_{*B}$	$\delta_{ve} = \Gamma_0 \frac{\upsilon}{u_*} - \frac{\alpha u_*^{\,2}}{g}$
$u_* \ge u_{*B}$	$\delta_{ve} = 0$

where u_{*A} = shear velocity at point A in Figure 4.2, m/s ; u_{*B} = shear velocity at point B in Figure 4.2, m/s.

In the first two segments, molecular diffusion in the viscous layer will be predominant since the effective viscous layer thickness is greater than zero. In the third segment, turbulent diffusion in the outer layer will be predominant since the viscous layer is pierced completely by the roughness.

At point A in Figure 4.2, the roughness thickness satisfies both Eq.4.23 and Eq.4.24:

$$z = \frac{1}{\lambda_l}\frac{\nu}{u_*} = \frac{\alpha u_*^{\,2}}{g} \tag{4-27}$$

Thus, the shear velocity at point A can be obtained from Eq.4.27 as:

$$u_{*A} = \left(\frac{g\nu}{\lambda_l \alpha} \right)^{\frac{1}{3}} \tag{4-28}$$

At point B in Figure 4.2, the roughness thickness satisfies both Eq.4.24 and Eq.4.5:

$$z = \frac{\alpha u_*^{\,2}}{g} = \Gamma \frac{\nu}{u_*} \tag{4-29}$$

Thus, the shear velocity at point B can be obtained from Eq.4.29 as:

$$u_{*B} = \left(\frac{\Gamma g \nu}{\alpha} \right)^{\frac{1}{3}} \tag{4-30}$$

Substitution Eq.4.30 in Eq.4.29 yields:

$$z_e = \left(\frac{\alpha}{g} \right)^{\frac{1}{3}} (\Gamma \nu)^{\frac{2}{3}} \tag{4-31}$$

4.2.1.5. Model of combined effects of wind and stream on gas-liquid transfer rate

Substitution Eq.4.15 into Eq.4.16 yields the wind-stream-driven gas-liquid transfer rate formulae as:

$$K_L = \sqrt{D \left[\frac{1}{D} \left(\frac{1}{\frac{1}{\frac{D}{\delta_{1ve}}} + \frac{1}{\sqrt{Dr_1}}} \right)^2 + r_2 \right]} \tag{4-32}$$

where δ_{1ve} = effective thickness of viscous layer in turbulent boundary layer at the air-water interface, m. In Eq.4.32 the effective viscous layer thickness has three segments correlating to the three segments of the roughness thickness formulae:

$$\delta_{1ve} = \Gamma \frac{\nu}{u_{*1}} - \frac{1}{\lambda_l} \frac{\nu}{u_{*1}} \qquad 0 \le u_{*1} \le \left(\frac{g\nu}{\lambda_l \alpha} \right)^{\frac{1}{3}} \tag{4-33}$$

$$\delta_{1ve} = \Gamma \frac{\nu}{u_{*1}} - \frac{\alpha u_{*1}^{\ 2}}{g} \qquad \left(\frac{g\nu}{\lambda_l \alpha} \right)^{\frac{1}{3}} \le u_{*1} \le \left(\frac{\Gamma g \nu}{\alpha} \right)^{\frac{1}{3}} \tag{4-34}$$

$$\delta_{1ve} = 0 \qquad u_{*1} \ge \left(\frac{\Gamma g \nu}{\alpha} \right)^{\frac{1}{3}} \tag{4-35}$$

where δ_{1ve} = effective thickness of viscous layer in turbulent boundary layer at the air-water interface, m; Γ = equivalent coefficient of viscous layer thickness; ν = kinematic viscosity, m^2/s; u_{*1} = shear velocity at the air-water interface, m/s; λ_l = roughness coefficient; g = acceleration of gravity, m/s^2; and α = roughness coefficient.

In Eq.4.33 r_1 is recalled from Eq.4.11:

$$r_1 = \frac{u_{*1}^{\ 2}}{121.5\nu} \tag{4-36}$$

r_2 is recalled from Eq.3.5:

$$r_2 = \frac{U}{H} \tag{4-37}$$

where r_1 = surface renewal rate at the air-water interface, s^{-1}; r_2 = surface renewal rate at the water-bed interface, s^{-1}; u_{*1} = shear velocity at air-water interface, m/s; ν = kinematic viscosity, m^2/s; U = flow velocity, m/s; and H = water depth, m.

In Eq.4.35 u_{*1} is the shear velocity which are caused by wind and stream at the air-water interface. The formula of u_{*1} is recalled from Eq.4.22 as:

$$u_{*1} = \sqrt{\left(\sqrt{\frac{\rho_a}{\rho_w}}\sqrt{\frac{C_{f1}}{2}}W_x - \sqrt{\frac{C_{f1}}{2}}U_x\right)^2 + \left(\sqrt{\frac{\rho_a}{\rho_w}}\sqrt{\frac{C_{f1}}{2}}W_y - \sqrt{\frac{C_{f1}}{2}}U_y\right)^2} \tag{4-38}$$

where u_{*1} = shear velocity at air-water interface, m/s; C_{f1} = skin-friction coefficient at air-water interface; ρ_a = density of air, kg/m^3; ρ_w = density of water, kg/m^3; W_x = wind speed at x direction, m/s; W_y = wind speed at x direction, m/s; U_x = streamflow velocity at x direction, m/s; and U_y = streamflow velocity at y direction, m/s. The wind-stream-driven gas-liquid transfer rate formulae are composed of Eq.4.32-4.38. The

model formulated as Eq.4.32-4.38 is named as “Wind-stream-driven KL Model” in this study.

4.2.2. Model testing

The gas-liquid transfer rate model developed in section 4.2.1 incorporates the combined effects of wind and streamflow. Thus, this model can be applied to stream-driven systems, wind-driven systems, and wind-stream-driven systems. For the former two kinds of systems, considerable formulae and experimental data sets have been developed or obtained. Thus, they can be used to test the model established in section 4.2.1. Then this model will be applied for the wind-stream-driven systems while only a few experimental data for the combined effects of wind and streamflow are available.

In order to test the model, it is applied in the stream-driven systems by setting the wind speed to be zero, in the wind-driven systems by setting the stream velocity to be zero, and in the wind-stream-driven systems by letting both the wind speed and stream velocity to be greater than zero. The predictions and the observations are displayed in Figures 4.3-4.6.

The predicted stream-driven gas-liquid transfer rates with this model and the observed data in the rivers are displayed in Figure 4.3. The wind speed was set to be zero when the wind-stream-driven gas-liquid transfer rate formulae were applied in the stream-driven systems. The observations in Figure 4.3 were from the experiments

conducted to measure the reaeration rates and flow velocities in several rivers (O'Connor and Dobbins 1956). Figure 4.3 shows that this model has reasonable predictions compared with these observations in the stream-driven systems.

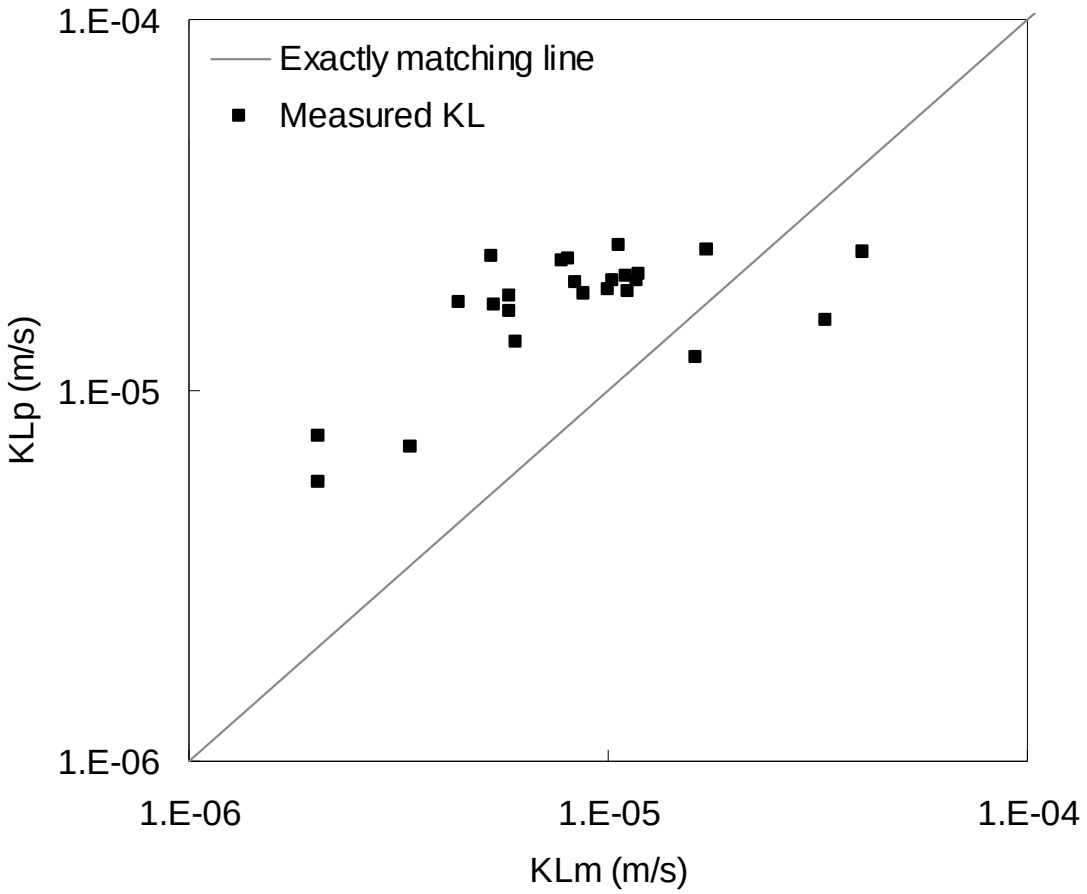

Figure 4.3. Comparison of the calculations and the observations of stream-driven gas-liquid transfer rate from O'Connor and Dobbins (1956)

The predicted wind-driven gas-liquid transfer rates with this model and observations are displayed in Figure 4.4 and Figure 4.5. The flow velocity was set to be zero when the wind-stream-driven gas-liquid transfer rate formulae were applied in the wind-driven

systems. The observed data in Figure 4.4 and Figure 4.5 were from the experiments conducted to measure the reaeration rates and wind speeds in wind-driven systems (Broecker et al. 1978; Jahne et al. 1979). Both Figure 4.4 and Figure 4.5 show that this model has reasonable predictions compared with the observations in the wind-driven systems. A specific value of Γ_0 in this model formed a prediction curve to tally with a specific data set, which will be discussed in details in section 4.3.

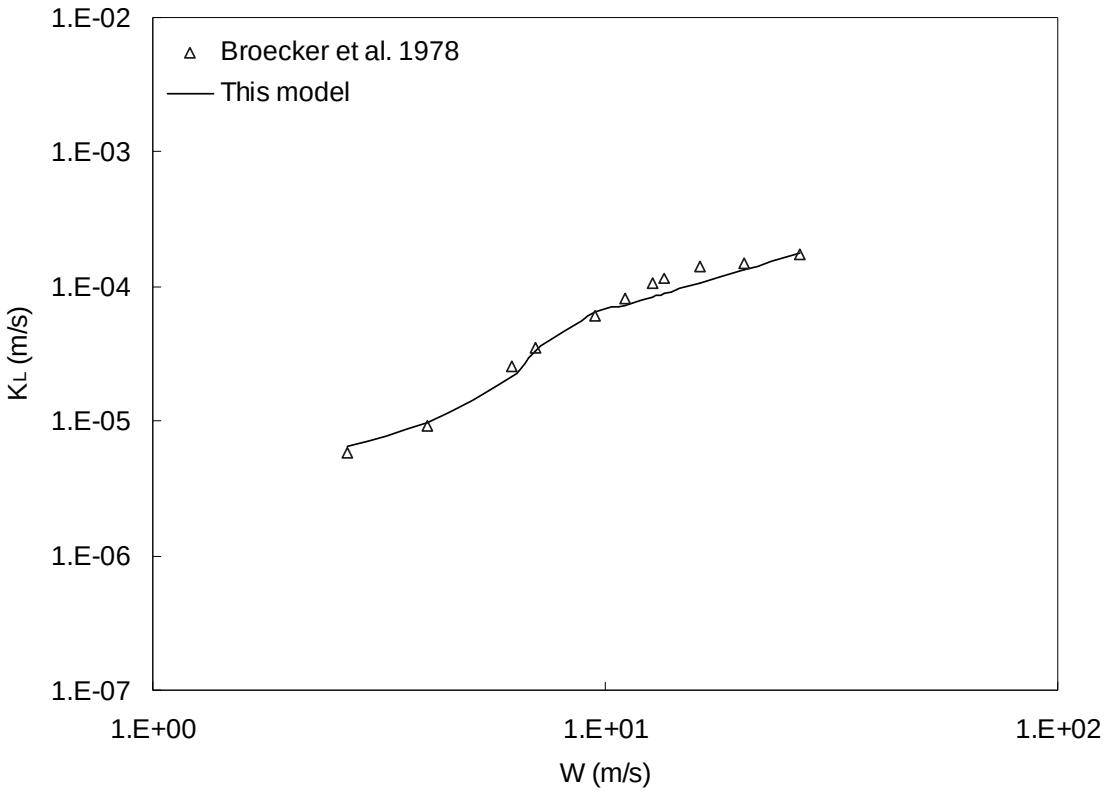

Figure 4.4. Comparison of the calculations and the observations of wind-driven gas-liquid transfer rate obtained by Broecker et al. (1978)

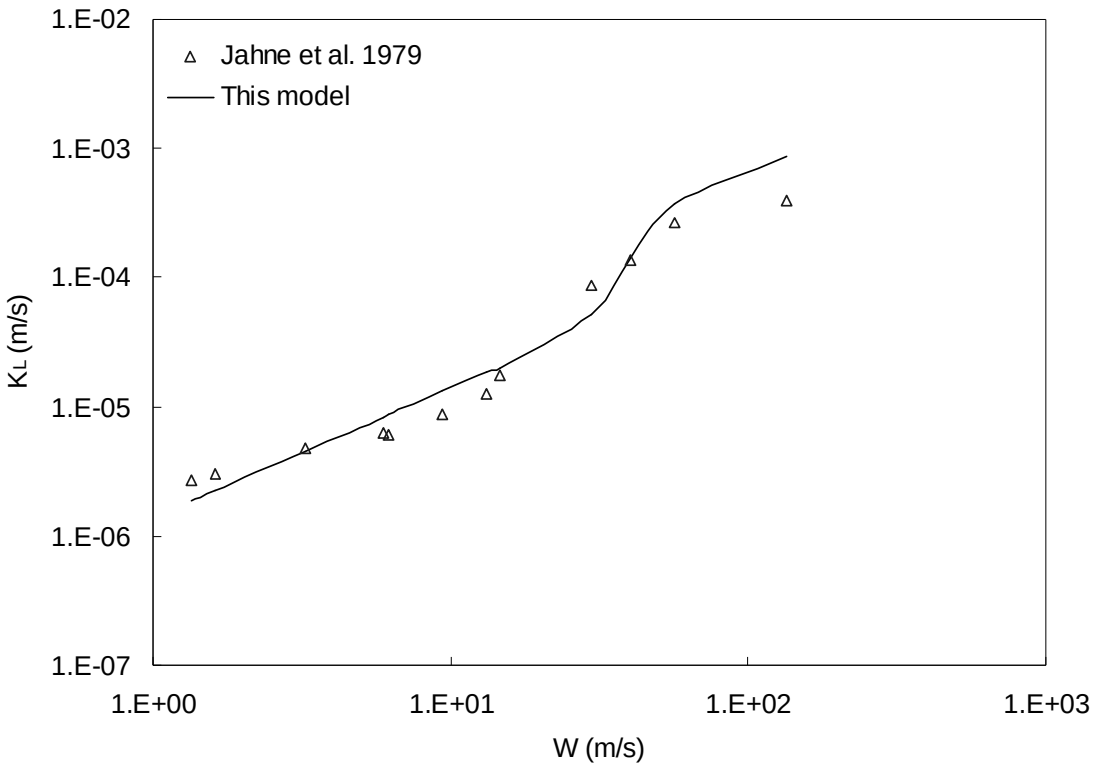

Figure 4.5. Comparison of the calculations and the observations of stream-driven gas-liquid transfer rate obtained by Jahne et al. (1979)

A few experiments have been conducted to measure the wind speeds, the stream velocities, and the gas-liquid transfer rates in the wind-stream-driven systems (Chu and Jirka 1995, 2003). The results of five cases in these experiments were used to test the model developed in this study. Case 3 is a countercurrent case, namely the wind speed is opposite to the flow velocity in this case; case 1, 2, 4 and 5 are cocurrent cases, namely the direction of wind speed is the same as that of flow velocity in these cases. The value of 0.03 for the coefficient of Cr is obtained by adjusting the predictions of case 1 to tally the measured values in case 1. Then, Cr = 0.03 is applied for cases 2-5. As Figure 4.6

shows, the predictions made by this model (computed KLp) tallied well with the measured values (KLm) of the above experiments for each case.

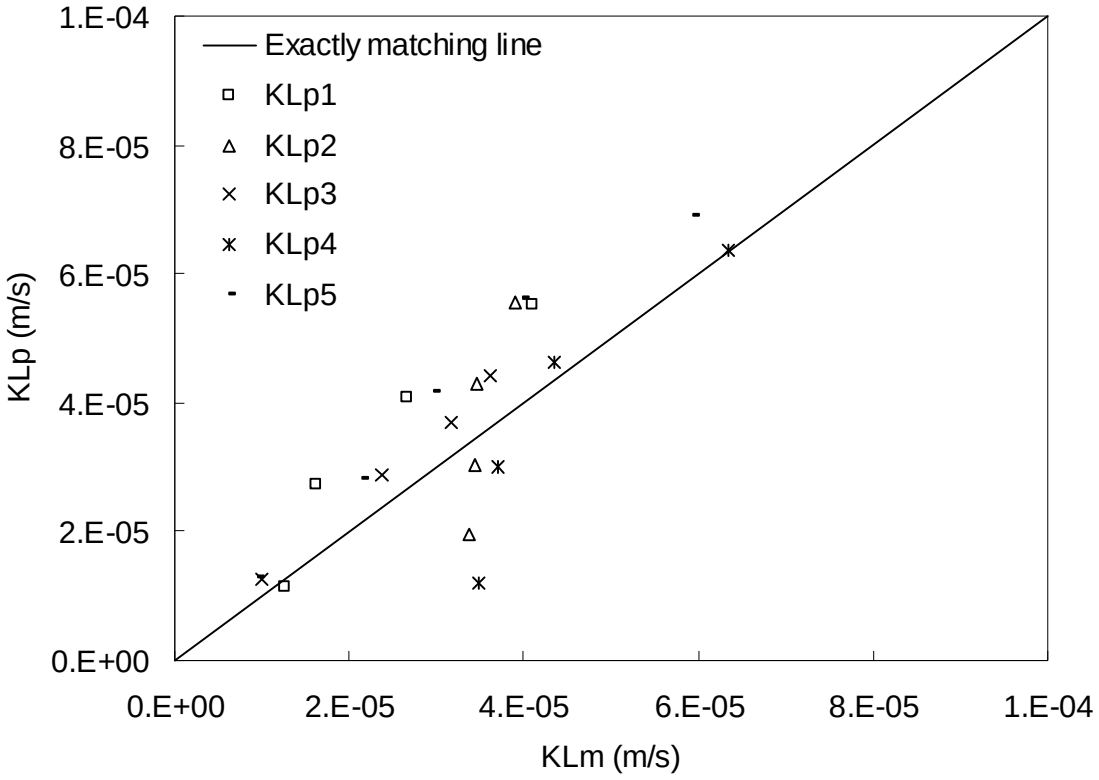

Notes: KLp1, KLp2, KLp3, KLp4, and KLp5 are five groups of predicted gas-liquid transfer rates in wind-stream-driven systems with the model developed in this research

Figure 4.6. Comparison of the calculations and the observations of wind-stream-driven gas-liquid transfer rate from Chu and Jirka (1995, 2003)

The above comparisons of predictions with this model and the observations from the experiments showed that this model has reasonable predictions on the gas-liquid transfer rate.

4.2.3. Conclusions

In this study, a model named as Wind-stream-driven KL Model and its related formulae were developed to describe the gas-liquid transfer rate from air to water bulk under the combined effects of wind and stream. This model was developed based on Two Film Theory and Surface Renewal Theory. The concept of turbulent boundary layer structure, vector sum of shear velocities, effective viscous layer thickness, and sequential resistance exerted by the turbulent boundary layer play important roles in the development of this model. This model correlates the gas-liquid transfer rate with the hydrodynamic parameters like wind speed, stream velocity, water depth, air density, water density, water viscosity, etc. The gas-liquid transfer rates predicted with this model show reasonable agreement with the observations when applied to stream-driven systems, wind-driven systems, and wind-stream-driven systems. This model considered the combined effects on gas-liquid transfer rate from both wind and stream processes. Thus, it can be applied for one-dimensional streams with or without wind blowing over the stream flows, one-dimensional estuaries with or without wind blowing over the estuaries, and static lakes with wind blowing over the water surface.

4.3. Formulations for Wind-driven Gas-liquid Transfer Rate

4.3.1. Wind-driven gas-liquid transfer rate model

A wind-stream-driven gas-liquid transfer rate model has been developed in section 4.2. It will be reduced to a wind-driven gas-liquid transfer rate model in this section. Considerable empirical formulae have been established for the wind-driven gas-liquid transfer rate. Some of them such as Broecker's and Jahne's formulae discussed in section 4.2 were developed based on experiments conducted in laboratories, while some of them were developed based on experiments conducted in oceans. For the high wind speed segments of these empirical formulae, wave breaking or bubble-mediated gas-liquid transfer may occur, which causes much more increase of the total gas-liquid transfer rate than the pure wind-driven gas-liquid transfer. Thus, the predictions of the empirical formulae in the high wind speed segments are greater than those of the pure wind-driven gas-liquid transfer rate model. In order to test this, a theoretical wind-driven gas-liquid transfer rate model needs to be established.

The formula of wind-streamflow-driven gas-liquid transfer rate (Eq.4.32-4.38) represented the combined effects of wind and stream on gas-liquid transfer rate. By setting the flow velocity to equal zero, a formula of wind-driven gas-liquid transfer rate can be obtained. When the flow velocity equals zero, r_2 equals zero, and U_x and U_y equal

zero respectively. Then, a formula of wind-driven gas-liquid transfer rate can be derived as:

(4-39)

when $0 \le u_{*1} \le \left(\frac{g\upsilon}{\lambda_l \alpha}\right)^{\frac{1}{3}}$,

$$K_L = \frac{1}{\frac{\left(\Gamma - \frac{1}{\lambda_l}\right)\nu}{D\sqrt{\frac{\rho_a}{\rho_w}\frac{C_{f1}}{2}}} + \sqrt{\frac{121.5\nu}{D\frac{\rho_a}{\rho_w}\frac{C_{f1}}{2}}}} W = C_1 W$$

when $\left(\frac{g\upsilon}{\lambda_l \alpha}\right)^{\frac{1}{3}} \le u_{*1} \le \left(\frac{\Gamma g\upsilon}{\alpha}\right)^{\frac{1}{3}}$,

$$K_L = \frac{1}{\left(\frac{\Gamma\nu}{D\sqrt{\frac{\rho_a}{\rho_w}\frac{C_{f1}}{2}}} + \sqrt{\frac{121.5\nu}{D\frac{\rho_a}{\rho_w}\frac{C_{f1}}{2}}}\right) W^{-1} - \frac{\alpha\frac{\rho_a}{\rho_w}\frac{C_{f1}}{2}}{Dg} W^2} = \frac{1}{C_{21}W^{-1} + C_{22}W^2}$$

when $u_{*1} \ge \left(\frac{\Gamma g\upsilon}{\alpha}\right)^{\frac{1}{3}}$,

$$K_L = \sqrt{D\frac{\rho_a}{\rho_w}\frac{C_{f1}}{2}}W = C_3 W$$

where C_1 = coefficient of wind-driven gas-liquid transfer rate in segment 1; C_{21}, C_{22} = coefficient of wind-driven gas-liquid transfer rate in segment 2; and C_3 = coefficient of wind-driven gas-liquid transfer rate in segment 3. The wind-driven gas-liquid transfer rate formula is reasonable as a specific case of the wind-stream-driven gas-liquid transfer rate formula which has been successfully tested.

4.3.2. Model applications

In section 4.2, when the wind-stream-driven gas-liquid transfer rate model is applied to a specific wind-driven system, the equivalent thickness coefficient of the overlap layer Γ introduced in Eq.4.10 needs to be adjusted to tally the predictions of this model with the experimental data set in the specific wind-driven system. However, it is difficult to determine this coefficient theoretically as it is determined by the specific conditions of experiments or applications. The equivalent thickness coefficient of the overlap layer needs to be adjusted when this wind-driven gas-liquid transfer rate formula was applied for specific sets of experimental data or empirical formulae.

Broecker et al. (1978) measured the carbon dioxide exchange rate in a large wind wave tunnel with 18 m length, 1 m width and 0.5 m water depth. The wind was generated

by a fan with the speed up to 26 m/s. The referenced gas-liquid transfer rates were up to 2.2×10^{-4} m/s. As Figure 4.4 showed, agreements between the general model and the Broecker's experimental data were obtained when $\alpha = 6$ and $\Gamma = 1$.

Jahne et al. (1979) did an experiment on wind-driven gas-liquid transfer rate in a wind tunnel with 0.1 m depth and 0.1 m width. As Figure 4.5 showed, agreements between the general model and the Jahne's experimental data were obtained when $\alpha = 0.06$ and $\Gamma = 2$.

Each empirical formula on wind-driven gas-liquid transfer rate was established from a specific set of experimental data. As the experiments were conducted under specific experimental conditions, the obtained empirical formulae have limited application ranges. The wind-driven gas-liquid transfer rate formula obtained in this study is a theoretical formula and thus has general application ranges. Figures 4.4-4.5 show that gas-liquid transfer rate has different values under the same wind speed for different wind-driven systems. It is postulated that the value of Γ is determined by specific conditions of the wind-driven systems. Agreements between the general model and the empirical formulae were obtained by adjusting the value of Γ. Furthermore, the predictions of the general formula developed in this study can be compared with the existing empirical formulae to check their application ranges.

Liss and Merlivat (1986) established an empirical formula on wind-driven gas-liquid transfer rate stated in three segments as:

$$K_L = 0.17W \quad (\text{W} < 3.6 \text{ m/s})$$

$$K_L = 2.85W - 9.65 \quad (3.6 \text{ m/s} < \text{W} < 13 \text{ m/s}) \qquad (4\text{-}40)$$

$$K_L = 5.9W - 49.3 \quad (\text{W} > 13 \text{ m/s})$$

Comparison between the general model and the Liss-Merlivat formula (1986) was obtained for wind speeds from 1 to 8 m/s when $\Gamma = 16$. As Figure 4.7 shows, for wind speed less than 8 m/s, reasonable agreements were obtained between this model and Liss-Merlivat formula; while for wind speeds greater than 8 m/s, the Liss-Merlivat formula predicted greater values than the model developed in this study.

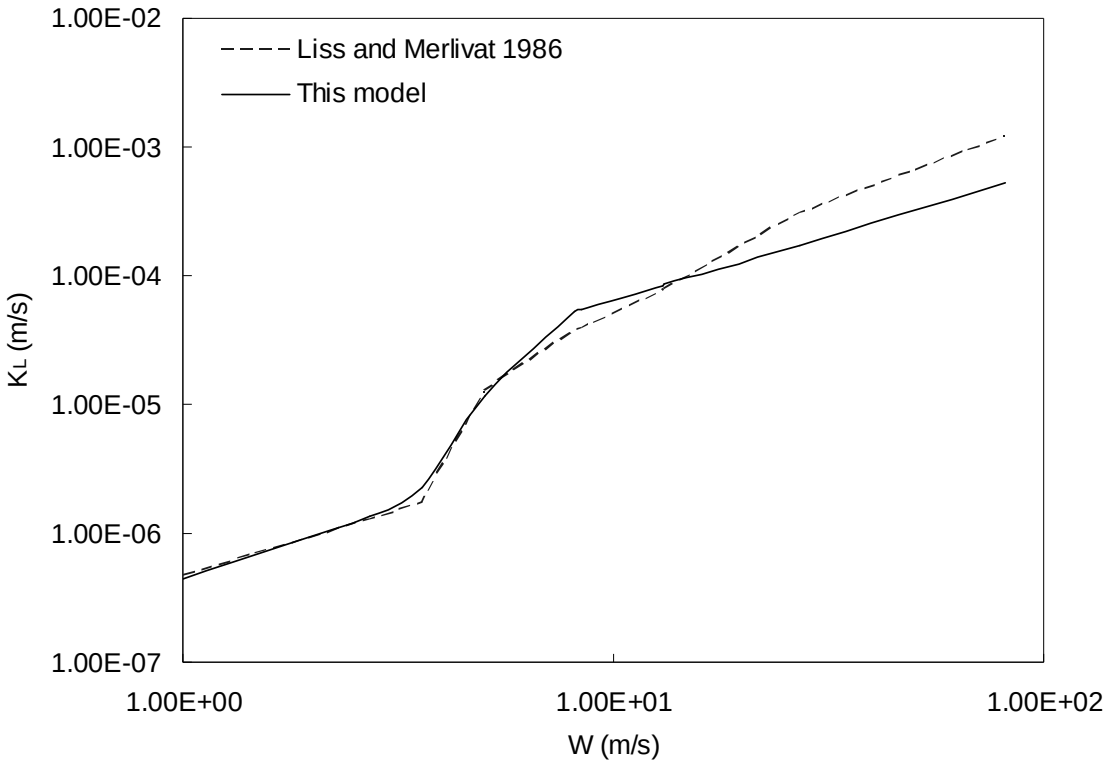

Figure 4.7. Comparison between this model and the Liss-Merlivat empirical formula when $\alpha = 125$ and $\Gamma = 7$ (W = wind speed; and K_L = gas-liquid transfer rate)

A cubic relationship between wind-driven gas-liquid transfer rate and wind speed was developed by Wanninkhof and McGillis (1999):

$$K_L = 1.09W - 0.333W^2 + 0.078W^3 \quad (4\text{-}41)$$

Comparison between the general model and the Wanninkhof-McGillis formula (1999) was obtained for wind speeds from 1 to 8 m/s when $\Gamma = 4$. Similar to Figure 4.7, Figure 4.8 shows that for wind speed less than 8 m/s, reasonable agreements were obtained between this model and Wanninkhof-McGillis formula, while for wind speeds greater than 8 m/s, the Wanninkhof-McGillis formula predicted greater values than the model developed in this study.

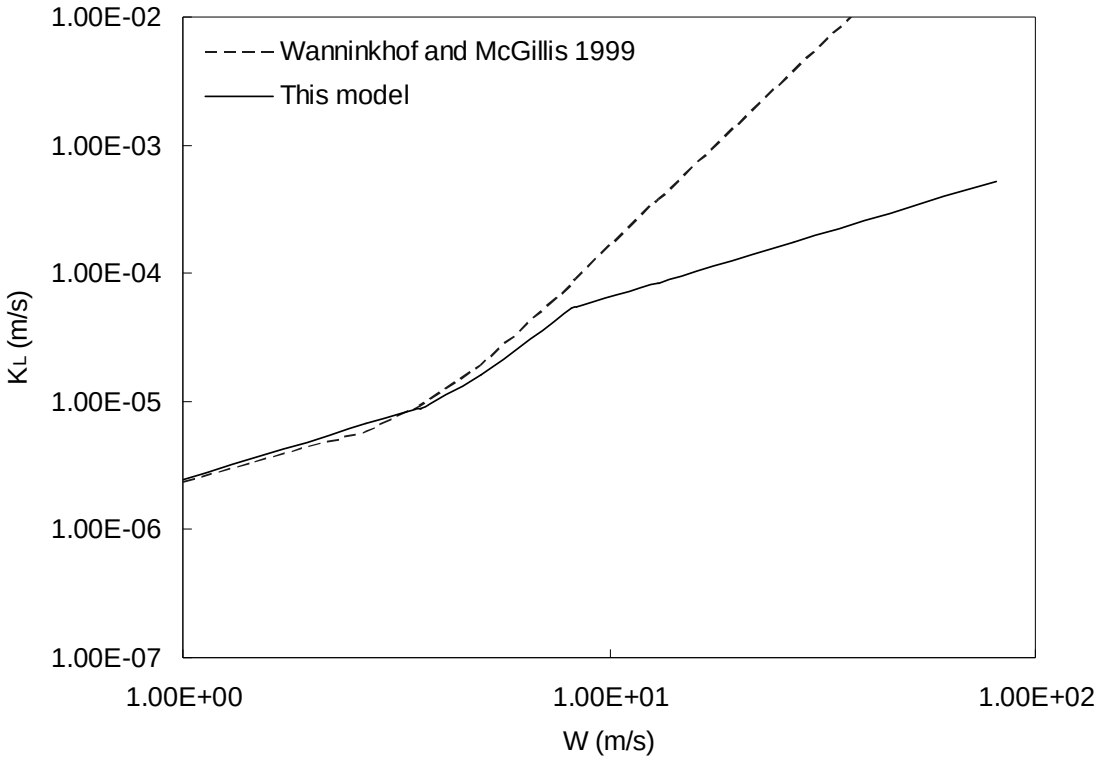

Figure 4.8. Comparison between this model and the Wanninkhof-McGillis empirical formula when $\alpha = 10$ and $\Gamma = 1$. (W = wind speed; and K_L = gas-liquid transfer rate)

In Figure 4.4 and Figure 4.5, all of the three segments of the formula developed in this study had reasonable agreements with the experimental data sets. However, in Figure 4.7 and Figure 4.8, only the first two segments of the formula had reasonable agreements with the empirical formulae while the third segment had lower predictions than the empirical formulae. Broecker's and Jahne's experiments were conducted at the laboratory scale, while Wanninkhof-McGillis formula was obtained from the experiments conducted in oceans. Thus, other factors like wave breaking or bubble-mediated gas-liquid transfer

in oceans could have important effects when wind speed is large enough, which would increase the gas-liquid transfer rate.

For the coefficient of equivalent thickness of the viscous layer in Eq.4.10 Gulliver and Stefan (1984) suggested a value of 10 based on some flume experiments. In this study multiple values ranging from 1 to 7 were selected to adjust this coefficient (Γ) and multiple values ranging from 0.06 to 125 were selected to adjust α in the formula of wind-driven gas-liquid transfer rate (Eq.4.32-4.38) to match the experimental data and empirical formulae.

The experimental conditions can be divided into three categories: laboratory scale, intermediate scale and field scale (O'Connor 1983). Normally the depths of the wind tunnels used for laboratory scale range from 0.1 m to 0.5 m (Broecker et al. 1978). The water depths in field scale are normally greater than those in laboratory scale, e.g. many experiments on carbon dioxide exchange rate were conducted in oceans. Table 4.2 showed the roughness coefficients in field scale were greater than those in laboratory scale; but it was not certain if this is a general situation. More empirical formulae with known experimental conditions need to be explored.

Table 4.2. Comparison of coefficients of equivalent thickness of overlap layer

Empirical formulae or experimental data sets	Scale	Roughness coefficient, α	Equivalent coefficient of viscous layer thickness, Γ	References
Wanninkhof-McGillis formulae	field scale	10	1	Wanninkhof and McGillis 1986
Broecker's experimental data	laboratory scale	6	1	Broecker et al. 1978
Jahne's experimental data	laboratory scale	0.06	2	Jahne et al. 1979

4.3.3. Conclusions

A theoretical formula of wind-driven gas-liquid transfer rate was derived from the formula of wind-stream-driven gas-liquid transfer rate developed in section 4.2. The formula was adjusted to match existing experimental data sets and empirical formulae by specifying the equivalent thickness coefficient of viscous layer Γ and roughness coefficient α in Eq.4.32-4.38. Agreements between the general model and the Liss-Merlivat formula were obtained for wind speed from 1 to 8 m/s when $\alpha = 125$ and $\Gamma = 7$; while for similar wind speeds, agreements with Wanninkhof's formulae were obtained when $\alpha = 10$ and $\Gamma = 1$. Some other values of Γ and α were obtained by applying this general formula on other sets of experimental data. It was found that the empirical formulae had greater predictions than the third segments of the model

developed in this study. Thus, other factors like wave breaking or bubble-mediated gas-liquid transfer in oceans could speed the gas-liquid transfer rate in field conditions. Comparisons showed that the roughness coefficients in field scale were greater than those in laboratory scale; but it would not be certain if this was a general conclusion until more empirical formulae and experimental data sets were explored.

CHAPTER V

SURFACE RENEWAL RATES FROM THREE TYPES OF TURBULENCE SOURCE LOCATIONS IN WATER BODIES

5.1. Introduction

As discussed in section 3.2.1, according to the Surface Renewal Theory, the gas-liquid transfer rate is determined by the surface renewal rate and molecular diffusion coefficient.

$$K_L = \sqrt{Dr} \tag{5-1}$$

In the natural water bodies, the air-water interface, the water-bed interface and the transition location of shear flows are three types of locations where the surface renewal rate is caused by the friction.

In the gas-liquid transfer rate formulae for uniform one-dimensional flow such as O'Connor and Dobbins formula (1956), the surface renewal rate caused by turbulence generated from the water-bed interface was considered to be predominant in determining the gas-liquid transfer rate at the air-water interface. When wind blows over water and water flow is negligible, turbulence is generated from the air-water interface.

Considerable empirical relationships have been established for the wind-driven gas-liquid transfer rate (Broecker 1978; Jahne 1979; Liss and Merlivat 1986; Wanninkhof 1992; Wanninkhof and McGillis 1999). A theoretical model on wind reaeration rate has been developed (O'Connor 1983), in which the surface renewal rate caused by the turbulence generated from the air-water interface is considered to determine the gas-liquid transfer rate in the wind-driven system. Apart from friction at the air-water interface and the water-bed interface, in complex flow fields the friction at the transition location of shear flows is another source of the surface renewal movement of the water parcels which brings the dissolved oxygen from air to water bulk. Thus, a formula of gas-liquid transfer rate caused by the turbulence at a transition location of shear flows needs to be developed.

5.2. Formulae development

5.2.1. Gas-liquid transfer rate caused by turbulence generated from transition location of shear flows

Shear flows often exist in non-uniform flows like stratified flows and complex three-dimensional flows. The friction at the transition location of shear flows in complex flow fields is the driving source of turbulence which causes the surface renewal movement of water parcels to bring the dissolved oxygen from air to water bulk.

The flow velocity profile in free shear flows was proposed by Gortler (1942) as:

$$\bar{u}(y) = U_1 + (U_2 - U_1)\frac{1}{2}\left[1 + erf\left(\frac{\sigma y}{x}\right)\right] \tag{5-2}$$

Where $\bar{u}$ = flow velocity in shear layers, m/s; σ = 13.5; y = distance from the interface, m; x = streamwise coordinate tangential to the moving interface, m; U_1 = flow velocity in upper flow layer, m/s; and U_2 = flow velocity in lower flow layer, m/s. The symbol of "erf" is an abbreviation for the error function which is defined as:

$$erf(z) = \int \frac{2}{\sqrt{\pi}} e^{-z^2} dz \tag{5-3}$$

where z = argument of the error function. After substituting Eq.5.3 into Eq.5.2, differentiation of the left side and the right side of Eq.5.2 yields:

$$\frac{d\bar{u}}{dy} = (U_2 - U_1)\frac{1}{\sqrt{\pi}}\frac{\sigma}{x} e^{-\left(\frac{\sigma y}{x}\right)^2} \tag{5-4}$$

The maximum of the derivative, $\frac{d\bar{u}}{dy}$, can be obtained by letting y equal zero in Eq.5.4:

$$\left(\frac{d\bar{u}}{dy}\right)_{\max} = \frac{(U_2 - U_1)\sigma}{\sqrt{\pi} x} \tag{5-5}$$

Eq.5.5 is used to formulate the shear stress.

Turbulent viscosity is a function of the flow velocity in the upper layer and the flow velocity in the lower layer (White 2006):

$$\nu_T = K U_{\max}(U_1, U_2) b \tag{5-6}$$

where ν_T = turbulent viscosity, m^2/s; K = 0.016; $U_{max}(U_i,U_{i-1})$ = maximum of U_i and U_{i-1} (White 2006); and b = the shear layer spreading rate and is given as:

$$b(x) = 0.121x \tag{5-7}$$

Eq.5.6 and Eq.5.7 are also used to formulate the shear stress.

Shear stress is proportional to the flow velocity gradient. In turbulent flow, the coefficient is the turbulent viscosity (White 2006):

$$\tau = \nu_T \left(\frac{d\bar{u}}{dy} \right)_{\max} \tag{5-8}$$

where τ = shear stress, N/m^2. Substitution of Eq.5.5, Eq.5.6 and Eq.5.7 into Eq.5.8 yields:

$$\tau = \frac{0.121}{\sqrt{\pi}} \sigma K U_{\max} (U_1, U_2)(U_2 - U_1) \tag{5-9}$$

Shear velocity is defined by (Munson 1994):

$$u_* = \sqrt{\frac{\tau}{\rho}} \tag{5-10}$$

where u_* = shear velocity, m/s; ρ = phase density, kg/m^3. Substitution of Eq.5.9 into Eq.5.10 yields:

$$u_* = \sqrt{\frac{0.121 \sigma K |U_2 - U_1| U_{\max} (U_1, U_2)}{\sqrt{\pi} \rho}} \tag{5-11}$$

As discussed in section 3.2.1, the surface renewal rate (r) is the function of the mixing length (l) and the vertical fluctuation velocity ($|\bar{v}|$) as:

$$r = \frac{|\bar{v}|}{l} \tag{5-12}$$

The vertical fluctuation velocity decreases across the space from the friction interface to the isotropic turbulent flow bulk. At the friction interface where the turbulence is

generated, the vertical fluctuation velocity has a maximum and is assumed to be equal to shear velocity:

$$\left|\overline{v}\right| = u_{*i} \tag{5-13}$$

where u_{*i} = shear velocity at friction interface, m/s. Though the fluctuating velocity scale in the bulk isotropic turbulent flow is in fact the same order of magnitude as that at the interface, the shear velocity is considered to be approximate zero in the bulk isotropic turbulent flow for convenience:

$$\left|\overline{v}\right| = u_{*b} \approx 0 \tag{5-14}$$

where u_{*b} = shear velocity in isotropic bulk flow far away from friction interface, m/s. In order to simplify the formula, the arithmetic average of u_{*i} and u_{*b} will be considered as the equivalent vertical fluctuation velocity used in the calculation of the gas-liquid transfer rate:

$$\left|\overline{v}\right| = \frac{u_{*i} + u_{*b}}{2} \tag{5-15}$$

A more general expression from Eq.5.15 is as:

$$\left|\overline{v}\right| = C_{sv} u_{*} \tag{5-16}$$

where C_{sv} = coeffcient of equivalent vertical fluctuation velocity.

For the isotropic turbulent flows, an empirical relationship between the mixing length and the water depth is as (Hamada 1953; Kalinske 1943; Schijf and Schonfeld 1953):

$$l = 0.1H \tag{5-17}$$

where H is the water depth.

Substitution of Eq.5.15 and Eq.5.17 in Eq.5.12 yields:

$$r = \frac{\frac{u_{*i} + u_{*b}}{2}}{0.1H} = \frac{5}{H}\left(u_{*i} + u_{*b}\right) \tag{5-18}$$

where u_{*i} = shear velocity at the two-phase interface, m/s, and thus can be replaced with Eq.5.11 and u_{*b} can be replaced with Eq.5.14. Then, the surface renewal rate r is:

$$r = \frac{5}{H}\sqrt{\frac{0.121\sigma K\left|U_2 - U_1\right|U_{\max}\left(U_1, U_2\right)}{\sqrt{\pi}\rho}} \tag{5-19}$$

The gas-liquid transfer rate caused by the surface renewal movement of water parcels driven by the turbulence from the transition location of shear flows is as Eq.5.20 by substituting Eq.5.19 into Eq.5.1:

$$K_L = \sqrt{\frac{5D}{H}\sqrt{\frac{0.121\sigma K\left|U_2 - U_1\right|U_{\max}\left(U_1, U_2\right)}{\sqrt{\pi}\rho}}} \tag{5-20}$$

where K_L = gas-liquid transfer rate, m/s; D = diffusion coefficient, m^2/s; H = water depth, m; K = 0.016; σ = 13.5;

ρ = density, kg/m^3; U_1 = flow velocity in upper layer, m/s; U_2 = flow velocity in lower layer, m/s; and U_{max} = maximum of U_1 and U_2, m/s.

5.2.2. Gas-liquid transfer rate caused by turbulence generated from water-bed interface

Based on the definition of the skin friction coefficient C_f, the shear stress is as (Munson 1994):

$$\tau = \rho \frac{C_f}{2} U^2 \tag{5-21}$$

where τ = shear stress, N/m^2; C_f = skin friction coefficient; and U = free flow velocity, m/s. The shear velocity is defined as (Munson 1994):

$$u_* = \sqrt{\frac{\tau}{\rho}} \tag{5-22}$$

Substitution of Eq.5.21 into Eq.5.22 yields the shear velocity as a function of free flow velocity:

$$u_* = \sqrt{\frac{C_f}{2}} U \tag{5-23}$$

Similar to the formula development of gas-liquid transfer rate caused by turbulence generated from transition location of shear flows, the equivalent vertical fluctuation velocity in Eq.5. 15 and the empirical relationship on mixing length in Eq.5.17 were used for the formula development of gas-liquid transfer rate caused by turbulence generated from water-bed interface. Substitution of Eq.5.16, Eq.5.17 and Eq.5.23 in Eq.5.12 yields:

$$r = \frac{C_{sv} \sqrt{\frac{C_f}{2}} U}{0.1H} \tag{5-24}$$

Substitution of Eq.5.24 into Eq.5.1 yields:

$$K_L = \sqrt{\frac{C_{sv} \sqrt{\frac{C_f}{2}} DU}{0.1H}} = A \frac{U^{\frac{1}{2}}}{H^{\frac{1}{2}}} \tag{5-25}$$

where K_L = gas-liquid transfer rate, m/s; D = diffusion coefficient, m^2/s; U = free flow velocity, m/s; H = water depth, m; A = coefficient of gas-liquid transfer rate; C_{sv} =

coeffcient of equivalent vertical fluctuation velocity; and C_f = skin friction coefficient. Eq.5.26 is the formula of gas-liquid transfer rate caused by the surface renewal movement of water parcels driven by the turbulence from water-bed interface. It has the same form as the formula of riverine reaeration rate developed by O'Connor and Dobbins in 1956.

5.2.3. Gas-liquid transfer rate caused by turbulence generated from air-water interface

A formula of shear velocity at the air-water interface was developed in Chapter 4:

$$u_{*1} = \sqrt{\left[\sqrt{\frac{\rho_a}{\rho_w}}\sqrt{\frac{C_{f1}}{2}}\left(W_x - U_x\right)\right]^2 + \left[\sqrt{\frac{\rho_a}{\rho_w}}\sqrt{\frac{C_{f1}}{2}}\left(W_y - U_y\right)\right]^2} \quad (5\text{-}26)$$

where u_{*1} = shear velocity at air-water interface, m/s; ρ_a = air density, kg/m^3; ρ_w = water density, kg/m^3; C_{f1} = skin-friction coefficient at air-water interface; U_x = streamflow velocity at x direction, m/s; U_y = streamflow velocity at y direction, m/s; W_x = wind speed at x direction, m/s; and W_y = wind speed at y direction, m/s. This formula incorporated the combined effects of wind speed and flow velocity on the shear velocity at the air-water interface. When wind speed is uniform one-dimensional and water flow is at rest, Eq.5.26 can be simplified as:

$$u_{*1} = \sqrt{\frac{C_{f1}\rho_a W^2}{2\rho_w}} \quad (5\text{-}27)$$

where W = uniform one-dimensional wind speed, m/s. Substitution of Eq.5.17 and Eq.5.27 into Eq.5.12 yields:

$$r = \frac{5}{H}\sqrt{\frac{C_{f1}\rho_a W^2}{2\rho_w}} \tag{5-28}$$

Substitution of Eq.5.28 into Eq.5.1 yields:

$$K_L = \sqrt{\frac{5D}{H}\sqrt{\frac{C_{f1}\rho_a W^2}{2\rho_w}}} \tag{5-29}$$

where K_L = gas-liquid transfer rate, m/s; D = diffusion coefficient, m^2/s; W = wind speed, m/s; H = water depth, m; ρ_a = density of air, kg/m^3; ρ_w = density of water, kg/m^3; and C_{f1} = skin-friction coefficient at air-water interface. Eq.5.29 is the formula of gas-liquid transfer rate caused by the surface renewal movement of water parcels driven by the turbulence from air-water interface. It can be considered as a formula of wind-driven gas-liquid transfer rate that is simplified from the formula of wind-stream-driven gas-liquid transfer rate that is developed in Chapter 4.

5.3. Comparison of effects of three kinds of interfaces on gas-liquid transfer rate

In natural water bodies, the water-bed interface can be the predominant turbulence source, e.g. in stream-driven gas-liquid transfer system; the air-water interface can stand alone as the turbulence source, e.g. in the wind-driven gas-liquid transfer system. Thus, the formulae of shear velocity, shear stress, surface renewal rate and gas-liquid transfer rate caused by turbulence generated from these two kinds of interfaces can be tested with

the stream-driven or wind-driven gas-liquid transfer experimental data and empirical formulae. However, normally the transition location of shear flows will not stand alone as the turbulence source in the natural water bodies. For example, in complex three-dimensional flows, the air-water interface, the water-bed interface, or both will stand together with the transition location of shear flows as the turbulence sources. Thus, it is difficult to directly verify the formula of shear velocity, shear stress, surface renewal rate and gas-liquid transfer rate caused by turbulence generated from the transition location of shear flows. However, the comparison of calculation results from the formulae on these three kinds of interfaces will be an indirect method to test whether the formulae for transition location of shear flows are reasonable. As the friction at the transition location of shear flows is greater than that at the air-water interface and less than that at the water-bed interface with the same amount of water flow velocity or wind speed, the magnitudes of the shear velocity, shear stress, surface renewal rate and gas-liquid transfer rate for the transition location of shear flows are between those for the air-water interface and those for the water-bed interface.

Based on the formulae of Eq.5.20, Eq.5.25 and Eq.5.29, the shear velocity, shear stress, surface renewal rate and gas-liquid transfer rate at the air-water interface, the transition location of shear flows and the water-bed interface can be calculated. Figure 5.1 shows two layers that are separated by an interface. The layers could be air, water, or bed. The interface could be the air-water interface, the transition location of shear flows,

or the water-bed interface. The phase velocity could be streamflow velocity or wind speed.

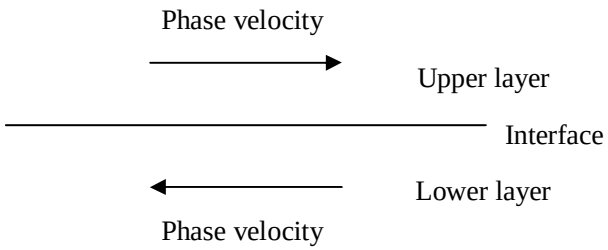

Figure 5.1. Two layers (air, water, or bed) separated by an interface (air-water interface, transition location of shear flows, or water-bed interface)

Four cases are tested. In case 1, it is supposed that for the air-water interface, a wind of 0.2 m/s blows over a water surface; for the transition location of shear flows, the upper layer of water moves at 0.2 m/s over the lower layer of water which is stagnant; for the water-bed interface, a turbulent flow moves along its water bed and the free stream velocity is 0.2 m/s. The corresponding calculation results were displayed in Table 5.1. Similarly another three cases were explored where the water flow velocities or wind speeds were 0.8 m/s, 2 m/s and 6 m/s respectively. The responding calculation results are displayed in Tables 5.1-5.4 respectively. The velocity of 0.2 m/s and 0.8 m/s represented the low and high water flow velocities respectively; the velocity of 2 m/s and 6 m/s represented the low and high wind speeds respectively.

Table 5.1. Calculation results when the phase velocity is 0.2 m/s

Parameters	Air-water interface	Transition location of shear flows	Water-bed interface
Phase in upper layer	air	water	water
Phase in lower layer	water	water	bed
Phase density in upper layer, ρ, kg/m^3	1.225	1000	1000
Phase density in lower layer, ρ, kg/m^3	1000	1000	>1000
Shear velocity, u_*, m/s	3.10×10^{-4}	7.69×10^{-4}	2.88×10^{-2}
Shear stress, τ, N/m^2	9.60×10^{-5}	5.90×10^{-4}	8.31×10^{-1}
Surface renewal rate, r, s^{-1}	6.20×10^{-4}	1.54×10^{-3}	5.77×10^{-2}
Gas-liquid transfer rate, K_L, m/s	1.11×10^{-6}	1.74×10^{-6}	1.07×10^{-5}

Table 5.2. Calculation results when the phase velocity is 0.8 m/s

Parameters	Air-water interface	Transition location of shear flows	Water-bed interface
Phase in upper layer	air	water	water
Phase in lower layer	water	water	bed
Phase density in upper layer, ρ, kg/m^3	1.225	1000	1000
Phase density in lower layer, ρ, kg/m^3	1000	1000	>1000
Shear velocity, u_*, m/s	1.24×10^{-3}	3.07×10^{-3}	1.15×10^{-1}
Shear stress, τ, N/m^2	1.54×10^{-3}	9.44×10^{-3}	1.33×10^{-1}
Surface renewal rate, r, s^{-1}	2.48×10^{-3}	6.15×10^{-3}	2.31×10^{-1}
Gas-liquid transfer rate, K_L, m/s	2.21×10^{-6}	3.48×10^{-6}	2.13×10^{-5}

Table 5.3. Calculation results when the phase velocity is 2 m/s

Parameters	Air-water interface	Transition location of shear flows	Water-bed interface
Phase in upper layer	air	water	water
Phase in lower layer	water	water	bed
Phase density in upper layer, ρ, kg/m^3	1.225	1000	1000
Phase density in lower layer, ρ, kg/m^3	1000	1000	>1000
Shear velocity, u_*, m/s	3.10×10^{-3}	7.69×10^{-3}	2.88×10^{-1}
Shear stress, τ, N/m^2	9.60×10^{-3}	5.90×10^{-2}	8.31×10^{-1}
Surface renewal rate, r, s^{-1}	6.20×10^{-3}	1.54×10^{-2}	5.77×10^{-1}
Gas-liquid transfer rate, K_L, m/s	3.50×10^{-6}	5.50×10^{-6}	3.37×10^{-5}

Table 5.4. Calculation results when the phase velocity is 6 m/s

Parameters	Air-water interface	Transition location of shear flows	Water-bed interface
Phase in upper layer	air	water	water
Phase in lower layer	water	water	bed
Phase density in upper layer, ρ, kg/m^3	1.225	1000	1000
Phase density in lower layer, ρ, kg/m^3	1000	1000	>1000
Shear velocity, u_*, m/s	9.30×10^{-3}	2.31×10^{-2}	8.65×10^{-1}
Shear stress, τ, N/m^2	8.64×10^{-2}	5.31E-01	7.47×10^{2}
Surface renewal rate, r, s^{-1}	1.86×10^{-2}	4.61×10^{-2}	1.73×10^{0}
Gas-liquid transfer rate, K_L, m/s	6.05×10^{-6}	9.53×10^{-6}	5.84×10^{-5}

Tables 5.1-5.4 show that the shear velocity, shear stress and their corresponding surface renewal rate and gas-liquid transfer rate at the water-bed interface are the greatest, followed by those at the transition location of shear flows and then by those at the

air-water interface. With the same flow velocity or wind speed, the friction at the transition location of shear flows is between that at the air-water interface and that at the water-bed interface. Thus, the predictions using Eq.5.20 are considered reasonable.

5.4. Conclusions

The gas-liquid transfer rate is determined by the total surface renewal rate and the molecular diffusion coefficient. The total surface renewal rate is a function of the shear velocity which is determined by the friction at air-water interface, transition location of shear flows, and water-bed interface. The formulae of shear velocity, shear stress, surface renewal rate and gas-liquid transfer rate caused by turbulence generated from these three types of turbulence source locations are developed in this study. The comparison of these parameters showed that these three kinds of interfaces have different significance in affecting the gas-liquid transfer rate. The water-bed interface has the greatest significance; followed by the transition location of shear flows and then by the air-water interface.

CHAPTER VI

GAS-LIQUID TRANSFER RATE IN WIND AND DYNAMIC THREE-DIMENSIONAL FLOW SYSTEMS

6.1. Gas-liquid transfer rate in wind and dynamic three-dimensional flows systems

6.1.1. Introduction

Many factors like streamflow, wind, etc. influence the gas-liquid transfer rate, K_L. In wind-driven systems, wind is the predominant factor for the gas transfer process. When wind blows over water, turbulence is generated at the air-water interface, which is the driving force for the surface renewal movement of the water parcels. Considerable empirical relationships have been established for the wind-driven gas-liquid transfer rate (Broecker 1978; Jahne 1979; Liss and Merlivat 1986; Wanninkhof 1992; Wanninkhof and McGillis 1999). A theoretical model on wind gas-liquid transfer rate has been developed (O'Connor 1983). In stream-driven system, when wind is negligible, stream is the predominant factor for the gas transfer process. When stream flows over bed, turbulence is generated at the water-bed interface and the air-water interface. Both kinds of turbulence are driving forces of the water parcels' surface renewal movement. Efforts

have been exerted to build empirical formulae (Churchill 1962; Owens and Gibbs 1964). Some theoretical models have been developed (O'Connor and Dobbins 1956; Langbein and Durum 1967; Wilcock 1984).

Widely used stream-driven gas-liquid transfer rate formulae include the O'Connor-Dobbins' formulae (Eq.6.1), Churchill's formulae (Eq.6.2), and Owens-Gibbs' formulae (Eq.6.3) (Chapra 1997):

$$K_L = 4.55 \times 10^{-5} \times \frac{U^{0.5}}{H^{0.5}} \tag{6-1}$$

$$K_L = 5.82 \times 10^{-5} \times \frac{U}{H^{0.67}} \tag{6-2}$$

$$K_L = 6.16 \times 10^{-5} \times \frac{U^{0.67}}{H^{0.85}} \tag{6-3}$$

where U = depth-averaged water flow velocity, m/s; and H = water depth, m. All of these formulae are expressed in the form of:

$$K_l = A\frac{U^B}{H^C} \tag{6-4}$$

where A, B and C = constant coefficients. These formulae work well with rivers that have one-dimensional uniform flow velocities. However, in application to water bodies with complex three-dimensional flows like tidal estuaries, it is difficult to determine what water depth and average flow velocity should be used in the formulae. For example, in an

estuary with two stratified layers, the upper layer and lower layer typically have opposite flow directions as Figure 6.1 shows:

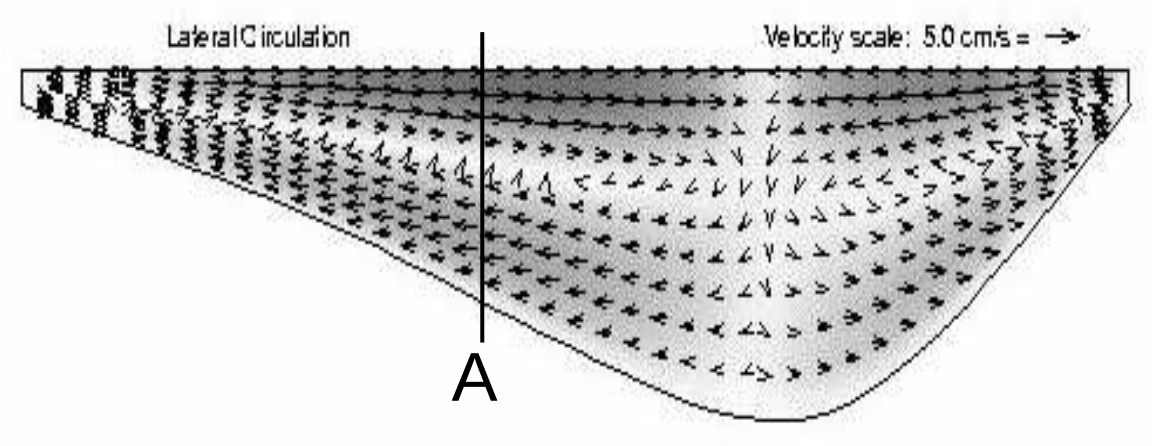

Figure 6.1. Velocity fields in flood tide simulation in Conway Estuary (modified from Scott, 2005)

It is assumed that the average velocity at location A is equal to zero (as in the null zone). If the average velocity and the total water depth at location A are used in Eq.6.4, the gas-liquid transfer rate is equal to zero. However, the gas-liquid transfer rate at location A is actually greater than zero. Thus, the use of the depth-averaged velocity and total water depth in the formulae like Eq.6.4 for stratified flows is problematic. The same problem will exist in more complex wind and dynamic three-dimensional flow systems. Thus, a new model and related formulae for gas-liquid transfer rate needs to be developed for application to complex systems with wind and dynamic three-dimensional flows.

6.1.2. Model development

6.1.2.1. Boxes model

In one-dimensional uniform flow there are no shear flows inside the water body. The surface renewal rates caused by the turbulence only come from the air-water interface and the water-bed interface but not from the transition location of shear flows inside the water body. Thus, the whole water body can be considered as a single water column. The average velocity and total water depth are used for the calculation of gas-liquid transfer rate using Eq.6.4.

However, for the water bodies with complex three-dimensional flow, their hydraulic characters cannot be represented by a single average velocity and the total water depth. They have to be divided into many small computational elements (boxes) with each one having three-dimensional velocities. The interfaces of the water boxes are composed of the air-water interface, the transition location of shear flows or the water-bed interface. The total surface renewal rates can be determined with the hydraulic parameters of the water boxes. All of the turbulence generated from the air-water interface, the transition location of shear flows and the water-bed interface may affect the gas-liquid transfer rate.

Surface Renewal Theory (Danckwerts 1951; Danckwerts 1953; Higbie 1935) is a classical theory to describe the gas-liquid transfer process. This theory proposes that the turbulent eddies carry the water parcels up to near the air-water interface for a period

when the gas is transferred from air to the water parcel. Then the water parcel is entrained down to the water column. Another parcel is brought up and the gas transfer process is repeated. The gas-liquid transfer rate at the air-water interface is determined by the total surface renewal rate and the molecular diffusion coefficient as:

$$K_L = \sqrt{Dr} \tag{6-5}$$

where D = diffusion coefficient, m^2/s; and r = surface renewal rate, s^{-1}. In the present study, it is assumed that the total surface renewal rate is the arithmetic sum of all of the effective surface renewal rates which are caused by the turbulence generated from the air-water interface, the effective horizontal and vertical transition location of shear flows and/or water-bed interface:

$$r = \sum r_n \tag{6-6}$$

where r_n = surface renewal rate, s^{-1}. This assumption will be tested with the predictions of the model of gas-liquid transfer rate in wind and dynamic three-dimensional flow systems. If the predictions are reasonable, this assumption will also be considered reasonable. In dynamic flows, the flow field changes as a function of time. The transition location of shear flows formed in later time steps possibly blocks the turbulent movement of the water parcels from the lower transition location of shear flows formed in the earlier time step. All of these effects need to be incorporated into the new model.

Hydrodynamic computer software models like the Environmental Fluid Dynamics Computer Code (EFDC) divide the water body into three-dimensional cells by gridding

the water surface and dividing the water depth into several layers. These hydrodynamic models can provide hydraulic parameter files containing water depth distribution data and three-dimensional flow velocity data. Thus, for three-dimensional flows, a box model can be developed to develop the formula of gas-liquid transfer rate at the air-water interface from the predicted layer depths and three-dimensional flow field. The schematic diagram is as Figure 6.2:

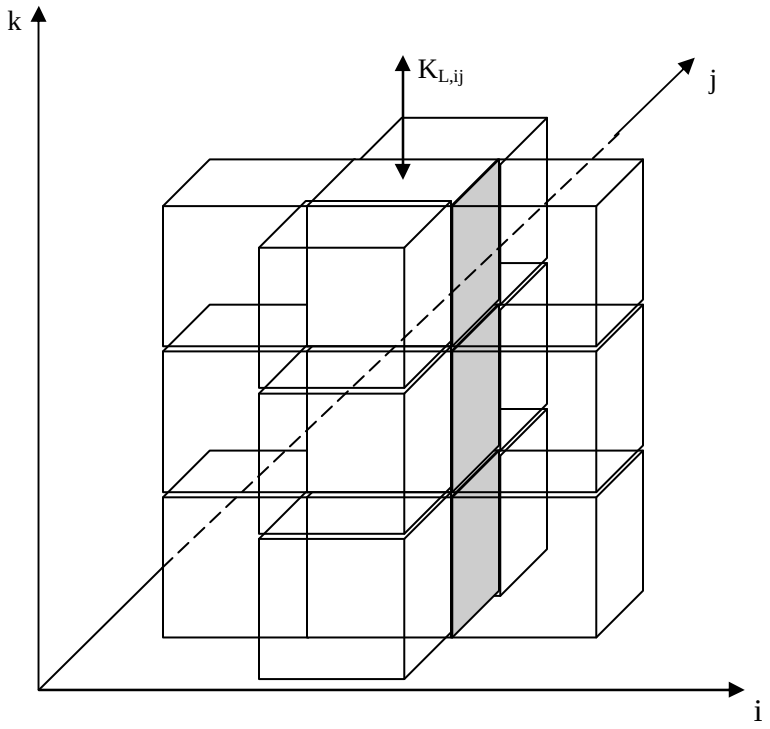

Figure 6.2. The objective water column and its adjacent water columns

The objective water column is located at (i,j). The objective gas-liquid transfer rate is $K_{L,ij}$ at the air-water surface of this water column (i,j). For the purpose of this study, it is assumed that $K_{L,ij}$ is affected by the turbulence generated from the interfaces at the edge of or inside this water column including the air-water interface, the horizontal transition location of shear flows, the vertical transition location of shear flows, and the water-bed interface. It is further assumed that the total surface renewal rate will be the arithmetic sum of all of the surface renewal rates from these effective interfaces. The horizontal spatial distribution of the gas-liquid transfer rates can be obtained after the gas-liquid transfer rate at the air-water interface on each water column is determined.

6.1.2.2. Effects of friction at air-water interface on gas-liquid transfer rate

The surface renewal movement caused by the turbulence generated from the air-water interface is a driving force of the gas-liquid transfer process. The formula of surface renewal rate has been developed in Chapter 5 as:

$$r_{aw} = \frac{5}{H}\sqrt{\frac{C_{f1}\rho_a W^2}{2\rho_w}} \tag{6-7}$$

where r_{aw} = surface renewal rate cuased by the turbulence from air-water interface, s^{-1}; H = water depth, m; C_{f1} = skin-coefficient coefficient at air-water interface; ρ_a = density of air, kg/m^3; ρ_w = density of water, kg/m^3; and W = wind speed, m/s. The combined effects of wind and the flow layer next to the air-water interface are incorporated into Eq.6.7.

6.1.2.3. Effects of friction at horizontal transition location of shear flows on gas-liquid transfer rate

When horizontal transition location of shear flows exist in the water body, the one next to the air-water interface is considered as the effective horizontal transition location of shear flows. The friction at this interface damps the turbulent movement from the lower transition location of shear flows though some water parcels may transfer from lower flow layer to this layer. The surface renewal movement caused by the turbulence generated from this effective transition location of shear flows is a driving force of the gas transfer at the air-water interface. The related formula of surface renewal rate has been developed in Chapter 5 as:

$$r = \frac{5}{H}\sqrt{\frac{0.121\sigma K\left|U_2 - U_1\right|U_{\max}\left(U_1, U_2\right)}{\sqrt{\pi}\rho}} \tag{6-8}$$

where $\sigma = 13.5$; $K = 0.016$; ρ = density of medium, kg/m^3; U_1 = flow velocity in upper layer, m/s; U_2 = flow velocity in upper layer, m/s; and U_{max} = maximum of U_1 and U_2, m/s.

In the objective water column, there is a horizontal transition location of shear flows between any two adjacent water boxes, but only one will work as the effective horizontal transition location of shear flows. The determination of the location of the effective transition location of shear flows is as the algorithm shown below. A typical flow velocity profile in the objective water column with multiple boxes piling up vertically is as Figure 6.3:

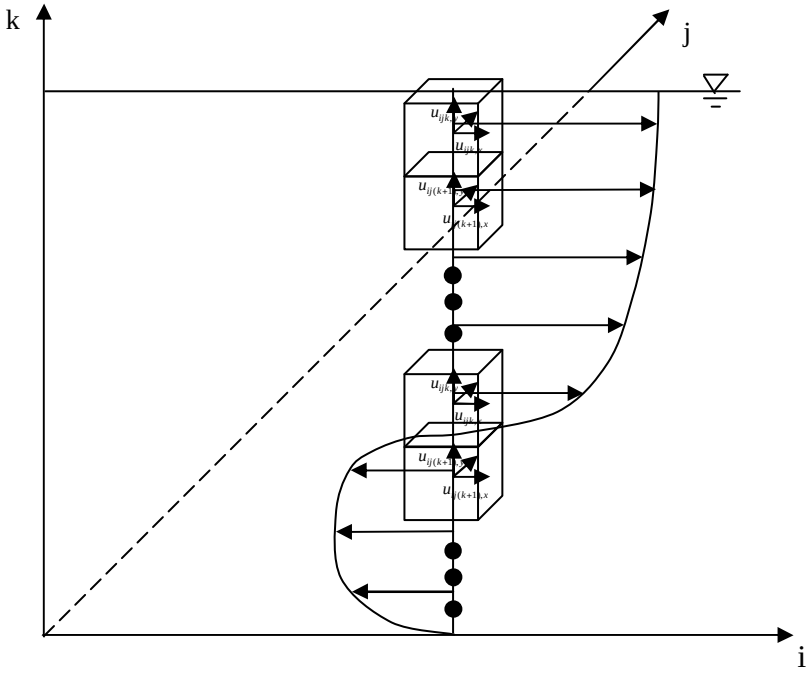

Figure 6.3. Flow velocity profile in the objective water column with multiple boxes piling up vertically

In the objective water column, the horizontal boxes interfaces are analyzed from top to bottom. Figure 6.4 shows two adjective water boxes piling up in the objective water column with each one having a three-dimensional flow velocity.

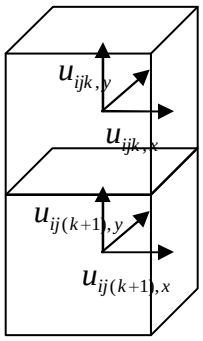

Figure 6.4. Two adjective water boxes piling up in the objective water column

The included-angle of two vectors can be calculated with the vector dot product. The horizontal included-angle of the velocities of the adjacent boxes is calculated as:

$$\cos\theta_z = \frac{\left(u_{ijk,x}i + u_{ijk,y}j\right)\cdot\left(u_{ij(k+1),x}i + u_{ij(k+1),x}j\right)}{\left|u_{ijk,x}i + u_{ijk,y}j\right|\left|u_{ij(k+1),x}i + u_{ij(k+1),x}j\right|} \quad (6\text{-}9)$$

where θ_z = included-angle in xy planes; $u_{ijk,x}$ = velocity at x direction in layer k, m/s; $u_{ij(k+1),x}$ = velocity at x direction in layer (k+1), m/s; $u_{ijk,y}$ = velocity at y direction in layer k, m/s; $u_{ij(k+1),y}$ = velocity at y direction in layer (k+1), m/s; i = water surface location at i coordinate, and I is the maximum at i coordinate; and j = water surface location at j coordinate, and J is the maximum at j coordinate. The included-angle of the flow velocities in two adjacent water boxes ranges from 0 to 2π. It is assumed in this study that if $\frac{\pi}{2} < \theta_z < \frac{3\pi}{2}$, this horizontal interface is considered as an effective horizontal transition location of shear flows. The effective water depth is as:

$$H = h \quad (6\text{-}10)$$

where h = water depth in layer 1, m. Otherwise, the friction at this horizontal interface will be ignored and the next horizontal transition location of shear flows will be analyzed

in the same way. This analysis needs to be processed repeatedly until the first effective horizontal interface with horizontal included-angle greater than $\frac{\pi}{2}$ and less than $\frac{3\pi}{2}$ is found. The effective water depth is considered to be as:

$$H = \sum_{k=1}^{k} h_k \tag{6-11}$$

where k = layer number where the effective transition location of shear flows is located.

6.1.2.4. Effects of friction at water-bed interface on gas-liquid transfer rate

If the effective horizontal transition location of shear flows stated in section 6.1.2.3 can be found from one of the transition location of shear flows in the objective water column, the water-bed interface will not be considered to contribute to the total surface renewal rate. Otherwise, if such effective horizontal transition location of shear flows cannot be found, the surface renewal rate caused by the turbulence from the water-bed interface will be considered as the effective horizontal interface. Under this situation, the turbulence generated from the water-bed interface is considered to be an effective driving force of the gas transfer at the air-water interface. The related formula of surface renewal rate is discussed in Chapter 5 as:

$$r = \frac{5\sqrt{\frac{C_{f2}}{2}}U}{H} \tag{6-12}$$

where C_{f2} = skin-friction coefficient at water-bed interface. The effective water depth equals to the total water depth of the objective water column as:

$$H = \sum_{k=1}^{K} h_k \tag{6-13}$$

where K = the total number of layers of the objective water column. When this effective horizontal transition location of shear flows is determined with the above algorithm, lower horizontal transition location of shear flows do not need to be considered since the turbulence generated from them has no direct contribution to the surface renewal movement of the water parcels in the water column between the air-water interface and the effective horizontal transition location of shear flows.

6.1.2.5. Effects of friction at vertical transition location of shear flows on gas-liquid transfer rate

Friction occurs at the vertical transition location of shear flows between the objective water column ij and those around it. The water columns (i-1)j, (i+1)j, i(j-1), and i(j+1) affect the objective gas-liquid transfer rate, $K_{L,ij1}$, in the same way (see Figure 6.2). The surface renewal rates caused by the turbulence generated from the interfaces in yz planes between the objective column and the (i-1)j one or the (i+1)j one contribute to the total surface renewal rate. The included-angle on the xz plane of the velocities of the adjacent water boxes are as:

$$\cos\theta_x = \frac{\left(u_{ijk,y} i + u_{ijk,z} j\right) \cdot \left(u_{ij(k+1),y} i + u_{ij(k+1),z} j\right)}{\left|u_{ijk,y} i + u_{ijk,z} j\right| \left|u_{ij(k+1),y} i + u_{ij(k+1),z} j\right|} \tag{6-14}$$

where θ_x = included-angle in yz planes; $u_{ijk,y}$ = velocity at y direction in layer k, m/s; $u_{ij(k+1),y}$ = velocity at y direction in layer (k+1), m/s; $u_{ijk,z}$ = velocity at z direction in layer k, m/s; and $u_{ij(k+1),z}$ = velocity at z direction in layer (k+1), m/s. Similar to θ_z in section 6.1.2.3, if $\frac{\pi}{2} < \theta_x < \frac{3\pi}{2}$, this interface is considered as an effective vertical transition location of shear flows. Since normally the number of the water flow layers is basically limited, the calculation complexity of the algorithm used for the horizontal interfaces in the objective water column is limited. However, since the water column number (I x J) is much greater than the flow layers amount (K), the algorithm used for the horizontal transition location of shear flows will not work efficiently. Another algorithm is needed as follows to provide a rough estimate of effects of the surrounding water columns on the gas-liquid transfer rate at the air-water surface of the objective water column: The shear velocity at the vertical interface of the objective water column is always considered as an effective one and the effects of the water columns not adjacent to the objective water column are ignored. The shear velocity at the vertical transition location of shear flows in xz plane is discussed in Chapter 5 as:

$$u_* = \sqrt{\frac{0.121\sigma K|U_i - U_{i-1}|U_{\max}(U_i, U_{i-1})}{\sqrt{\pi}\rho}} \qquad (6\text{-}15)$$

where u_* = shear velocity, m/s; U_i = flow velocity in water box i, m/s; and U_{i-1} = flow velocity in water box (i-1), m/s.

The surface renewal rates caused by the turbulence generated from the interfaces in yz plane between the objective column and the i(j-1) one or the i(j+1) one contribute to

the total surface renewal rate. The included-angle on the yz plane of the velocities of the adjacent boxes is calculated as:

$$\cos\theta_y = \frac{\left(u_{ijk,z} i + u_{ijk,x} j\right)\cdot\left(u_{ij(k+1),z} i + u_{ij(k+1),x} j\right)}{\left|u_{ijk,z} i + u_{ijk,x} j\right|\left|u_{ij(k+1),z} i + u_{ij(k+1),x} j\right|} \tag{6-16}$$

where θ_y = included-angle in zx planes; $u_{ijk,x}$ = velocity at x direction in layer k, m/s; $u_{ij(k+1),x}$ = velocity at x direction in layer (k+1), m/s; $u_{ijk,z}$ = velocity at z direction in layer k, m/s; and $u_{ij(k+1),z}$ = velocity at z direction in layer (k+1), m/s. Similar to θ_z in section 6.1.2.3, if $\frac{\pi}{2} < \theta_y < \frac{3\pi}{2}$, this interface is considered as an effective vertical transition location of shear flows. Similar to Eq.6.15, the shear velocity at the vertical transition location of shear flows in yz plane is discussed in Chapter 5 as:

$$u_* = \sqrt{\frac{0.121\sigma K\left|U_j - U_{j-1}\right| U_{\max}(U_j, U_{j-1})}{\sqrt{\pi}\rho}} \tag{6-17}$$

The surface renewal movement of the water parcels caused by the friction at the vertical transition location of shear flows is assumed to have similar mechanism as that caused by the friction at the horizontal transition location of shear flows. Thus, Eq.6.8 can also be used to calculate the surface renewal rate. The objective water column has transition location of shear flows with four adjective water columns with multiple water boxes. The included-angles of flow velocities for different transition location of shear flows around the objective water column are different. Thus, some of these transition location of shear flows are effective ones, while others are not. Only the area of the effective transition location of shear flows is considered as effective area. Thus, an area

coefficient needs to be added into Eq.6.8. Thus, the surface renewal rate formula caused by the turbulence from the vertical transition location of shear flows is as:

(6-18)

$$r = \frac{\left|\bar{v}\right|}{l} = \frac{0.5\sum\left(C_A u_*\right)}{0.1H} = \frac{5\sum\left(C_A u_*\right)}{H} = \frac{5}{H}\sum\left(\sqrt{\frac{0.121\sigma K\left|U_2 - U_1\right|U_{\max}\left(U_2, U_1\right)}{\sqrt{\pi}\rho}}\right)$$

where C_A = area coefficient equal to the ratio of the effective vertical interface area over the total vertical interface area.

6.1.2.6. Effects of dynamic flows on gas-liquid transfer rate

The flow fields in some water bodies such as tidal estuaries are dynamic. The dynamic flows cause the re-distribution of transition location of shear flows inside the objective water column. If at time (t+1) a new effective transition location of shear flows is above the one at time t, and the distance between these two interfaces is greater than the distance of the water parcels moving up from the effective transition location of shear flows at time t and the part of the vertical transition location of shear flows which are below the effective transition location of shear flows at time of (t+1), this movement is assumed for this study to be ineffective and have no contribution to the gas transfer at the air-water interface of the objective water column. Otherwise, this movement is considered to be effective and the related surface renewal rates will be considered as components of the total surface renewal rate. The effects of dynamic flows on gas-liquid transfer rate cannot be expressed in form of a formula; but they can be implemented in

the computer program in calculating the gas-liquid transfer rate using the assumptions described above.

6.1.2.7. Model of gas-liquid transfer rate in wind and three-dimensional flows systems

It is assumed in this study that the total surface renewal rate is the arithmetic sum of the surface renewal rates.

$$r = \sum r_n = r_{aw} + r_{xy} + r_{yz} + r_{zx} \tag{6-19}$$

where r_{aw} = surface renewal rate caused by the turbulence from air-water interface, s^{-1}, which is formulated as Eq.6.7; r_{xy} = surface renewal rate caused by the turbulence from horizontal transition location of shear flows in xy planes, s^{-1}, which is formulated as Eq.6.8 when a transition location of shear flows is the effective horizontal interface and as Eq.6.12 when the water-bed interface is the effective horizontal interface; r_{yz} = surface renewal rate caused by the turbulence from vertical transition location of shear flows in yz planes, s^{-1}, which is formulated as Eq.6.8 when a transition location of shear flows is the effective horizontal interface and as Eq.6.12 when the water-bed interface is the effective horizontal interface; r_{zx} = surface renewal rate caused by the turbulence from vertical transition location of shear flows in zx planes, s^{-1}, which is formulated as Eq.6.18.

Substitution of Eq.6.19 into Eq.6.5 yields:

$$K_L = \sqrt{D(r_{aw} + r_{xy} + r_{yz} + r_{zx})} \quad (6\text{-}20)$$

where K_L = gas-liquid transfer rate, m/s; and D = diffusion coefficient, m^2/s. Eq.6.20 is the gas-liquid transfer rate at the air-water interface of the objective water column. Thus, the formula of gas-liquid transfer rate in wind and three-dimensional flow systems is composed of Eq.6.7, Eq.6.8, Eq.6.12, Eq.6.18 and Eq.6.20. This is a formula for non-dynamic flow fields. Because of the complexity of the algorithms used in developing this formula, a computer program needs to be coded to implement this formula. For the dynamic change of the flow fields, the related algorithm showed in section 6.1.2.6 needs to be incorporated into the computer program. The model developed in this section is named as “Wind-dynamic-3D-flows-driven KL Model” in this study.

6.1.3. Model testing

The complexity of the model of gas-liquid transfer rate in wind and dynamic three-dimensional flow systems requires a computer program to implement it. Especially when this model is applied into complex flow fields in tidal water bodies, only a computer program can process the complex tasks, e.g. recognizing the effective horizontal transition location of shear flows, incorporating the effects of dynamic change of the flow field on the gas-liquid transfer rate. Thus, a FORTRAN program named as "KL Program" was coded to implement the model developed in this study (Appendix B). This program can calculate the gas-liquid transfer rate values in wind and dynamic

three-dimensional flow systems to test the model in section 6.1.2 and are included in Appendix B along with representative input and output files (Appendix C-E). The schematic diagram of this program is as Figure 6.5. This program uses the water depth and flow velocity data generated by the EFDC model as inputs and then processes them based on the model of gas-liquid transfer rate in wind and dynamic three-dimensional flow systems to calculate the gas-liquid transfer rate on the water surface of each water column in the tidal estuaries.

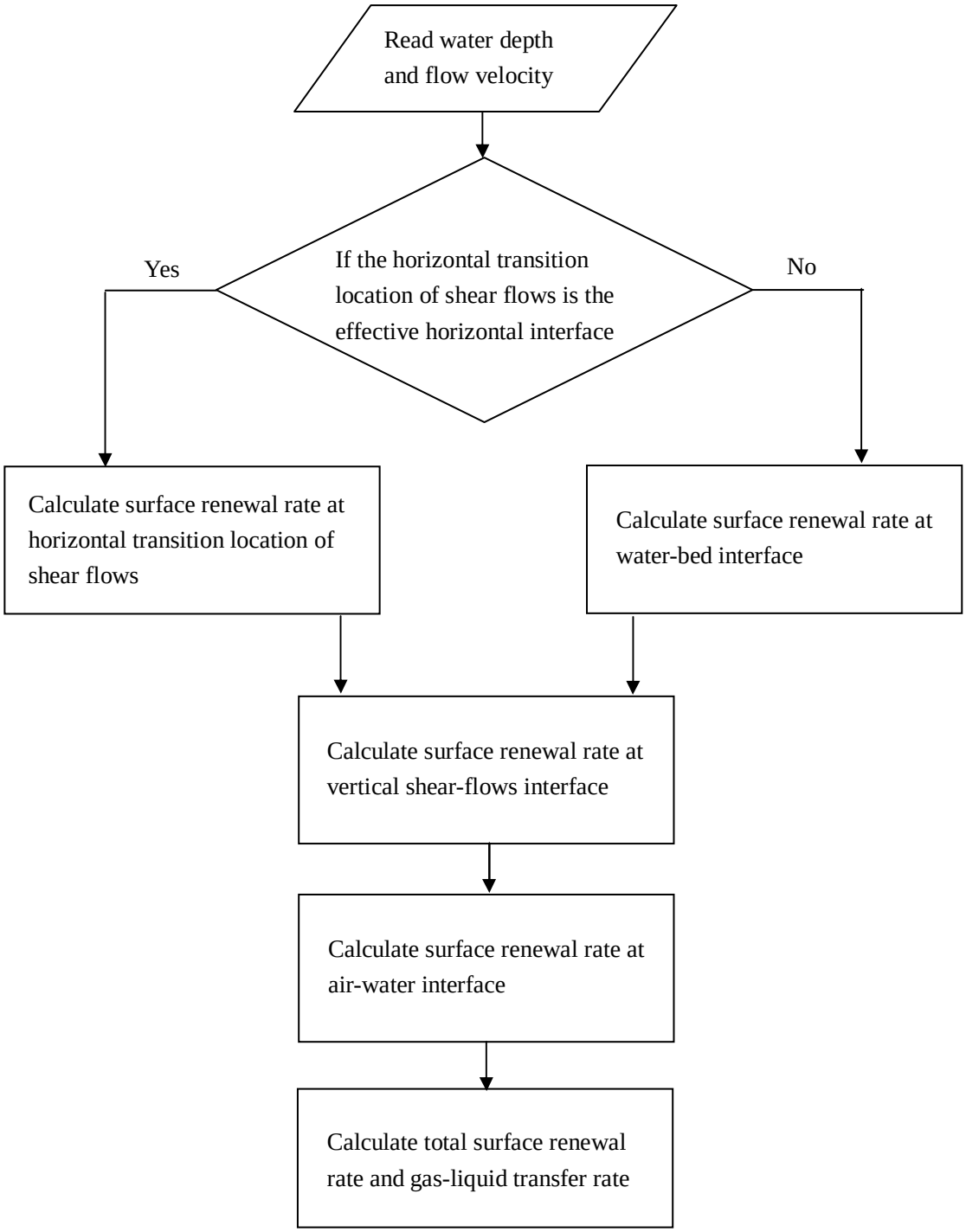

Figure 6.5. Schematic diagram of gas-liquid transfer rate program (KL Program)

Table 5.1-5.4 show that the gas-liquid transfer rate in the normal wind and flow systems has the value in the level of from 0.01 to 10 m/day. The wind-stream-driven gas-liquid transfer rate experimental results showed in Figure 4.6 also has value in this level. Thus, in this chapter, this value level will be used to check if the predictions with KL program are reasonable.

In order to test the models, this program were applied in various kinds of wind-water systems from simple one-dimensional uniform flow without wind blowing over the water surface to complex dynamic three-dimensional flows with wind blowing over the water surface. As Figure 6.6 shows, the water body used for model testing consists of 4 x 4 x 4 boxes and the total water depth is 9.9 m.

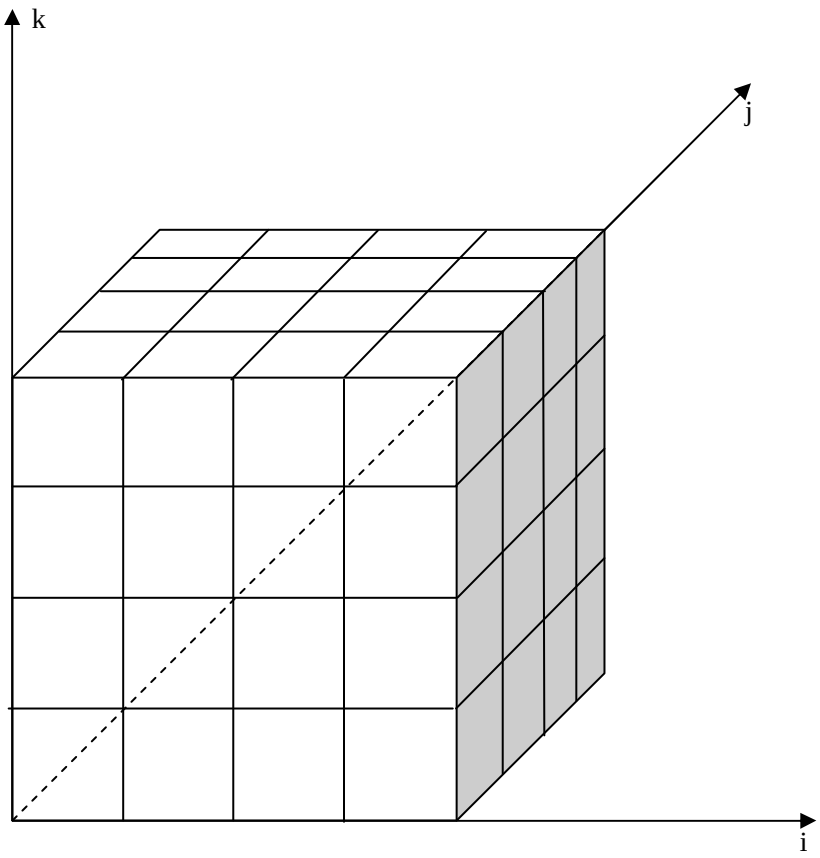

Figure 6.6. Water body used for model testing consisting of 4 x 4 x 4 boxes

6.1.3.1. In one-dimensional uniform flows

When this model was applied for the one-dimensional uniform flow with velocity of 0.5 m/s at positive i direction (Figure 6.7), positive j direction (Figure 6.8), and northeast direction (45^{o} to positive i direction) in ij plane (Figure 6.9) respectively, the calculated gas-liquid transfer rate values by the KL program are the same and equal to 0.758 m/day, which is also the same as that calculated with O'Connor and Dobbins' formula (Eq.6.1).

For this case, the effective interface is the water-bed interface, H = 9.9 m and U = 0.5 m/s.

Thus, the model was verified in case of one-dimensional uniform flow in any direction.

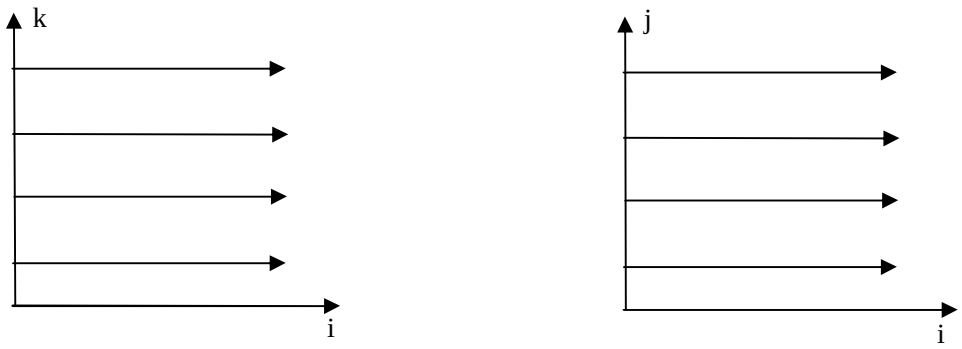

Figure 6.7. One-dimensional uniform flow with velocity of 0.5 m/s at positiove i direction

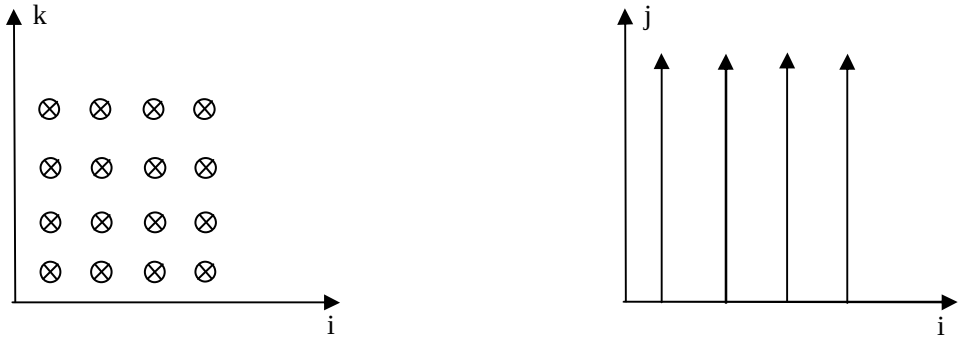

Figure 6.8. One-dimensional uniform flow with velocity of 0.5 m/s at positive j direction

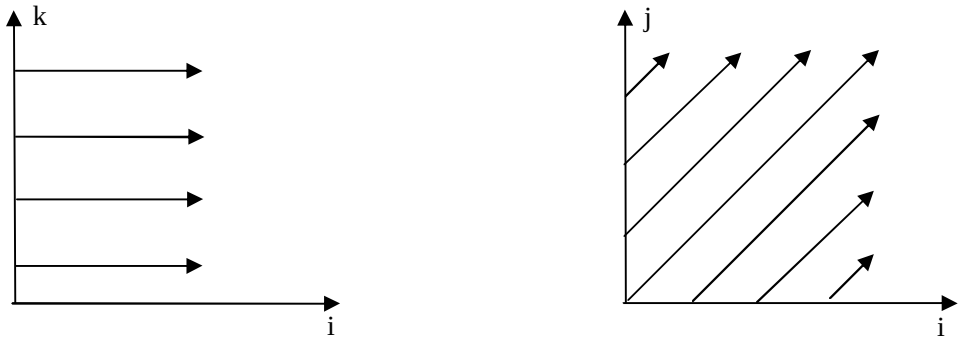

Figure 6.9. One-dimensional uniform flow with velocity of 0.5 m/s at northeast direction (45^{o} to positive i direction) in ij plane

When this model was applied for the one-dimensional stratified flows with velocity of 0.5 m/s in positive i direction in the upper two flow layers and velocity of 0.5 m/s in negative i direction in the lower two flow layers (namely the net depth-averaged velocity equals to zero as in Figure 6.10), the calculated gas-liquid transfer rate by the KL program is 0.235 m/day. This value is less than that in the one-dimensional uniform flow of 0.758 m/day. This is considered reasonable since in the stratified flows the surface renewal rate is mainly caused by the friction at the transition location of shear flows; while in the one-dimensional uniform flow the surface renewal rate is mainly caused by the friction at the water-bed interface.

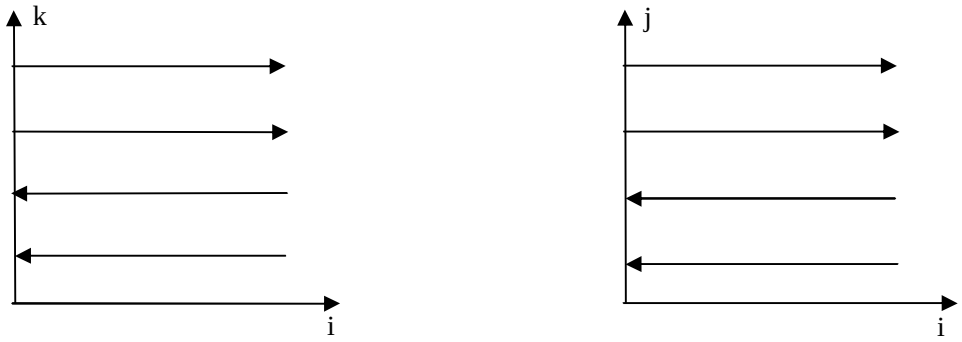

Figure 6.10. One-dimensional stratified flows with two layers

When this model was applied for a more complex one-dimensional stratified flow as Figure 6.11 shows, the calculated gas-liquid transfer rate by the KL program is 0.41 m/day.

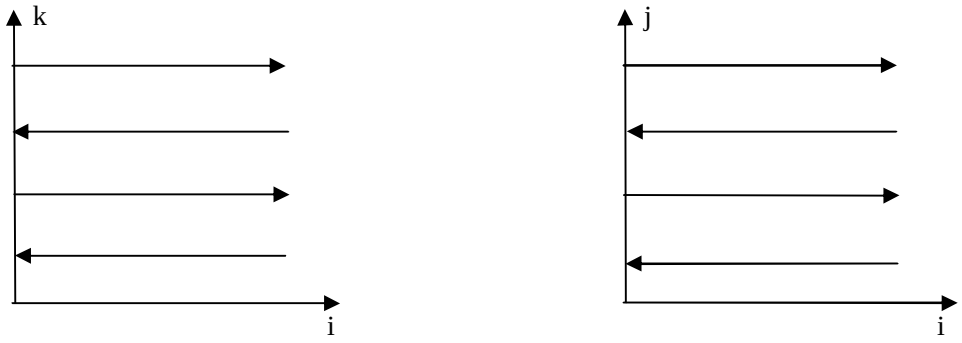

Figure 6.11. One-dimensional stratified flows with three layers

6.1.3.2. In two-dimensional complex flows

When this model was applied to two-dimensional flows where the velocity magnitude is a constant of 0.5 m/s but the velocity direction is random at positive i, negative i, positive j, or negative j direction, the calculated gas-liquid transfer rates by this KL program ranged from 0.18 m/day to 0.84 m/day, which are considered reasonable since they are in the value level from 0.1 to 5 m/day as stated at the beginning of section 6.1.3.

When this model was applied for the two-dimensional flow where the velocity magnitude is a constant of 0.5 m/s but the velocity direction is random at northeast (1,1,k), northwest (-1,1,k), southeast (1,-1,k), southwest (-1,-1,k) direction, the calculated gas-liquid transfer rates by the KL program ranged from 0.24 m/day to 0.83 m/day, which are considered reasonable since they are in the value level from 0.01 to 10 m/day as stated at the beginning of section 6.1.3.

6.1.3.3. In three-dimensional flows

A data file with three-dimensional flow fields was constructed for the model testing (Appendix F). This program was applied for this constructed flow field and the gas-liquid transfer rate values were calculated for all water columns. The statistical results of these values are as Table 6.1, which shows the computed gas-liquid transfer rates for the test

are within a reasonable range of value since they are in the value level from 0.01 to 10 m/day as stated at the beginning of section 6.1.3.

Table 6.1. Statistical results of gas-liquid transfer rate values in three-dimensional flows

Statistic parameters	Maximum, m/day	Minimum, m/day	Average, m/day	Mode, m/day	count of records
values	0.83	0.24	0.53	0.41	16

6.1.3.4. In dynamic flow fields

A data file with dynamic three-dimensional flow fields was constructed for model testing (Appendix G). At time (t+1), a new effective transition location of shear flows (named as interface 2 here) is formed above that at time t (named as interface 1 here). In case 1, if the distance between interface 1 and interface 2 is less than the distance of the water parcels moving up from the interface 1 during the time from (t+1) to t, the surface renewal movement of these water parcels contribute to the total surface renewal rate. In case 2, if the distance between interface 1 and interface 2 is greater than the distance of the water parcels moving up from the interface 1 during the time from (t+1) to t, the surface renewal movement of these water parcels do not contribute to the total surface renewal rate. For case 1, the calculated gas-liquid transfer rate value is 0.23 m/s. For case 2, the calculated gas-liquid transfer rate value is 0.11 m/s, which is less than that in case 1.

This is considered reasonable since the blocked surface renewal movements in case 2 do not contribute to the total surface renewal rate.

6.1.4. Conclusions

In this study, a model named as Wind-dynamic-3D-flows-driven KL Model and its related formulae were developed for the gas-liquid transfer rate in the wind and dynamic three-dimensional flow systems. This model was developed based on the Surface Renewal Theory. The assumption of arithmetic accumulation of surface renewal rates, shear flows, boxes model, and the shear velocities at the air-water interface, the water-bed interface, the horizontal transition location of shear flows and the vertical transition location of shear flows played important roles in the development of this model. This model correlates the gas-liquid transfer rate with time and the hydrodynamic parameters like wind speed, three-dimensional flow velocities, water depth, air density, water density, etc. The gas-liquid transfer rates predicted with this model appeared reasonable when applied to one-dimensional uniform systems, wind and one-dimensional flow systems. The gas-liquid transfer rates predicted with this model also appeared reasonable when applied to three-dimensional flow systems, wind and dynamic three-dimensional flow systems.

6.2. Gas-liquid Transfer Rate in Tidal Water Bodies

6.2.1. Introduction

The application examples in section 6.1 are synthetic water bodies which have only 64 water boxes. The natural tidal water bodies such as estuaries that delineated by hydrodynamic models typically include many computational elements (water boxes), where complex flow fields exist. These dynamical water bodies include three-dimensional flow, stratified flows, periodical tides, etc. The application of the existing formulae of gas-liquid transfer rate is problematic as they were developed from rivers with one-dimensional flow. When tides move periodically in the water bodies, they cause the water flow to forward and back periodically, cause the water depth to increase and decrease periodically, introduce water waves on the surface, and provoke stratified flows inside the water bodies.

A model of gas-liquid transfer rate in wind and dynamic three-dimensional flow systems has been developed in section 6.1. The surface renewal rates caused by the turbulence from the air-water interface, water-bed interface and transition location of shear flows may contribute to the total surface renewal rate. This model also incorporates the effects of the wind and the dynamic change of flow field on the gas-liquid transfer

rate. In this section, this model is applied to tidal water bodies using predictions of the three-dimensional hydrodynamic model.

6.2.2. Methodology

6.2.2.1. EFDC model

The Environmental Fluid Dynamics Code (EFDC) is a three-dimensional hydrodynamic model (EPA 2007). "EFDC uses stretched or sigma vertical coordinates and Cartesian or curvilinear, orthogonal horizontal coordinates to represent the physical characteristics of a waterbody" (EPA 2007). It can be applied for water bodies such as estuaries to simulate three-dimensional flow velocites, which along with the water depth distribution can be used as the input hydraulic parameters files of the gas-liquid transfer rate calculation program (KL Program).

Savannah Estuary is located close to the border of Georgia and South Carolina with outlet to the Atlantic Ocean. The preprocessor of EFDC, VOGG, was used to delineate the Savannah Estuary (Tetra Tech, Inc. 2002). The result is as Figure 6.12 shows. The water surface of this estuary is gridded into 28 x 120 cells and the water body is divided into 3 layers.

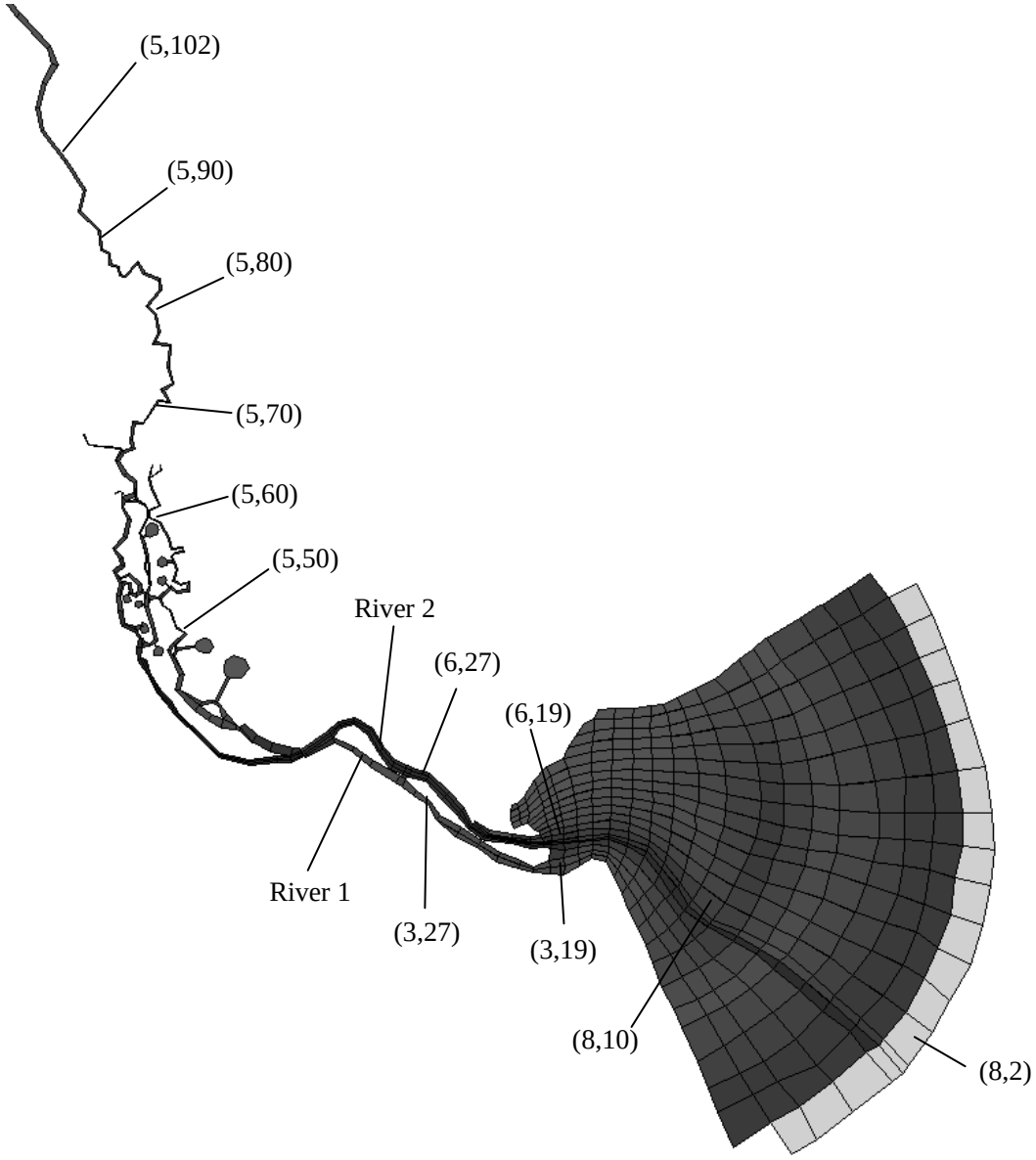

Figure 6.12. EFDC preprocessor results for Savannah Estuary (modified from Tetra Tech Inc. 2002)

6.2.2.2. KL Program

The KL Program in section 6.1 is applied to the Savannah Estuary to calculate the gas-liquid transfer rates by using the water depth and flow velocity data from the EFDC model applications.

6.2.3. Results and Discussions

6.2.3.1. Application in Savannah Estuary

The EFDC was applied to the Savannah Estuary (Tetra Tech, Inc. 2002). In this study, the water body is divided into 3 layers and the application period is 1 day with a set of records once an hour. After running the EFDC program, the three-dimensional flow velocity data are obtained. The KL Program in section 6.1 are used to calculate the dynamic gas-liquid transfer rate distribution all through the water surface of the Savannah Estuary. The statistical results of the calculated gas-liquid transfer rates are as Table 6.2 shows:

Table 6.2. Statistical results of the calculated gas-liquid transfer rates on the water surface of each water column in the Savannah Estuary

Statistic parameters	Maximum, m/day	Minimum, m/day	Average, m/day	Mode, m/day	Count of records
values	1.94	0.00	0.19	0.13	15720

Table 6.2 shows that the calculated gas-liquid transfer rates are in the reasonable value range since they are in the value level from 0.01 to 10 m/day as stated at the beginning of section 6.1.3.

6.2.3.2. Gas-liquid transfer rate at estuary outlet

The gas-liquid transfer rate and flow velocity as functions of time at location (8,2) are displayed in Figure 6.13. Location (8,2) is at the estuary outlet edge (Figure 6.12). Thus, Figure 6.13 shows the dynamic gas-liquid transfer rate values and flow velocities at estuary outlet edge during a day. At this location there is a semidiurnal tide in the Savannah Estuary with a tidal period of about 12.42 hours. The maximum flow velocity is about 0.04 m/s at positive i direction and 0.03 m/s at positive j direction. When the flow reaches its maximum magnitude, the computed gas-liquid transfer rate has maximum value; when the flow velocity crosses zero, the computed gas-liquid transfer rate has minimum value as would be expected.

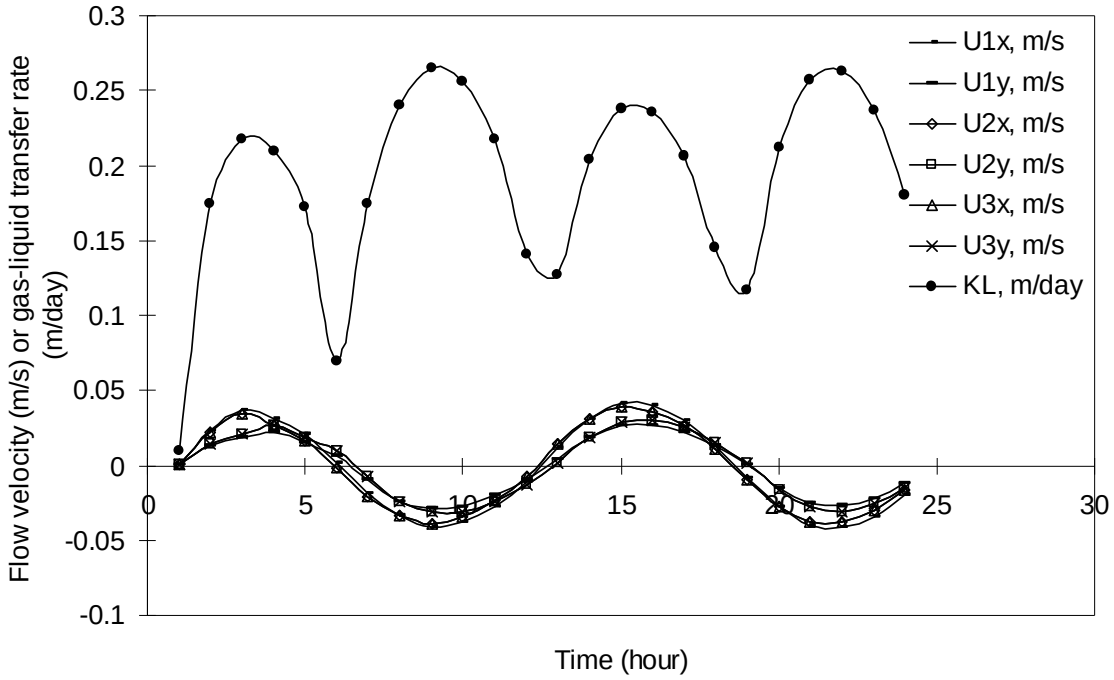

U_{1x} = flow velocity at x direction in layer 1; U_{1y} = flow velocity at y direction in layer 1; U_{2x} = flow velocity at x direction in layer 2; U_{2y} = flow velocity at y direction in layer 2; U_{3x} = flow velocity at x direction in layer 3; U_{3y} = flow velocity at y direction in layer 3; and K_L = gas-liquid transfer rate.

Figure 6.13. Gas-liquid transfer rate and flow velocity as functions of time at location (8,2) (Figure 6.12)

6.2.3.3. Gas-liquid transfer rate in the middle of estuary

The gas-liquid transfer rate and flow velocity as functions of time at location (8,10) (Figure 6.12) are displayed in Figure 6.14. Location (8,10) is in the middle of the estuary. The flow velocities at this location, especially the flow velocities at x direction, have fewer tidal wave characteristics than those at the estuary outlet. The separation of the

flow velocity at layers 1 and 3 and the flow velocity at layer 2 shows the flow is stratified and shear flows occur at this location. The existence of the transition location of the shear flows shows the turbulence generated at the transition location of shear flows is predominant in affecting the gas-liquid transfer, and the turbulence generated at the water-bed interface is blocked by the transition location of shear flows in computation. The average computed gas-liquid transfer rate is about 0.13 m/day, which is less than that at the estuary outlet edge of 0.19 m/day as would be expected.

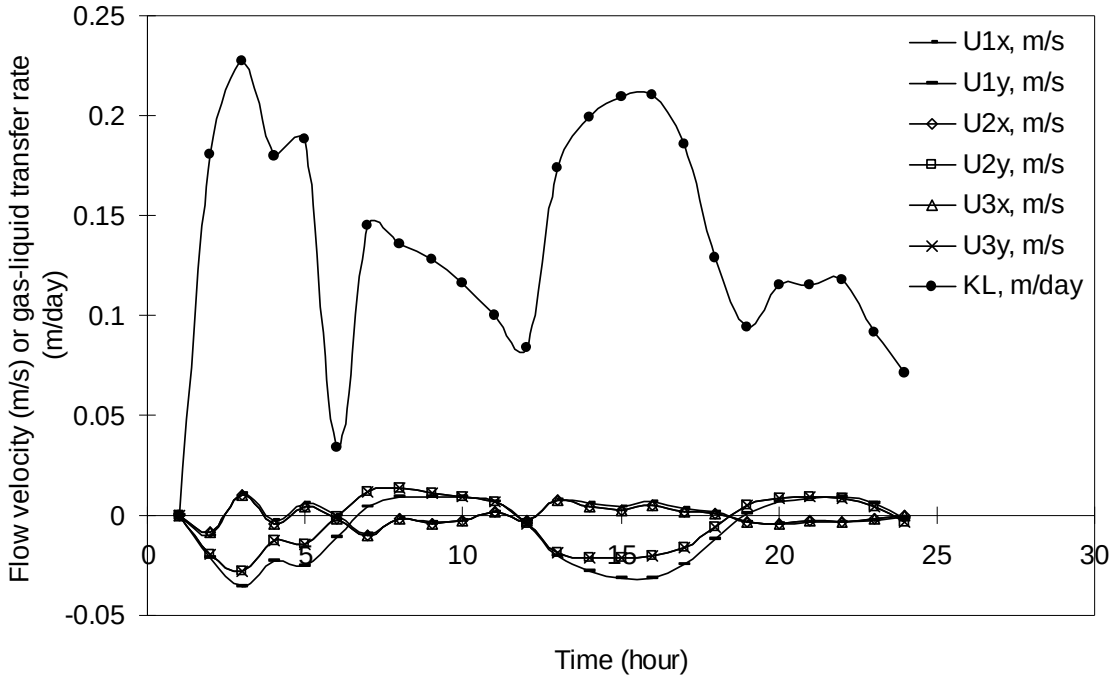

U1x = flow velocity at x direction in layer 1; U1y = flow velocity at y direction in layer 1; U2x = flow velocity at x direction in layer 2; U2y = flow velocity at y direction in layer 2; U3x = flow velocity at x direction in layer 3; U3y = flow velocity at y direction in layer 3; and KL = gas-liquid transfer rate.

Figure 6.14. Gas-liquid transfer rate and flow velocity as functions of time at location (8,10) (Figure 6.12)

6.2.3.4. Gas-liquid transfer rate at river outlet

The gas-liquid transfer rate and flow velocity as functions of time at location (3,19) (Figure 6.12) are displayed in Figure 6.12. Location (3,19) is at the entry of river 1 to the Savannah Estuary. Figure 6.15 shows that the magnitudes of the flow velocities are very small at the entry of the estuary and the flow has fewer tidal wave characteristics. The

flow velocities in all the layers are the same but their magnitudes are different. It was postulated that the gas-liquid transfer rate was determined mainly by the magnitudes of the flow velocities in this case. The values of the gas-liquid transfer rate varies with the magnitude of the flow velocity along the time axis. The average of the computed gas-liquid transfer rate at location (3,19) is 0.09 m/day, which are considered reasonable since they are in the value level from 0.01 to 10 m/day as stated at the beginning of section 6.1.3.

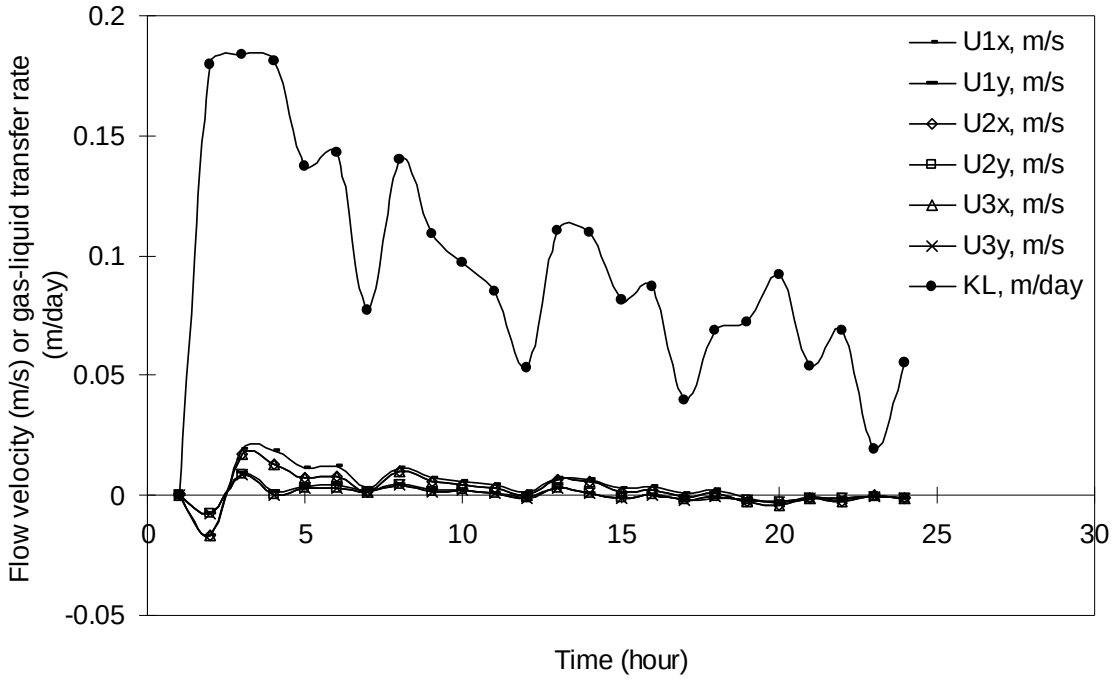

U1x = flow velocity at x direction in layer 1; U1y = flow velocity at y direction in layer 1; U2x = flow velocity at x direction in layer 2; U2y = flow velocity at y direction in layer 2; U3x = flow velocity at x direction in layer 3; U3y = flow velocity at y direction in layer 3; and KL = gas-liquid transfer rate.

Figure 6.15. Gas-liquid transfer rate and flow velocity as functions of time at location (3,19) (Figure 6.12)

The gas-liquid transfer rate and flow velocity as functions of time at location (6,19) (Figure 6.12) are displayed in Figure 6.16. Location (6,19) is at the entry of river 2 to the Savannah Estuary. The trends of gas-liquid transfer rate and flow velocity at location (6,19) are similar to those at location (3,19). The values of the gas-liquid transfer rate vary mainly with the magnitude of the flow velocity. The average of the computed gas-liquid transfer rate at location (6,19) is 0.07 m/day, which are considered reasonable

since they are in the value level from 0.01 to 10 m/day as stated at the beginning of section 6.1.3.

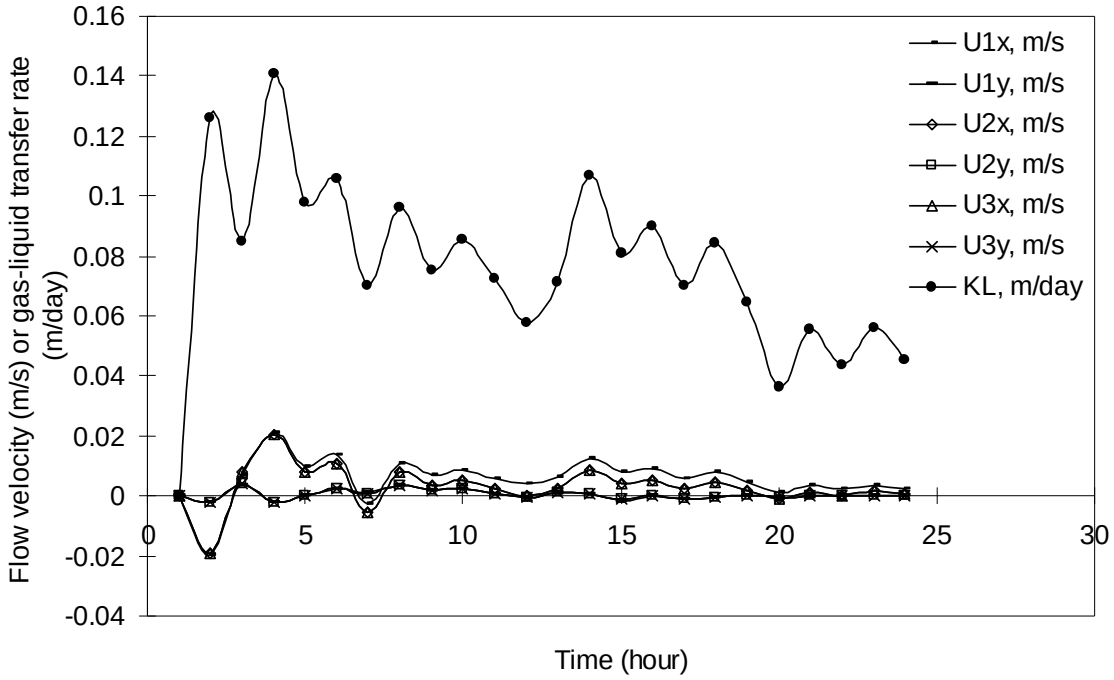

U1x = flow velocity at x direction in layer 1; U1y = flow velocity at y direction in layer 1; U2x = flow velocity at x direction in layer 2; U2y = flow velocity at y direction in layer 2; U3x = flow velocity at x direction in layer 3; U3y = flow velocity at y direction in layer 3; and KL = gas-liquid transfer rate.

Figure 6.16. Gas-liquid transfer rate and flow velocity as functions of time at location (6,19) (Figure 6.12)

6.2.3.5. Gas-liquid transfer rate in tidal river

The gas-liquid transfer rate and flow velocity as functions of time at location (3,27) (Figure 6.12) are displayed in Figure 6.17. The flow velocity has tidal wave characteristics, which shows that the effects of tide are significant. The period of the wave is about 20% of that in the estuary outlet. Thus, the gas-liquid transfer rate varies much more dramatically with the flow velocity.

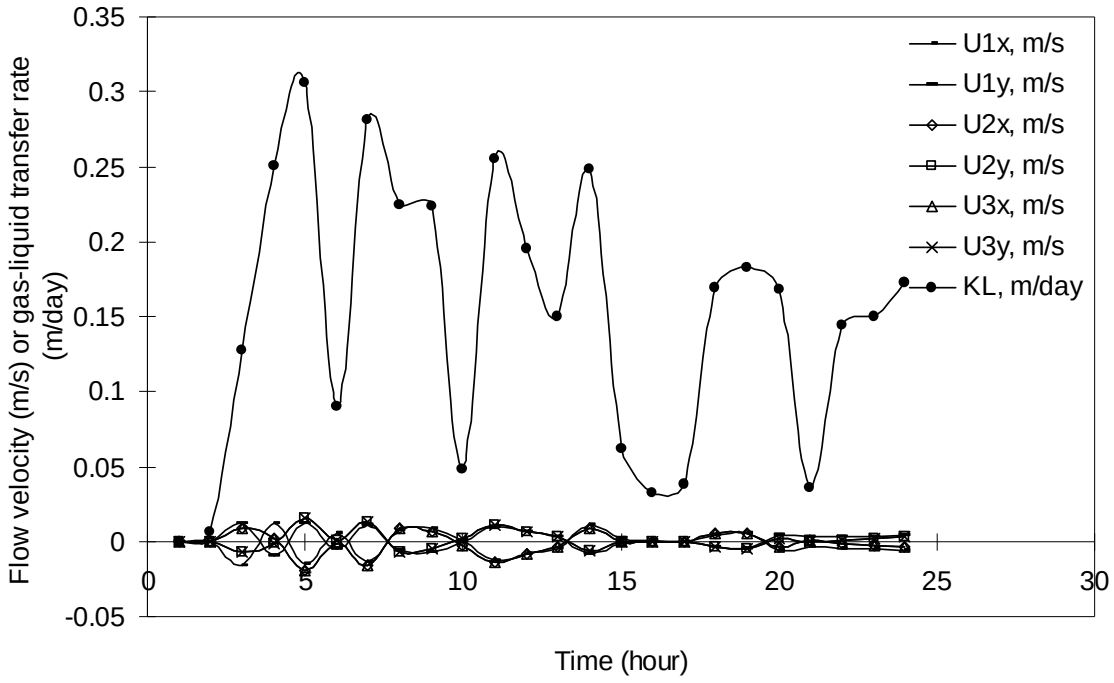

U1x = flow velocity at x direction in layer 1; U1y = flow velocity at y direction in layer 1; U2x = flow velocity at x direction in layer 2; U2y = flow velocity at y direction in layer 2; U3x = flow velocity at x direction in layer 3; U3y = flow velocity at y direction in layer 3; and KL = gas-liquid transfer rate.

Figure 6.17. Gas-liquid transfer rate and flow velocity as functions of time at location (3,27) (Figure 6.12)

The gas-liquid transfer rate and flow velocity as functions of time at location (6,27) (Figure 6.12) are displayed in Figure 6.18. The flow velocity also has significant tidal wave characteristics, but both the gas-liquid transfer rate and flow velocity in river 2 are different from those in river 1 as Figure 6.17 shows though they are located at the same distance from the estuary entry, which may be caused by the difference of the physical characteristics of River 1 and River 2.

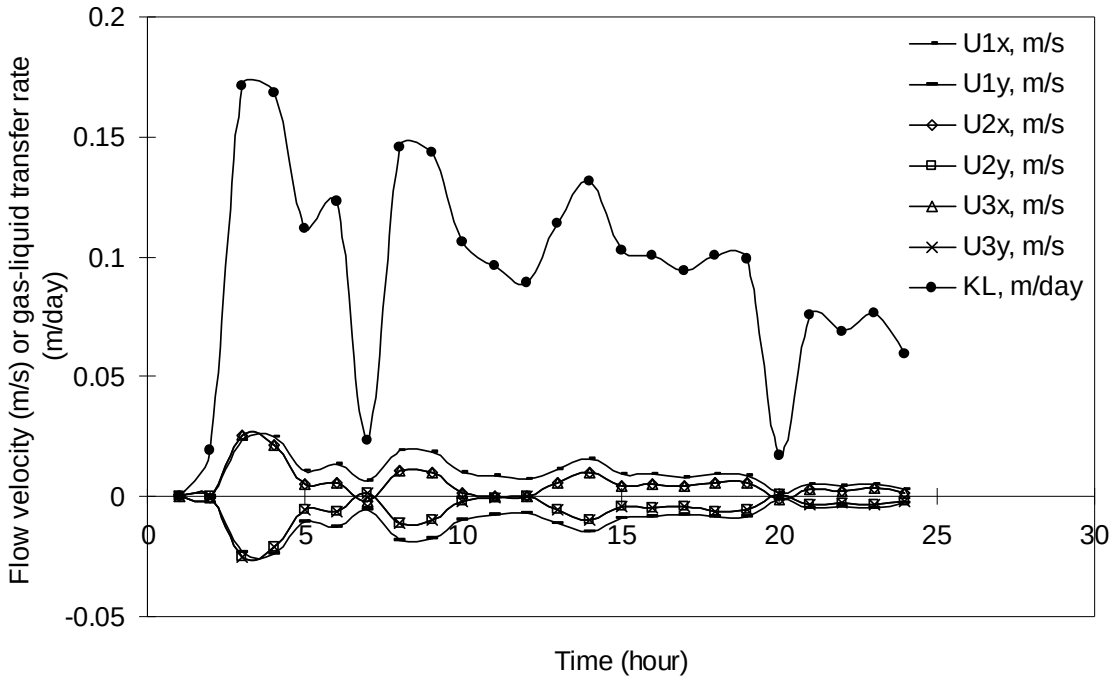

U1x = flow velocity at x direction in layer 1; U1y = flow velocity at y direction in layer 1; U2x = flow velocity at x direction in layer 2; U2y = flow velocity at y direction in layer 2; U3x = flow velocity at x direction in layer 3; U3y = flow velocity at y direction in layer 3; and KL = gas-liquid transfer rate.

Figure 6.18. Gas-liquid transfer rate and flow velocity as functions of time at location (6,27) (Figure 6.12)

6.2.3.6. Gas-liquid transfer rate in non-tidal river

The gas-liquid transfer rate and flow velocity as functions of time at location (5,50), (5,60), (5,70), (5,80), (5,90), and (5,102) (Figure 6.12) are displayed in Figure 6.19-6.24 respectively. With the increase of the distance from the estuary entry, the tidal wave characteristics in the flow decreased until they were completely lost. Thus, the turbulence generated from the water-bed interface becomes the dominant driving force of the gas-liquid transfer. The flow becomes slow when it goes from the rivers to the estuary as the water width increases. Figures 6.19-6.24 show that with the increase in distance from the estuary entry, the flow velocity magnitude increases from 0.05 m/s to 0.2 m/s which causes the gas-liquid transfer rate to increase from 0.37 m/day to 1.8 m/day.

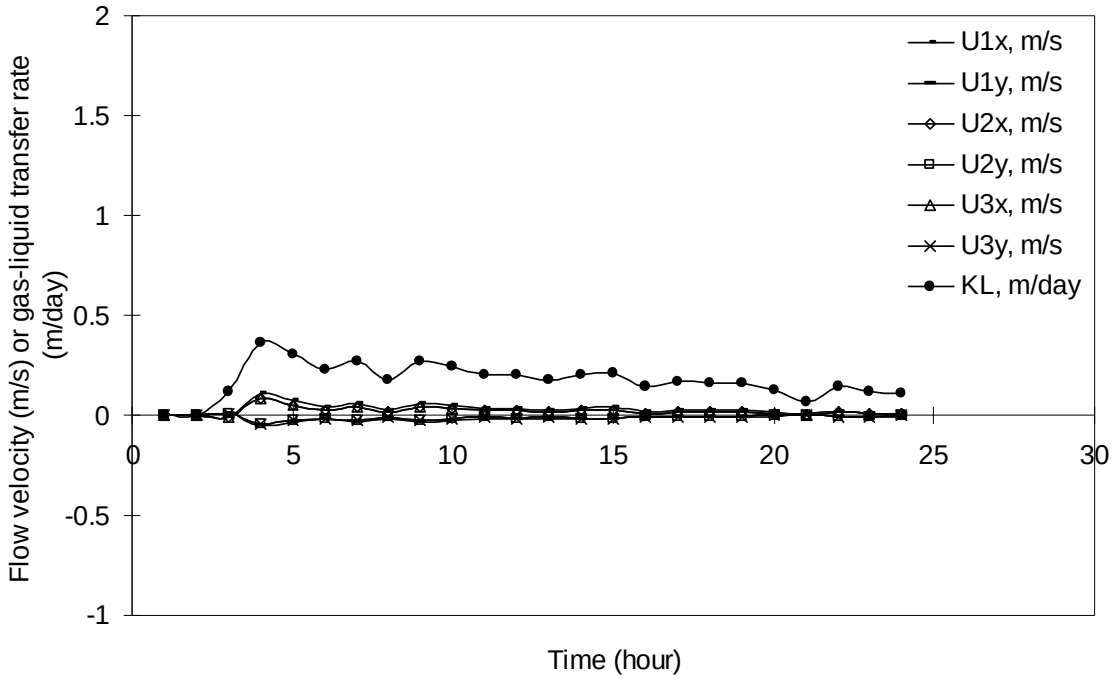

U1x = flow velocity at x direction in layer 1; U1y = flow velocity at y direction in layer 1; U2x = flow velocity at x direction in layer 2; U2y = flow velocity at y direction in layer 2; U3x = flow velocity at x direction in layer 3; U3y = flow velocity at y direction in layer 3; and KL = gas-liquid transfer rate.

Figure 6.19. Gas-liquid transfer rate and flow velocity as functions of time at location (5,50) (Figure 6.12)

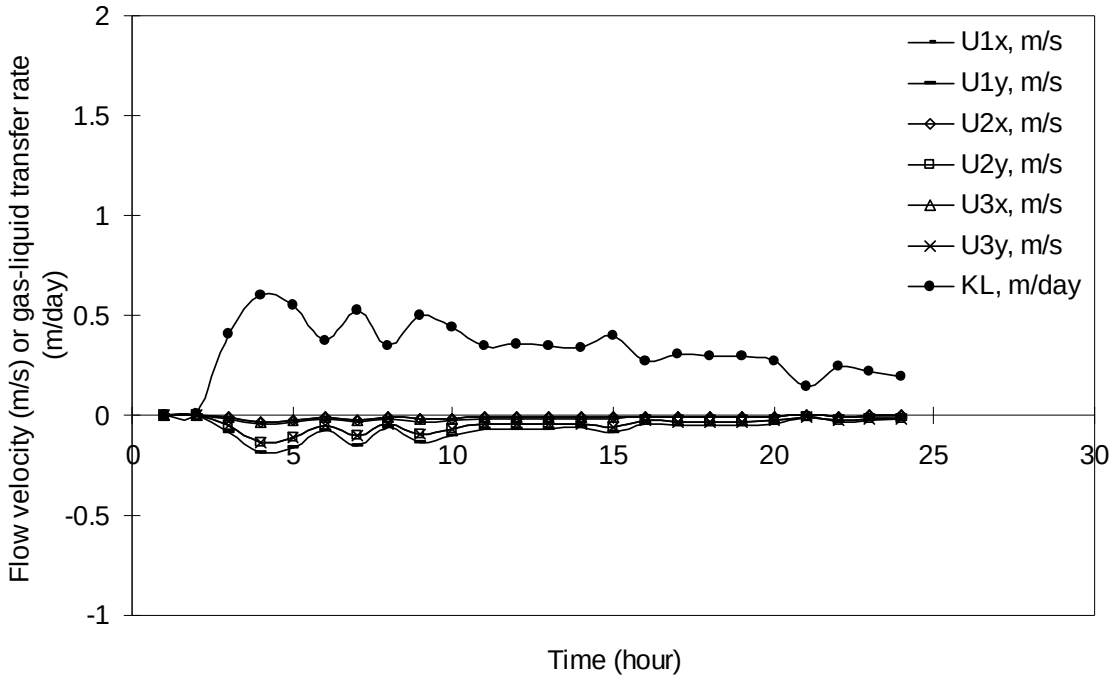

U1x = flow velocity at x direction in layer 1; U1y = flow velocity at y direction in layer 1; U2x = flow velocity at x direction in layer 2; U2y = flow velocity at y direction in layer 2; U3x = flow velocity at x direction in layer 3; U3y = flow velocity at y direction in layer 3; and KL = gas-liquid transfer rate.

Figure 6.20. Gas-liquid transfer rate and flow velocity as functions of time at location (5,60) (Figure 6.12)

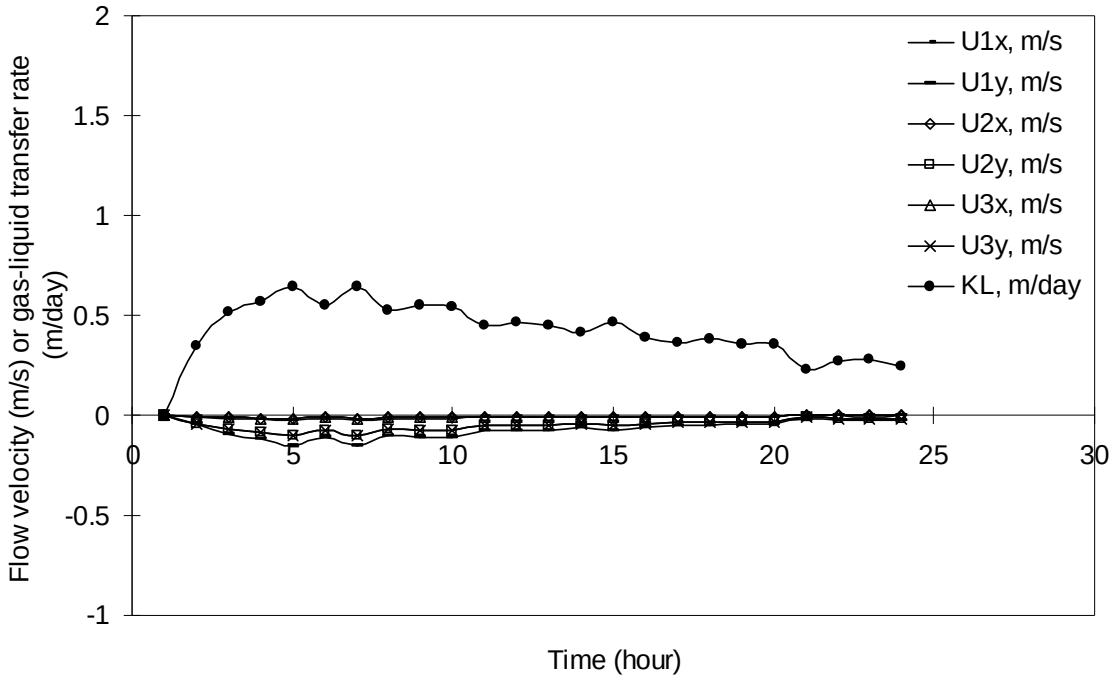

U1x = flow velocity at x direction in layer 1; U1y = flow velocity at y direction in layer 1; U2x = flow velocity at x direction in layer 2; U2y = flow velocity at y direction in layer 2; U3x = flow velocity at x direction in layer 3; U3y = flow velocity at y direction in layer 3; and KL = gas-liquid transfer rate.

Figure 6.21. Gas-liquid transfer rate and flow velocity as functions of time at location (5,70) (Figure 6.12)

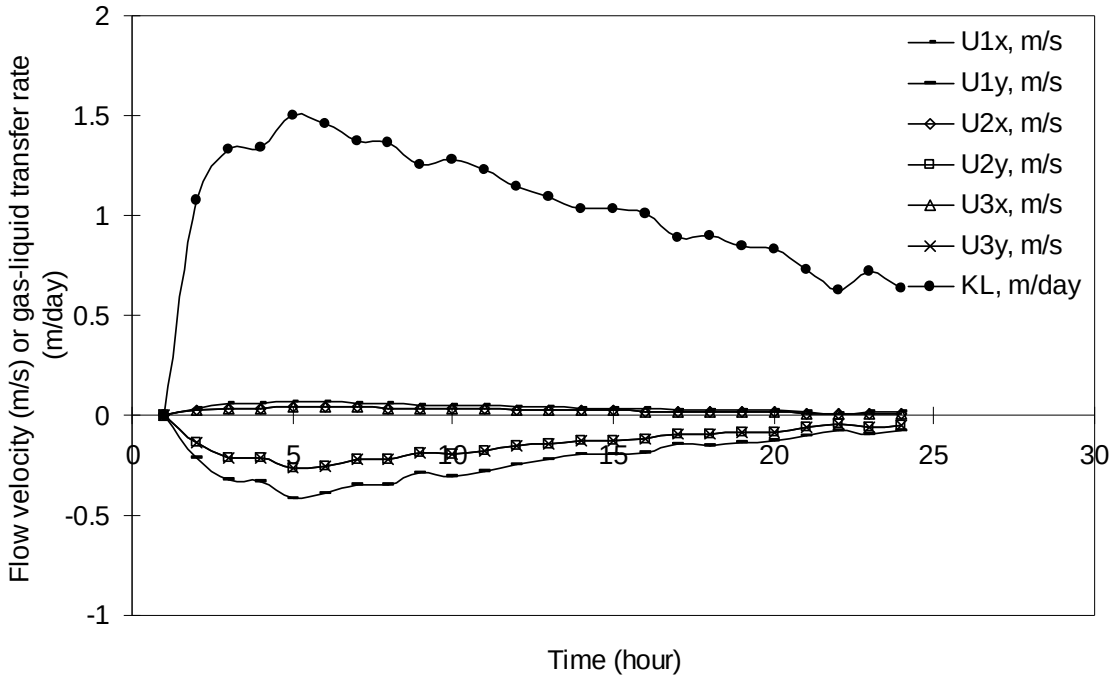

U1x = flow velocity at x direction in layer 1; U1y = flow velocity at y direction in layer 1; U2x = flow velocity at x direction in layer 2; U2y = flow velocity at y direction in layer 2; U3x = flow velocity at x direction in layer 3; U3y = flow velocity at y direction in layer 3; and KL = gas-liquid transfer rate.

Figure 6.22. Gas-liquid transfer rate and flow velocity as functions of time at location (5,80) (Figure 6.12)

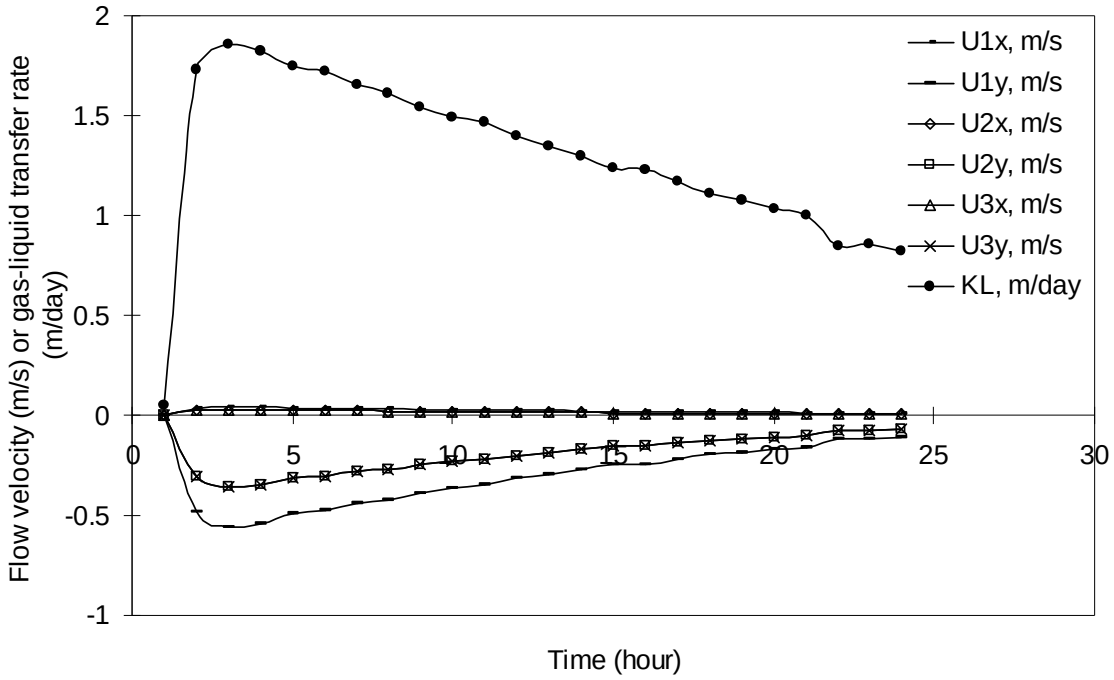

U1x = flow velocity at x direction in layer 1; U1y = flow velocity at y direction in layer 1; U2x = flow velocity at x direction in layer 2; U2y = flow velocity at y direction in layer 2; U3x = flow velocity at x direction in layer 3; U3y = flow velocity at y direction in layer 3; and KL = gas-liquid transfer rate.

Figure 6.23. Gas-liquid transfer rate and flow velocity as functions of time at location (5,90) (Figure 6.12)

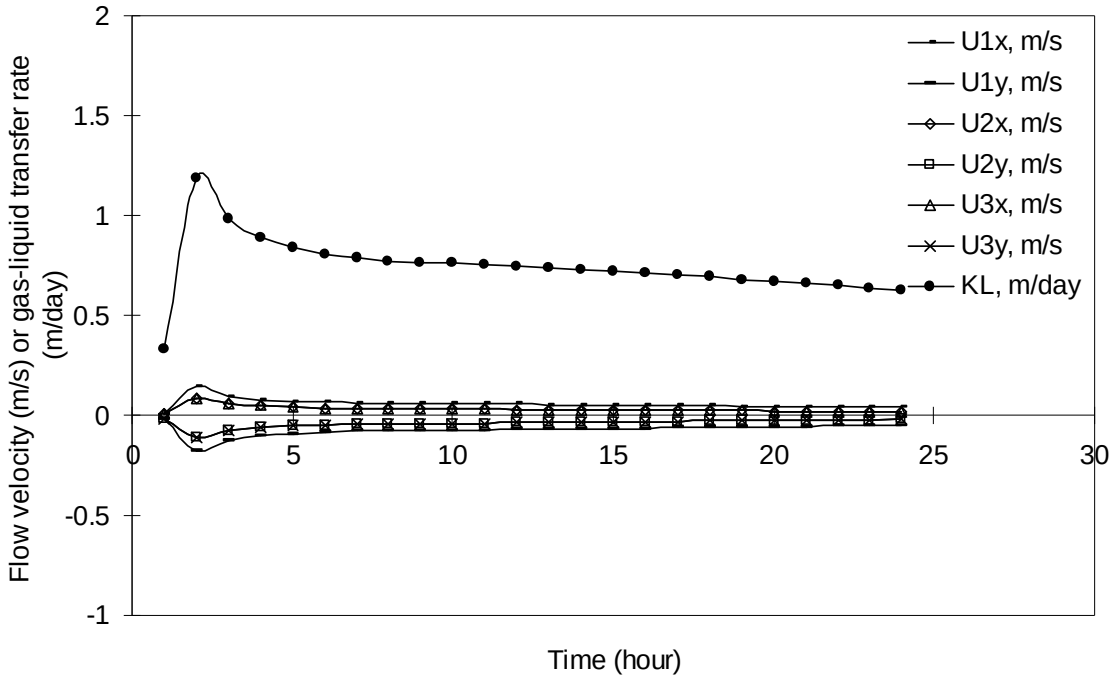

U1x = flow velocity at x direction in layer 1; U1y = flow velocity at y direction in layer 1; U2x = flow velocity at x direction in layer 2; U2y = flow velocity at y direction in layer 2; U3x = flow velocity at x direction in layer 3; U3y = flow velocity at y direction in layer 3; and KL = gas-liquid transfer rate.

Figure 6.24. Gas-liquid transfer rate and flow velocity as functions of time at location (5,102) (Figure 6.12)

6.2.4. Conclusions

The hydrodynamic model EFDC was used to simulate the dynamic flow field in the tidal Savannah Estuary based upon an application by Tetra Tech, Inc. (2002). A FORTRAN program were written based on the model of gas-liquid transfer rate in wind and dynamic three-dimensional flow systems developed in section 6.1. With the outputs

from the EFDC model including the water depth and flow velocities, the KL program predicted the gas-liquid transfer rate values on the surface of each gridded water column throughout the Savannah Estuary in multiple time steps. The application demonstrated that the space distribution and dynamic change of the gas-liquid transfer rate in tidal water bodies can be simulated with the combined applications of the EFDC and the FORTRAN program developed in this study. The statistical results of the calculated values showed they are reasonable since they are in the value level from 0.01 to 10 m/day as stated at the beginning of section 6.1.3.

CHAPTER VII

CONCLUSIONS

This study developed a series of gas-liquid transfer rate models in wind and water flow systems from the simple stream-driven gas-liquid transfer rate model to the more complex wind-stream-driven gas-liquid transfer rate model and then to the most complex gas-liquid transfer rate model for wind and dynamic three-dimensional flow systems.

In section 3.2, a model of gas-liquid transfer rate in non-isotropic turbulent flows was developed to explore why the theoretical formulae of gas-liquid transfer rates in isotropic turbulent flows have much lower predictions in non-isotropic turbulent flows than the empirical formulae. The non-isotropic turbulent flows are mainly composed of turbulent boundary layers. The shear velocity and mixing length in non-isotropic turbulent flows are different from those in isotropic turbulent flows. Thus, both the turbulence generated from the water-bed interface and the air-water interface have significant contributions to the gas-liquid transfer rate in non-isotropic turbulence.

In section 3.3, based on the model of gas-liquid transfer rate in non-isotropic turbulent flows, general expressions were constructed for shear velocity and mixing length in both non-isotropic turbulent flows and isotropic turbulent flows. Then, a general

stream-driven gas-liquid transfer rate model (named as Stream-driven KL Model) was developed with these expressions to cover the normal ranges of water depth and flow velocity in natural rivers, namely to cover both the non-isotropic turbulent flows and isotropic turbulent flows. The existing formulae need to be combined in applications for different ranges of water depth and flow velocity. Nevertheless, the establishment of the general model can simplify the engineering applications of reaeration expressions for one-dimensional streams and rivers. The comparisons of the predictions of this model with the experimental data and empirical formulae showed that this model has reasonable predictions.

In natural environments, both wind and stream have combined effects on gas-liquid transfer. For some simple cases, only one factor is dominant and thus the other one is ignored. For example, stream-driven turbulence is the main driving force of gas-liquid transfer in one-dimensional streams; thus, wind can often be ignored. Wind-driven turbulence is typically the main driving force of gas-liquid transfer in slow moving water bodies such as lakes; thus streamflow may often be ignored. However, in some water bodies such as estuaries, wind and streamflow both have important effects on gas-liquid transfer, and their effects need to be incorporated into the gas-liquid transfer rate model. In Chapter 4, based on the concepts of shear velocity, roughness, viscous layer, arithmetic accumulation of surface renewal rates, and the theories of Surface Renewal Theory and turbulent boundary layer theory, a wind-stream-driven gas-liquid transfer rate model

(Wind-stream-driven KL Model) is developed. This model is tested in wind-driven systems, stream-driven systems, and wind-stream-driven systems and showed reasonable predictions compared with the experimental data and empirical formulae.

The most complex cases occur in the wind and dynamic three-dimensional flow systems such as tidal estuaries. The employment of average water flow velocity and total water depth will lead to problematic results. The dynamic change of flow fields needs to be incorporated into the gas-liquid transfer rate model.

Surface renewal rates are caused by turbulence generated from three types of turbulence source locations including water-bed interface, air-water interface, and transition location of shear flows. The surface renewal rate for water-bed interface has been explored in the stream-driven model. The surface renewal rate for air-water interface has been explored in the wind-stream-driven model. But the surface renewal rate caused by turbulence from transition location of shear flows only exists in three-dimensional flows and is not considered in the simpler stream-driven or wind-stream-driven systems. Thus, the model of gas-liquid transfer rate driven by the turbulence from the transition location of shear flows is developed in Chapter 5. As the transition location of shear flows does not exist alone in water bodies (i.e., it cannot be isolated), the related gas-liquid transfer rate model cannot be directly tested with the experimental data. Thus, an indirect method is used for the test. The shear velocity, shear stress, surface renewal rate, and gas-liquid transfer rate for the transition location of shear

flows are compared with those for air-water interface and water-bed interface with the same water flow velocity or wind speed. As the turbulence generated from the transition location of shear flows should be greater than that generated from the air-water interface and less than that generated from water-bed interface with the same water flow velocity or wind speed, as the surface renewal rate model for transition location of shear flows was considered to have reasonable predictions if the shear velocity, shear stress, surface renewal rate, and established gas-liquid transfer rate for transition location of shear flows were between those for air-water interface and water-bed interface. A theoretical surface renewal rate model for transition location of shear flows is developed by using the flow velocity profile in shear flows and the Surface Renewal Theory and the turbulent boundary layer theory. A series of comparisons are done for low wind speed, high wind speed, low water flow velocity, and high water flow velocity and these comparisons showed that this model has reasonable predictions.

Based on the surface renewal rate model for transition location of shear flows, the formulae of surface renewal rate for the air-water interface, and that for the water-bed interface, a gas-liquid transfer rate model for wind and dynamic three-dimensional flow systems (named as Wind-dynamic-3D-flows-driven KL Model) was developed in Chapter 6. As complex algorithms are used in finding the efficient horizontal interface and incorporating the effects of dynamic change of flow fields, a computer program was written to implement this model for applications. A FORTRAN program named as KL

program was coded and applied to various cases from the simple one-dimensional uniform flow systems to the complex wind and dynamic three-dimensional flow systems (Appendix B). The calculated gas-liquid transfer rate values were found to be reasonable.

The series models have increased capabilities to predict gas-liquid transfer rate in wind and water flow systems. But at the same time, their computation complexity also increases. In other words, the more complex the wind and water flow systems are, the more complex the models are and the more complexity the computations have. A specific model can be selected from the series of models as presented in this study for a specific application based on the application requirements and the acceptable computation complexity.

The hydraulic parameters such as the effective thickness coefficient of overlap layer have effects on the predictions of gas-liquid transfer rate in the wind-driven systems. In this study, its value is adjusted for specific case according to the experimental data or empirical formulae. However, the theoretical determination of its value is still not clear. It is found that the equivalent thickness coefficients of overlap layer in laboratory scale are greater than those in field scale; but it is not certain if this is a general situation. Further studies need to focus on these issues.

REFERENCES

Asher, W. E., Wang, Q., Monahan, E. C., and Smith, P. M. (1998). "Estimation of air-sea gas transfer velocities from apparent microwave brightness temperature", *Mar. Tech. Soc. J.*, 32, 32-40.

Asher, W. E., and Wanninkhof, R. (1998). "Transient tracers and air-sea gas exchange", *J. Geophys. Res.*, 103C, 15,939-15,958.

Asher, W. E., and Wanninkhof, R. (1998), "The effect of bubble-mediated gas transfer on purposeful dual-gaseous tracer experiments." *J. Geophys. Res.*, 103(C5), 10,555-10,560.

Asher, W. E., Farley, P. J., Wanninkhof, R., Monahan, E. C., and Bates, T. S. (1992). "Laboratory and field measurements concerning the correlation of fractional area foam coverage with air/sea gas transport." *Proc., Precipitation Scavenging and Atmosphere-Surface Exchange, Volume 2-The Semonin Volume: Atmosphere-Surface Exchange Processes*, S. E. Schwartz and W. G. N. Slinn, eds., Hemisphere, Washington D.C., 815-828.

Asher, W. E., and Farley, P. J. (1995). "Phase-Doppler anemometer measurement of bubble concentrations in laboratory-simulated breaking waves", *J. Geophys. Res.*, 100C: 7045-7056.

Asher, W. E., Edson, J. B., McGillis, W. R., Wanninkhof, R., Ho, D. T., and Litchendorf, T. M. (2001). "Fractional area whitecap coverage and air-sea gas transfer velocities measured during GasEx-98", *Proc., Gas Transfer at Water Surfaces*, edited by M. A. Donelan, W. M. Drennan, E. S. Saltzman, and R. Wanninkhof, AGU.

Atkinson, J. F. (1995). "Surface Aeration." *J. Envir. Engrg.*, 121(1), 113-118.

Banerjee, S., Eaton, J. K. (1999). "Turbulence and Shear Flow Phenomena." Proc., First International Symposium, September 12-15, Santa Barbara, California.

Banerjee, S., Lakehal, D., Fulgosi, M. (2004). "Surface divergence models for scalar exchange between turbulent streams." *International Journal of Multiphase Flow*, 30, 963-977.

Banerjee, S., Rhodes, E., Scott, D.S. (1968). "Mass transfer to falling wavy liquid films in turbulent flow." *Ind. Eng. Chem. Fundam.*, 7, 22-27.

Banerjee, S. (1990). "Turbulence Structure and Transport Mechanisms at Interfaces, Keynote Lecture." *Proc., 9th Int. Heat Transfer Conf.*, Hemisphere Press, NY, 395-418.

Banks, R. B. (1975). "Some features of wind action on shallow lakes." *Proc. Am. Soc. Civ. Eng.*, 101, 813.

Boettcher, E. J., Fineberg, J., and Lathrop, D. P. (2000). "Turbulence and Wave Breaking Effects on Air-Water gas transfer." *Physical Review Letters*, 85, 2030-2033.

Bortkovski, R. S. (2002). "Atmosphere-ocean gas transfer due to bubbles generated by wind wave breaking." *Proc., Gas Transfer at Water Surfaces*, Ed. M. A. Donelan et al., Amer. Geophys. Un., Monograph Ser. 127, 261- 264.

Broecker, H. C., Petermann, J., and Siems, W. (1978). "The influence of wind on CO2-exchange in a wind-wave tunnel, including the effects of monolayers." *J. Marine Res.*, 36, 595-610.

Broecker, H. C. and Siems, W. (1984). "The role of bubbles for gas transfer from water to air at higher windspeeds. Experiments in the wind-wave facility in Hamburg." *Proc., Gas Transfer at Water Surfaces*, Kluwer Academic Publishers, Dordrecht, Holland, 229-236.

Cardone, V. J. (1969). "Specification of the wind distribution in the marine boundary layer for wave forecasting." *Report TR-69-01*, Geophysical Sciences Laboratory. New York University, New York, NY, 131 (Available from NTIS #AD 702-490, 137).

Chapra, S. C. (1997). *Surface water-quality modeling*, McGraw-Hill, New York, NY.

Chu, C. R. and Jirka, G. H. (1995). "Reaeration in combined wind/stream driven flows." *Proc., Air-Water Gas Transfer*, AEON Verlag and Studio, Hanau, Germany. 79-88.

Chu, C. R. and Jirka, G. H. (2003), "Wind- and Stream Flow-Induced Reaeration." *J. Environmental Engineering*, 129 (12), 1129-1136.

Churchill, M. A., Elmore, H. L., and Buckingham, R. A. (1962). "Prediction of stream reaeration rates." *J. San. Engr. Div. ASCE SA*, 4 (1), 3199.

Covar, A. P. (1976). "Selecting the Proper Reaeration Coefficient for Use in Water Quality Models." *Proc., U.S. EPA Conference on Environmental Simulation and Modeling*, Cincinnati, OH.

Danckwerts, P. V. (1953). "Continuous Flow Systems. Distribution of Residence Times." *Chem. Engr. Sci.*, 2, 1-13.

Danckwerts, P. V. (1970). *Gas Liquid Reactions*, McGraw-Hill, New York, NY .

Danckwerts, P. V. (1951). "Significance of Liquid-Film Coefficients in Gas Absorption." *Ind. Eng. Chem.*, 43(6), 1460-1467.

Deacon, E. L. (1977). "Gas transfer to and across an air–water interface." *Tellus*, 29, 363-374.

Donelan, M. A. and Wanninkhof, R. (2002). "Gas Transfer at Water Surfaces-Concepts and Issues." *Chapter in Gas Transfer at Water Surfaces*, Geophysical Monograph #127, American Geophysical Union, 1-10.

Donelan, M. A., Wanninkhof, C. R., Muhammad, S., William, H. K., Peirson, L. (2001). "Gas Transfer at Water Surfaces." *Proc., Air-Water Gas Transfer*, Donelan, M. A., and W. M. Drennan, E. S. Saltzman, R. Wanninkhof, eds.

Downing, A. L. and Truesdale, G. A. (1955). "Some factors affecting the rate of solution of oxygen in water." *Journal of Applied Chemistry*, 5, 570-581.

Dulov, V. A., Kudryavtsev, V. N., and Bol'shakov, A. N. (2001). "A field study of whitecap coverage and its modulations by energy containing surface waves." *Proc., Air-Water Gas Transfer*, Donelan, M.A., and W. M. Drennan, E. S. Saltzman, R. Wanninkhof, eds.

Eckenfelder W. W. (1959). "Factors affecting the aeration efficiency." *Sewage ind. Wastes*, 31, 61-70.

Eloubaidy, A. F., and Plate, E. J. (1972). "Wind shear turbulence and reaeration coefficient." *J. Hydraul. Div., Am. Soc. Civ. Eng.*, 98, 153-170.

EPA. (2007). "Environmental Fluid Dynamics Code (EFDC)." *Ecosystems Research Division*, <http://www.epa.gov/ATHENS/wwqtsc/html/efdc.html> (February 22, 2007).

Feely, R., Wanninkhof, A., R., Hansell, D. A., Lamb, M. F., Greeley, D., and Lee, K. (2001). "Water column CO_2 measurements during the gas Ex-98 expedition." *Proc., Air-Water Gas Transfer*, Donelan, M.A., and W. M. Drennan, E. S. Saltzman, R. Wanninkhof, eds.

Fortescue, G. E., Pearson, J. R. A. (1967). "On gas absorption into a turbulent liquid." *Chemical Engineering Science*, 22, 1163-1176.

Gortler, H. (1942). "Berechnung von Aufgaben der freien Turbulenz auf Grund eines neuen Naherungsansatzes." Z. Angew. Math. Mech., 22, 244-254.

Gulliver, J. S., and Stefan, H. G. (1984). "Prediction of non-reactive water surface gas exchange in streams and lakes." *Proc., Gas Transfer at Water Surface*, D. Reidel Publishing Co., Boston, MA.

Hamada, T. (1953). "Density Current Problems in an Estuary." *Proc., Minnesota International hydraulics Convention*, Minneapolis, MN.

Hara, T., B. M. Uz, H. Wei, J. B. Edson, N. M. Frew et al. (2001). "Surface wave and air-sea gas transfer during CoOP experiment." *Proc., Gas Transfer at Water Surfaces*, edited by M. A. Donelan, W. M. Drennan, E. S. Saltzman and R. Wanninkhof, AGU.

Higbie, R. (1935). "The Rate of Adsorption of a Pure Gas into a Still Liquid during Short Periods of Exposure." *Trans. Amer. Inst. Chem. Eng.*, 31, 365-389.

Ho, D. T., Asher, W. E., Schlosser, P., Bliven, L. and Gordon, E. (2000). "On the mechanisms of rain-induced air-water gas transfer." *J. Geophys. Res.*, 105 : 24,045-24,057.

Hunt, J. C. R., Graham, J. M. R. (1978). "Free stream turbulence near plane boundaries." *J. Fluid Mech.*, 84, 209-235.

Inhoff, K., and Fair, G. M. (1956). *Sewage Treatment* (2nd end.), John Wiley & Sons, New York, NY, 338.

Jahne, R., Munnich, K.O., and Siegeuthaler, U. (1979). "Measurements of gas exchange and momentum transfer in a circular wind-water tunnel." *Tellus*, 31, 321.

Jean-Baptiste, P., Fourre, E., and Poisson, A. (2001). "Gas transfer velocities for 3He in lake at high wind speeds." *Proc., Air-Water Gas Transfer*, Donelan, M.A., and W. M. Drennan, E. S. Saltzman, R. Wanninkhof, eds.

Kalinske, A. A. (1943). "The Role of Turbulence in River Hydraulics." *Bulletin 27, Proc., The 2nd Hydraulics Conference*, Univ. of Iowa Studies in Engineering., Iowa City, IA, 266-279.

Kanwisher, J. (1963). "On the exchange of gases between the atmosphere and the sea." *Deep-Sea Res.*, 10, 195–207.

Kato, H., Nobuoka, H., and Ooshima, N. (2001). "Measurements of wind-driven current near the water surface by the use of the PTV method." *Proc., Air-Water Gas Transfer*, Donelan, M. A., and W. M. Drennan, E. S. Saltzman, R. Wanninkhof, eds.

Keeling, R. F. (1993). "On the role of large bubbles in air-sea gas transfer and supersaturation in the ocean." *J. Mar. Res.*, 51, 237-271.

Kerman, B. R. (1984). "Underwater sound generation by breaking wind waves", *J. Acoust. Soc. Am.*, 75 (1), 149-165.

Komori, S. and Misumi, R. (2001). "The effects of bubbles on mass transfer across the breaking air–water interface." *Proc., Gas Transfer at Water Surfaces*, edited by M. A. Donelan, W. M. Drennan, E. S. Saltzman and R. Wanninkhof, AGU.

Kumar, S., Gupta, R., Banerjee, S. (1998). "An experimental investigation of the characteristics of free-surface turbulence in channel flow." *Phys. Fluids*, 10, 437-456.

Lamont, J. C. and Scott, D. S. (1970). "An eddy cell model of mass transfer into the surface of a turbulent liquid." *A.I.Ch.E.Jl.*, 16, 513-519.

Langbein, W. B. and Durum, W. J. (1967). "The aeration of streams." *Proc., U.S. Geological Survey Circular No. 542*. U.S. Geological Survey, Reston, Virginia.

Lee, G. Y., and Gill, W. N. (1977). “Note on velocity and eddy viscosity distributions in turbulent shear flows withfree surfaces." *Chem. Eng. Sci.*, 32, 967.

Lewis, W. K., and Whitman, W. G. (1924). “Principles of Gas Absorption.” *Ind. Eng. Chem.*, 16(12), 1215-1220.

Lide, D. R. (2000). *CRC Handbook of Chemistry and Physics: Version 2000*, Chapman & Hall/CRC, New York, NY.

Liss, P. S., Merlivat, L. (1986). “Air-sea gas exchange rates: introduction and synthesis”. *Proc., The Role of Air-Sea Exchange in Geochemical Cycling*, Norwell, MA, 113-129.

Macintyre, S., Wanninkhof, R. H. and Chanton, J. P. (1995). “Trace gas transfer across the air-water interface in freshwater and coastal marine environments.” *In Methods in ecology-biogenic trace gases: Measuring emissions from soil and water* (ed. P. A. Matson and R. C. Harris), 52. New York, Blackwell Science.

Martin, J. L. and Kennedy, R. H. (2000). “Total Maximum Daily Loads (TMDLs): A Perspective.” *DOTS Technical Note, 20, ERDC/TN EEDP-01-46*, ERDC Waterways Experiment Station, Vicksburg, MS.

McCready, M. J., Vassilliadou, E., and Hanratty, T. J. (1986). “Computer simulation of turbulent mass transfer at a mobile interface.” *AIChE J.*, 32, 1108-1115.

McKenna, S. P., McGillis, W. R. (2004). “The role of free-surface turbulence and surfactants in air-water gas transfer.” *International Journal of Heat and Mass Transfer*, 47, 539-553.

Merlivat, L., Memery, L. and Boutin, J. (1993). “Gas transfer at the air-sea interface: present status. Case of CO_2.” *Presented at the 4th International Conference on CO_2*, Carquerainne, France, 13-17.

Memery, L., and Merlivat, L. (1983). “Gas exchange across an air-water interface: experimental results and modelling of bubble contribution to transfer.” *J. Geophys. Res.*, 88, 707−724.

Mills, A. F., and Chung, D. K. (1973). “Heat-transfer across turbulent falling films.” *Int. J. Heat Mass Tran.*, 16, 694.

Monahan, E. C. (1986). "The ocean as a source of atmospheric particles." *Proc., The Role of Air- Sea Exchange in Geochemical Cycling*, P. Buat-Menard, ed., Kluwer Academic Publishers, Dordrecht, Holland, 129-163.

Monahan, E. C. and Spillane, M. C. (1984). "The role of oceanic whitecaps in air-sea gas transfer." *Proc., Gas Transfer at Water Surfaces*, W. Brutsaert and G. H. Jirka, eds., Kluwer Academic Publishers, Dordrecht, Holland, 495-503.

Moog, D. B., and Jirka, G. H. (1995). "Macroroughness effects on stream reaeration." *Proc., Air-Water Gas Transfer*, Jähne, B., and Monahan, E. C., eds.

Munson, B. R., Young, D. E., and Okiishi, T. H. (1994). *Fundamentals of fluid mechanics (2nd ed.)*. Wiley, New York, NY.

O'Connor, D. J., and Dobbins, W. E. (1956). "Mechanism of Reaeration in Natural Streams." *Trans. American Soc. of Civil Engrs.*, 123, 641-684.

O'Connor, D. J. (1983). "Wind effects on gas-liquid transfer coefficients." *J. Environ. Eng.*, 109(3), 731-752.

Ogston, A. S., Sherwood, C. R., and Asher, W. E. (1995). "Estimation of turbulence dissipation rates and gas transfer velocities in a surf pool: Analysis of the results from WABEX-93." *Proc., Air-Water Gas Transfer*, B. Jähne and E. C. Monahan, eds., Aeon Verlag, Hanau, 255-268.

Owens, M., Edwards, R., and Gibbs, J. (1964). "Some reaeration studies in streams." *Int. J. Air Water Poll.*, 8, 469-486.

Peirson, W. L., and Banner, M. L. (2001). "On the surface kinematics of microscale breaking wind waves." *Proc., Air-Water Gas Transfer*, Donelan, M. A., and W. M. Drennan, E. S. Saltzman, R. Wanninkhof, eds.

Peirson, W. L., and Banner, M. L. (2003). "Aqueous surface layer flows induced by micro-breaking wind waves." *J. Fluid Mech.*, 479, 1-38.

Prandtl, L. (1925). "Uber die ausgebildete Turbulenz." *Z. Angew. Math. Mech.*, 5, 136-139.

Reynolds, A. J. (1974). *Turbulent Flows in Engineering*, John Wiley, London/New York.

Richardson, S. M. (1989). *Fluid Mechanics*, Taylor & Francis, London/New York.

Ross, D. B., and Cardone, V. (1974). "Observations of oceanicwhitecaps and their relation to remote measurements ofsurface wind speed." *Journal of Geophysical Research*, 79, 444-452.

Rubin, H. and Atkinson, J. (2001). *Environmental Fluid Mechanics*, Marcel Dekker, New York, NY.

Schijf, J. B., Schonfeld, J. T. (1953). "Theoretical Considderations of the Motion of Salt and Fresh Water." *Proc., Minnesota International hydraulics Convention*, Minneapolis, MN.

Scott, J. C. (1975). "The preparation of water for surface-clean fluid mechanics." *J. Fluid Mech.*, 69, 339-351.

Scott, C. (2007). "Conway Estuary - Flood Tide Simulation." http://www-staff.lboro.ac.uk/-cvcfs/simulations/estuarinedynamics/flood.html (February 26, 2007)

Siddiqui, M., Mark, H. K., Loewen, R., Richardson, C., Asher, W. E., and Jessup, A. T. (2001). "Turbulence Generated by Microscale Breaking Waves and Its Influence on Air-Water Gas Transfer." *Proc., Air-Water Gas Transfer*, Donelan, M. A., and W. M. Drennan, E. S. Saltzman, R. Wanninkhof, eds.

Stevens, Craig L., Smith, M. J., and McGregor, J. A. (2001). "Estimation of whitecap coverage percentage using shallow grazing-angle video and FMICW Radar." *Proc., Air-Water Gas Transfer*, Donelan, M. A., and W. M. Drennan, E. S. Saltzman, R. Wanninkhof, eds.

Tetra Tech, Inc. (2002). *User's Manual for Environmental Fluid Dynamics Code Hydro Version (EFDC-Hydro) Release 1.00*, Fairfax, VA.

Thames Survey Committee. (1964). "Effects of polluting dischargeson the Thames estuary." *Water Pollution Research Technical Paper No. 11.*, Thames Survey Committee and the Water Pollution Research Laboratory, London, U.K.

Thorpe, S. A. (1982). "On the clouds of bubbles formed by breaking wind-waves in deep water, and their role in air-sea gas transfer." *Phil. Trans. R. Soc.*, London, A304, 155-210.

Thorpe, S. A. (1986). “Measurements with an automatically recording inverted echo sounder; ARIES and the bubble clouds.” *J. Phys. Oceanogr.*, 16, 1462-1478.

Thorsen, T. A. (1999). “The sea-surface microlayer and its role in global change.” *GESAMP Reports and Studies*, No. 59, <http://www.gesamp.imo.org/no59/intro.htm> (July 15, 2006).

Townsend, A. A. (1956). *The Structure of Turbulent Shear Flow*s, Cambridge University Press, Cambridge.

Wanninkhof, R. (1992). “Relationship between wind speed and gas exchange over the ocean.” *J. Geophys. Res.*, 97, 7373-7382.

Wanninkhof, R. H., and McGillis, W. R. (1999). “A cubic relationship between air–sea CO2 exchange and gas speed.” *Geophys. Res. Lett.*, 26, 1889-1892.

Weber, W. J. Jr. (2001). *Environmental Systems and Processes: Principles, Modeling, and Design*, Wiley-interscience, New York, NY.

White, F. M. (2006). *Viscous Fluid Flow (3rd ed.)*, McGraw-Hill, New York, NY.

Whitman, W. G. (1923). “The two-film theory of gas absorption.” *Chem. Metallurg. Eng.*, 29(4), 146-148.

Wilcock, R. J. (1984). “Methyl chloride as a gas-tracer for measuring stream reaeration coefficients-II.” *Water Research*, 18, 53-57.

Wilcock, R. J. (1988). “Study of River Reaeration at Different Flow Rates.” *Journal of Environmental Engineering (ASCE) JOEDDU*, 114(1), 91-105.

Wilhelms, Steven C. (Editor), Gulliver, John S. (Editor) (1990). *Air-Water Mass Transfer: Selected Papers from the Second Informational Symposium on Gas Transfer at Water Surfaces*, Minneapolis, MN, 11-14.

Woolf, D. K. (2001). “Parameterization of Gas Transfer Velocities and Sea-State-Dependent Wave Breaking.” *Proc., Air-Water Gas Transfer*, Donelan, M. A., and W. M. Drennan, E. S. Saltzman, R. Wanninkhof, eds.

Woolf, D. K. (2001). “Gas transfer in energetic conditions.” *Proc., Air-Water Gas Transfer*, Donelan, M. A., and W. M. Drennan, E. S. Saltzman, R. Wanninkhof, eds.

Woolf, D. K. (1993). “Bubbles & the air-sea transfer velocity of gases.” *Atmosphere-Ocean*, 31, 517-540.

Woolf, D. K. (1995). “Energy dissipation through wave breaking and the air-sea exchange of gases.” *Proc., Air-water Gas Transfer*, Jahne, B., and Monahan, E. C. eds, AEON Verlag, Hanau, Germany, 185-195.

Woolf, D. K. (1997). “Bubbles and their role in gas exchange." Proc., The Sea Surface and Global Change (Liss, P. S., and Duce, R. A., eds), Cambridge University Press, Cambridge, 173-205.

Woolf, D. K. and Thorpe, S. A. (1991). “Bubbles and the air-sea exchange of gases in near- saturation conditions.” *J. Mar. Res.*, 49, 435-466.

Yaws, C. L. (1999). Chemical Properties Handbook, McGraw-Hill, New York, NY.

Zappa, C. J., Asher, W. E., Jessup, A. T., Klinke, J. and Long, S. R. (2001). “Effect of microscale wave breaking on air-water gas transfer.” *Proc., Air-Water Gas Transfer*, Donelan, M. A., and Drennan, W. M., Saltzman, E. S., Wanninkhof, R. eds.

Zappa, C. J., Asher, W. E., and Jessup, A. T. (2001). “Microscale wave breaking and air-water gas transfer.” *J. Geophys. Res.*, 106(C5), 9385-9392.

Zhao, D., Toba, Y., Suzuki, Y. and Kmori, S. (2003). “Effect of wind waves on air-sea gas exchange: proposal of an overall CO_2 transfer velocity formula as a function of breaking-wave parameter.” *Tellus*, 55B, 478-487.

APPENDIX A

SYMBOLS

English Symbols

a	wind-driven gas-liquid transfer rate constant coefficient
A	reaeration rate constant coefficient
b	bubble-mediated gas-liquid transfer rate constant coefficient
b	width of shear layers, m
B	reaeration rate constant coefficient
C	wind-driven gas-liquid transfer rate constant coefficient
C	gas concentration, kg/m^3
C	reaeration rate constant coefficient
d	bubble radius, m
D	diffusion coefficient, 2.09×10^{-9} m^2/s at 20^oC
F	bubble-mediated gas-liquid transfer rate constant coefficient
g	acceleration of gravity, 9.8 m/s^2
H	water depth, m
K	wind-driven gas-liquid transfer rate constant coefficient
K	coefficient of turbulent viscosity
N	gas flux, $kg/(m^2s)$
l	mixing length, m
r	surface renewal rate, s^{-1}

R	orifice radius, m
t	average contact time of water parcel at air-water interface, sec
t	surface renewal time, sec
U	characteristic velocity of flow, m/s
U	free stream velocity, m/s
W	wind speed, m/s
x	axial distance, m
x	distance to air-water interface, m
x	Schmidt number dependent that is -2/3 for smooth surfaces and -1/2 for rough surfaces
x	streamwise coordinate tangential to the moving interface, m
y	axial distance, m
y	distance to the two-phase interface or the transition location of shear flows, m
y	spanwise coordinate tangential to the moving interface
z	roughness thickness, m
z	surface-normal coordinate
z	normal coordinate
z	argument of the error function

Greek Symbols

α	roughness coefficient
α	wind speed constant coefficient
δ	thickness of turbulent boundary layer, m
σ	surface tension, N/m
σ	constant coefficient of distance from the fraction interface
Γ	equivalent coefficient of viscous layer thickness
κ	von Karman constant, 0.41
ν	kinematic viscosity, 1 x 10^{-6} m^2/s at 20^{o}C
ρ	density, kg/m^3
Λ	flow characteristic length, m
ε	energy dissipation rate, m^2/s^3
τ	shear stress, N/m^2
γ	streamwise coordinate tangential to the moving interface

Symbol Groups

C_a	gas concentration in air, kg/m^3
C_b	gas concentration in water bulk, kg/m^3
C_D	drag coefficient
C_f	skin-friction coefficient

C_{f1} skin-friction coefficient at air-water interface

C_{f2} skin-friction coefficient at water-bed interface

C_i gas concentration at air-water interface, kg/m^3

C_l liquid concentration in the liquid bulk, kg/m^3

C_r effective coefficient of the surface renewal rate at water-bed interface

C_s concentration at air-water interface, kg/m^3

C_{sv} coeffcient of equivalent vertical fluctuation velocity

C_w concentration in water, kg/m^3

d_B bubble diameter, m

D_f the frictional drag, N

H_e Henry's law constant, $mol/(m^3atm)$

H_w wave height, m

K_L gas-liquid transfer rate, m/s

K_{L600} gas-liquid transfer rate when Schmidt number equls to 600, m/s

K_{LB} bubble-mediated gas-liquid transfer rate, m/s

K_{Lbw} gas-liquid transfer rate induced by breaking wave, m/s

K_{Lg} mass transfer velocity in gas laminar layer, m/s

K_{Ll} mass transfer velocity in liquid laminar layer, m/s

K_{Lnw} gas-liquid transfer rate induced by non-breaking wave, m/s

K_{Lbw} gas-liquid transfer rate induced by breaking wave, m/s

K_{LT} total gas-liquid transfer rate, m/s

K_{Lw} gas-liquid transfer rate due to wind stirring, m/s

$K_{L\delta}$ liquid film transfer coefficient for hydrodynamically smooth surface, m/s

K_{Lv} gas-liquid transfer rate controlled by molecular diffusion, m/s

$K_{L\tau}$ liquid film transfer coefficient for non-smooth surface, m/s

$K_{L\tau}$ gas-liquid transfer rate controlled by turbulent diffusion, m/s

l_v mixing length at the edge of viscous layer, m

l_{v1} mixing length at the edge of viscous layer at the air-water interface, m

l_{v2} mixing length at the edge of viscous layer at the water-bed interface, m

l_τ mixing length in isotropic turbulent flow, m

$l_{\tau 1}$ mixing length in isotropic turbulent flow at the air-water interface, m

$l_{\tau 2}$ mixing length in isotropic turbulent flow at the water-bed interface, m

P_g gas pressure in the gas bulk, N/m^2

r_1 surface renewal rate at the air-water interface, s^{-1}

r_{1e} equivalent surface renewal rate at air-water interface, s^{-1}

r_2 surface renewal rate at the water-bed interface, s^{-1}

R_e Reynolds number

Re_* shear Reynolds number

Re_t turbulent Reynolds number

Re_H a form of Reynolds number for wind waves

R_i	interfacial resistance, s/m
Sc	Schmidt number
Sc_a	Schmidt number of gas a
Sc_b	Schmidt number of gas b
Sh	Sherwood number
T_a	temperature in bulk air, K
u_*	shear velocity, m/s
u_{*1}	shear velocity at air-water interface, m/s
u_{*2}	shear velocity at water-bed interface, m/s
u_{*A}	shear velocity at point A, m/s
u_{*a}	shear velocity at the air-water interface in air phase, m/s
u_{*B}	shear velocity at point B, m/s
u_{*b}	shear velocity in isotropic turbulent flow bulk far away from friction interface, m/s
u_{*i}	shear velocity at friction interface, m/s
u_{*w}	shear velocity at the air-water interface in water phase, m/s
$\bar{u}$	flow velocity in shear layers, m/s
U_1	flow velocity in upper layer, m/s
U_2	flow velocity in lower layer, m/s
U_B	bubble velocity, m/s

U_x	streamflow velocity at x direction, m/s
U_x	surface velocity at x direction, m/s
U_y	streamflow velocity at y direction, m/s
U_y	surface velocity at y direction, m/s
U_z	water-side interface-normal velocity, m/s
$\left\|\overline{v}\right\|$	vertical velocity fluctuation, m/s
ν_v	net transfer velocity across the air-water interface, m/day
V_B	bubble volume, m^3
W_{10}	wind velocity at 10 m height, m/s
Wc	fractional area of whitecap whitecap coverage
We	Weber number
W_e	effective wind speed, m/s
W_x	wind speed at x direction, m/s
W_y	wind speed at x direction, m/s
z_1	roughness thickness in the first segment, m
z_2	roughness thickness in the second segment, m
z_3	roughness thickness in the third segment, m
z_e	roughness thickness when viscous layer is completely pierced, m
δ_0	empirical constant of the thickness sum of turbulent boundary layers, m

δ_1 thickness of viscous layer in turbulent boundary layer at the air-water interface, m

δ_{1ve} effective thickness of viscous layer in turbulent boundary layer at the air-water interface, m

δ_v effective thickness of viscous layer in turbulent boundary layer, m

δ_{v1} thickness of viscous layer at the air-water interface, m

δ_{v2} thickness of viscous layer at the water-bed interface, m

δ_{ve} effective thickness of viscous layer in turbulent boundary layer, m

Γ_0 equivalent coefficient of viscous layer thickness

ν_a air kinematic viscosity, m^2/s

ν_w water kinematic viscosity, m^2/s

ν_T turbulent viscosity, m^2/s

λ_l roughness coefficient

ρ_l density of liquid, kg/m^3

ρ_a density of air, 1.2 kg/m^3

ρ_w density of water, 998.2 kg/m^3

ρ_B density of bubble, kg/m^3

$\Delta\rho$ density difference, kg/m^3

APPENDIX B

KL PROGRAM

```
program KL_Program

implicit none

character (len=20) :: filename1,filename2
character (len=20) :: filename11,filename12
character (len=20) :: filename21
integer :: ni = 0
integer :: nj = 0
integer :: ni2 = 0
integer :: nj2 = 0
integer :: status1,status2
integer :: status11,status12
integer :: status21
integer :: n1,n2,n3,n4,n5,n6,n7,n8,nmax,nt,t_num
real :: u1,u2
real :: vel_mod_max0,area_ratio,diff_depth
real :: ustar_sl_temp,ustar_xy_wb_temp

integer,dimension (4,4,9) :: i,j,dx,dy
real,dimension (4,4,9) :: depth
real,dimension (4,4,4,9) :: u,v,u0,v0
real,dimension (4,4,4,9) :: vel_mod,theta_xy,vel_mod_max,depth_maxvel
real,dimension (4) :: ustar_sl
real,dimension (4,4,4,9) ::
diff_theta_xy,diff_theta_yz1,diff_theta_yz2,diff_theta_zx1,diff_theta_zx2
real,dimension (4,4,9) :: sum_ustar_xy_sl,ustar_xy_wb,ustar_xy_aw,ustar_xy
real,dimension (4,4,9) :: ustar_yz1,ustar_yz2,ustar_zx1,ustar_zx2,sum_ustar
real,dimension (4,4,9) :: r,kl,klday
integer,dimension (4,4,9) :: nmaxvel
integer,dimension (4,4,4,9) :: layernum_maxvel
integer,dimension (9) :: time
real,dimension (9) :: sal

real :: diffusion=2.09E-09
real :: thou_water=998.2
real :: thou_air=1.225
real :: sigma=13.5
real :: k_sl=0.016
real :: pi=3.14159
```

```
real :: cf1=4.00E-03
real :: cf2=4.16E-02
real :: w=0.0
integer :: time_step_length=720

write (*,*) 'program is starting:'

filename1='depth1.txt'
filename2='vel1.txt'
filename11='kl1.txt'
filename12='kl2.txt'
filename21='debug1.txt'

open (unit=3,file=filename1,status='old',action='read',iostat=status1)
open (unit=4,file=filename2,status='old',action='read',iostat=status2)
open (unit=11,file=filename11,status='old',action='write',iostat=status11)
open (unit=12,file=filename12,status='old',action='write',iostat=status12)
open (unit=21,file=filename21,status='old',action='write',iostat=status21)

openif: if( (status1==0).and.(status2==0).and.(status11==0).and.(status12==0) ) then
      write (11,1000)
      1000 format ('VELOCITY (CM/S),DEPTH (M),GAS TRANSFER RATE,KL
(M/S),GAS TRANSFER RATE,KL2 (M/DAY)')
      write (11,1010)
      1010 format
(T6,'I',T12,'J',T18,'DX',T26,'DY',T34,'DEPTH',T47,'U1',T60,'V1',T72,'U2',&

T84,'V2',T96,'U3',T108,'V3',T120,'U4',T132,'V4',T144,'KL',T153,'KL2')
      write (11,1020)
      1020 format
(1X,T5,'===',T11,'===',T17,'====',T25,'====',T34,'=====',T46,'===',T59,'===',T71,'==
=',&

T83,'===',T95,'===',T107,'===',T119,'===',T131,'===',T143,'===',T153,'===')
      write (12,1030)
      1030 format
(T6,'I',T12,'J',T18,'ustar_xy_wb',T32,'ustar_xy_aw',T46,'ustar_xy',T60,'ustar_yz1',T74,&

'ustar_yz2',T88,'ustar_zx1',T102,'ustar_zx2',T116,'sum_ustar',T133,'r',T148,'KL',T161,'K
L2')
```

```
      write (12,1040)
      1040 format
(1X,T5,'===',T11,'===',T22,'====',T36,'====',T50,'====',T64,'====',T78,'====',T92,'=
===',&
                              T106,'====',T120,'====',T131,'===',T146,'====',T160,'====')
      read (3,1060,iostat=status1)
      1060 format (//)
      read (4,1070,iostat=status2)
      1070 format (/)

      t_num=0
      readloop_t: do nt=1,1
      t_num=t_num+1
            read (4,*,iostat=status2) time(nt),sal(nt)
            readloop_i: do ni=1,4
                  readloop_j: do nj=1,4
                        read (3,*,iostat=status1)
i(ni,nj,nt),j(ni,nj,nt),dx(ni,nj,nt),dy(ni,nj,nt),depth(ni,nj,nt)
                        read (4,*,iostat=status2)
i(ni,nj,nt),j(ni,nj,nt),u0(ni,nj,1,nt),v0(ni,nj,1,nt),&
                                    u0(ni,nj,2,nt),v0(ni,nj,2,nt),u0(ni,nj,3,nt),v0(ni,nj,3,nt)
                        u(ni,nj,1,nt)=u0(ni,nj,1,nt)*0.01
                        v(ni,nj,1,nt)=v0(ni,nj,1,nt)*0.01
                        u(ni,nj,2,nt)=u0(ni,nj,2,nt)*0.01
                        v(ni,nj,2,nt)=v0(ni,nj,2,nt)*0.01
                        u(ni,nj,3,nt)=u0(ni,nj,3,nt)*0.01
                        v(ni,nj,3,nt)=v0(ni,nj,3,nt)*0.01
                        read (4,*,iostat=status2)
i(ni,nj,nt),j(ni,nj,nt),u0(ni,nj,4,nt),v0(ni,nj,4,nt)
                        u(ni,nj,4,nt)=u0(ni,nj,4,nt)*0.01
                        v(ni,nj,4,nt)=v0(ni,nj,4,nt)*0.01
                        if (status1/=0) exit
                  end do readloop_j
            end do readloop_i
      end do readloop_t

      readif: if( (status1>0).or.(status2>0).or.(status11>0).or.(status12>0) ) then
            write (*,2000) ni*nj+1
            2000 format ('0','An error occurred reading line',I6)
      else
```

```
        write (*,2010) ni*nj
        2010 format ('0','End of file reached. There were',I6,'values in the file.')
      end if readif

      nt=0
      ni=0
      nj=0
      kl_calculation_t: do nt=1,1
          kl_calculation_i: do ni=1,4
              kl_calculation_j: do nj=1,4

                  do n1=1,4
                      vel_mod(ni,nj,n1,nt)=sqrt( u(ni,nj,n1,nt)**2+v(ni,nj,n1,nt)**2 )
                  end do

                  do n2=1,4
                      if ( (u(ni,nj,n2,nt)==0).and.(v(ni,nj,n2,nt)==0) ) then
                          theta_xy(ni,nj,n2,nt)=0
                      end if
                      if ( (u(ni,nj,n2,nt)==0).and.(v(ni,nj,n2,nt)>0) ) then
                          theta_xy(ni,nj,n2,nt)=pi/2.0
                      end if
                      if ( (u(ni,nj,n2,nt)==0).and.(v(ni,nj,n2,nt)<0) ) then
                          theta_xy(ni,nj,n2,nt)=3.0*pi/2.0
                      end if
                      if ( (u(ni,nj,n2,nt)>0).and.(v(ni,nj,n2,nt)==0) ) then
                          theta_xy(ni,nj,n2,nt)=0.0
                      end if
                      if ( (u(ni,nj,n2,nt)<0).and.(v(ni,nj,n2,nt)==0) ) then
                          theta_xy(ni,nj,n2,nt)=pi
                      end if
                      if ( (u(ni,nj,n2,nt)/=0).and.v(ni,nj,n2,nt)/=0 ) then
                          if (v(ni,nj,n2,nt)>0) then

theta_xy(ni,nj,n2,nt)=atan( v(ni,nj,n2,nt)/u(ni,nj,n2,nt) )
                          end if
                          if (v(ni,nj,n2,nt)<0) then

theta_xy(ni,nj,n2,nt)=atan( v(ni,nj,n2,nt)/u(ni,nj,n2,nt) )+pi
                          end if
```

```
                    end if
                end do

                nmax=0
                vel_mod_max0=vel_mod(ni,nj,1,nt)
                do n3=1,3

diff_theta_xy(ni,nj,n3,nt)=abs( theta_xy(ni,nj,n3+1,nt)-theta_xy(ni,nj,n3,nt) )
                    if
( ((pi/2.0<diff_theta_xy(ni,nj,n3,nt)).and.(diff_theta_xy(ni,nj,n3,nt)<3.0*pi/2.0)).or.&

((vel_mod(ni,nj,n3,nt)==0.0).and.(vel_mod(ni,nj,n3+1,nt)/=0.0)).or.&

((vel_mod(ni,nj,n3+1,nt)==0.0).and.(vel_mod(ni,nj,n3,nt)/=0.0)) ) then
                            nmax=nmax+1
                            vel_mod_max(ni,nj,nmax,nt)=vel_mod_max0
                            vel_mod_max0=vel_mod(ni,nj,n3+1,nt)
                            layernum_maxvel(ni,nj,nmax,nt)=n3

depth_maxvel(ni,nj,nmax,nt)=(n3-1+0.5)*depth(ni,nj,nt)/3.0
                    elseif (vel_mod(ni,nj,n3+1,nt)>vel_mod(ni,nj,n3,nt)) then
                        vel_mod_max0=vel_mod(ni,nj,n3+1,nt)
                    end if
                end do

                nmax=nmax+1
                vel_mod_max(ni,nj,nmax,nt)=vel_mod_max0
                nmaxvel(ni,nj,nt)=nmax
                if (nmax<=1) then
                    layernum_maxvel(ni,nj,nmax,nt)=4
                    depth_maxvel(ni,nj,nmax,nt)=depth(ni,nj,nt)
                else

layernum_maxvel(ni,nj,nmax,nt)=layernum_maxvel(ni,nj,nmax-1,nt)+1
                    depth_maxvel(ni,nj,nmax,nt)=0.0
                end if
                do
                    if (nmax+1>4) exit
                    nmax=nmax+1
                    vel_mod_max(ni,nj,nmax,nt)=0.0
```

```
                    layernum_maxvel(ni,nj,nmax,nt)=0.0
                    depth_maxvel(ni,nj,nmax,nt)=0.0
                end do

            end do kl_calculation_j
        end do kl_calculation_i
    end do kl_calculation_t

    nt=0
    ni=0
    nj=0
    kl_calculation_t2: do nt=1,1
        kl_calculation_i2: do ni=1,4
            kl_calculation_j2: do nj=1,4

                sum_ustar_xy_sl(ni,nj,nt)=0
                if (nmaxvel(ni,nj,nt)>=2) then
                    do n4=1,1
                        u1=vel_mod_max(ni,nj,n4,nt)
                        u2=vel_mod_max(ni,nj,n4+1,nt)

ustar_sl(n4)=sqrt(0.121*sigma*k_sl*max(u2,u1)*abs(u2+u1)/sqrt(pi)/thou_water)

sum_ustar_xy_sl(ni,nj,nt)=sum_ustar_xy_sl(ni,nj,nt)+ustar_sl(n4)
                    end do
                end if

                if (nt>8) then

ustar_xy_wb(ni,nj,nt)=sqrt(cf2/2.0)*vel_mod_max(ni,nj,nmaxvel(ni,nj,nt),nt)
                else

ustar_xy_wb_temp=sqrt(cf2/2.0)*vel_mod_max(ni,nj,nmaxvel(ni,nj,nt),nt)
                    if ( (depth_maxvel(ni,nj,1,nt+1) <
depth_maxvel(ni,nj,1,nt)).and.&
                        ((0.5*ustar_sl_temp)*(time(nt+1)-time(nt)) <
depth_maxvel(ni,nj,1,nt+1)) ) then
                        ustar_xy_wb(ni,nj,nt)=0
                    else
                        ustar_xy_wb(ni,nj,nt)=ustar_xy_wb_temp
```

```
                    end if
                end if


ustar_xy_aw(ni,nj,nt)=sqrt(cf1*thou_air*(w-vel_mod_max(ni,nj,1,nt))**2/2.0/thou_wate
r)

                if (nmaxvel(ni,nj,nt)>=2) then

ustar_xy(ni,nj,nt)=0+ustar_xy_aw(ni,nj,nt)+sum_ustar_xy_sl(ni,nj,nt)
                else

ustar_xy(ni,nj,nt)=ustar_xy_wb(ni,nj,nt)+ustar_xy_aw(ni,nj,nt)+sum_ustar_xy_sl(ni,nj,nt
)
                end if

                ustar_yz1(ni,nj,nt)=0.0
                do n5=1,layernum_maxvel(ni,nj,1,nt)

area_ratio=(dy(ni,nj,nt)*depth(ni,nj,nt)/3.0)/(dx(ni,nj,nt)*dy(ni,nj,nt))
                    if (ni>1) then

diff_theta_yz1(ni,nj,n5,nt)=abs( theta_xy(ni-1,nj,n5,nt)-theta_xy(ni,nj,n5,nt) )
                        if
( (pi/2.0<diff_theta_yz1(ni,nj,n5,nt)).and.(diff_theta_yz1(ni,nj,n5,nt)<3.0*pi/2.0) ) then
                            u1=vel_mod(ni-1,nj,n5,nt)
                            u2=vel_mod(ni,nj,n5,nt)

ustar_sl(n5)=sqrt(0.121*sigma*k_sl*max(u2,u1)*abs(u2+u1)/sqrt(pi)/thou_water)
                            ustar_yz1(ni,nj,nt)=ustar_yz1(ni,nj,nt)+ustar_sl(n5)
                        end if
                    end if
                end do

                ustar_yz2(ni,nj,nt)=0.0
                do n6=1,layernum_maxvel(ni,nj,1,nt)

area_ratio=(dy(ni,nj,nt)*depth(ni,nj,nt)/3.0)/(dx(ni,nj,nt)*dy(ni,nj,nt))
                    if (ni<4) then
```

```
diff_theta_yz2(ni,nj,n6,nt)=abs( theta_xy(ni+1,nj,n6,nt)-theta_xy(ni,nj,n6,nt) )
                                    if
( (pi/2.0<diff_theta_yz2(ni,nj,n6,nt)).and.(diff_theta_yz2(ni,nj,n6,nt)<3.0*pi/2.0) ) then
                                        u1=vel_mod(ni+1,nj,n6,nt)
                                        u2=vel_mod(ni,nj,n6,nt)

ustar_sl(n6)=sqrt(0.121*sigma*k_sl*max(u2,u1)*abs(u2+u1)/sqrt(pi)/thou_water)
                                        ustar_yz2(ni,nj,nt)=ustar_yz2(ni,nj,nt)+ustar_sl(n6)
                                    end if
                                end if
                            end do

                            ustar_zx1(ni,nj,nt)=0.0
                            do n7=1,layernum_maxvel(ni,nj,1,nt)

area_ratio=(dy(ni,nj,nt)*depth(ni,nj,nt)/3.0)/(dx(ni,nj,nt)*dy(ni,nj,nt))
                                if (nj>1) then

diff_theta_zx1(ni,nj,n7,nt)=abs( theta_xy(ni,nj-1,n7,nt)-theta_xy(ni,nj,n7,nt) )
                                    if
( (pi/2.0<diff_theta_zx1(ni,nj,n7,nt)).and.(diff_theta_zx1(ni,nj,n7,nt)<3.0*pi/2.0) ) then
                                        u1=vel_mod(ni,nj-1,n7,nt)
                                        u2=vel_mod(ni,nj,n7,nt)

ustar_sl(n7)=sqrt(0.121*sigma*k_sl*max(u2,u1)*abs(u2+u1)/sqrt(pi)/thou_water)
                                        ustar_zx1(ni,nj,nt)=ustar_zx1(ni,nj,nt)+ustar_sl(n7)
                                    end if
                                end if
                            end do

                            ustar_zx2(ni,nj,nt)=0.0
                            do n8=1,layernum_maxvel(ni,nj,1,nt)

area_ratio=(dy(ni,nj,nt)*depth(ni,nj,nt)/3.0)/(dx(ni,nj,nt)*dy(ni,nj,nt))
                                if (nj<4) then

diff_theta_zx2(ni,nj,n8,nt)=abs( theta_xy(ni,nj+1,n8,nt)-theta_xy(ni,nj,n8,nt) )
                                    if
( (pi/2.0<diff_theta_zx2(ni,nj,n8,nt)).and.(diff_theta_zx2(ni,nj,n8,nt)<3.0*pi/2.0) ) then
                                        u1=vel_mod(ni,nj+1,n8,nt)
```

```
                                    u2=vel_mod(ni,nj,n8,nt)

ustar_sl(n8)=sqrt(0.121*sigma*k_sl*max(u2,u1)*abs(u2+u1)/sqrt(pi)/thou_water)
                                    ustar_zx2(ni,nj,nt)=ustar_zx2(ni,nj,nt)+ustar_sl(n8)
                                end if
                            end if
                        end do


sum_ustar(ni,nj,nt)=ustar_xy(ni,nj,nt)+ustar_yz1(ni,nj,nt)+ustar_yz2(ni,nj,nt)+ustar_zx1(
ni,nj,nt)+&
                                                    ustar_zx2(ni,nj,nt)
                        r(ni,nj,nt)=(0.5*sum_ustar(ni,nj,nt))/(0.1*depth_maxvel(ni,nj,1,nt))
                        kl(ni,nj,nt)=sqrt(diffusion*r(ni,nj,nt))
                        klday(ni,nj,nt)=kl(ni,nj,nt)*24*60*60

                    end do kl_calculation_j2
                end do kl_calculation_i2
            end do kl_calculation_t2

            kl_calculation_t3: do nt=1,1
                kl_calculation_i3: do ni=1,4
                    kl_calculation_j3: do nj=1,4

                        write (11,3000)
i(ni,nj,nt),j(ni,nj,nt),dx(ni,nj,nt),dy(ni,nj,nt),depth(ni,nj,nt),u(ni,nj,1,nt),&

v(ni,nj,1,nt),u(ni,nj,2,nt),v(ni,nj,2,nt),u(ni,nj,3,nt),v(ni,nj,3,nt),u(ni,nj,4,nt),&
                                    v(ni,nj,4,nt),kl(ni,nj,nt),klday(ni,nj,nt)
                        3000 format (2I6,2I8,F10.6,8F12.6,2F12.8)
                        write (12,3010)
i(ni,nj,nt),j(ni,nj,nt),ustar_xy_wb(ni,nj,nt),ustar_xy_aw(ni,nj,nt),&

ustar_xy(ni,nj,nt),ustar_yz1(ni,nj,nt),ustar_yz2(ni,nj,nt),ustar_zx1(ni,nj,nt),&

ustar_zx2(ni,nj,nt),sum_ustar(ni,nj,nt),r(ni,nj,nt),kl(ni,nj,nt),klday(ni,nj,nt)
                        3010 format (2I6,10F14.8,F14.8)
                        write (21,3020)
theta_xy(ni,nj,1,nt),theta_xy(ni,nj,2,nt),theta_xy(ni,nj,3,nt),theta_xy(ni,nj,4,nt),&
```

```
vel_mod_max(ni,nj,1,nt),vel_mod_max(ni,nj,2,nt),vel_mod_max(ni,nj,3,nt),vel_mod_ma
x(ni,nj,4,nt)
                    3020 format (4F12.6,4F12.6)

                end do kl_calculation_j3
            end do kl_calculation_i3
        end do kl_calculation_t3

else openif
        write (*,4000) status1
        4000 format (','Error opening file: iostat=',I6)
end if openif

close (unit=3)
close (unit=4)
close (unit=11)
close (unit=12)
close (unit=21)

end program KL_Program
```

APPENDIX C

WATER DEPTH FILE

C Water depth file, in free format across columns

C

C I J DX DY DEPTH BOTTOM ELEV ZROUGH VEG TYPE CELL NAME

C

0 0 1900 2260 9.9 -9.9 -0.1 0 'I3-J2'

0 1 2640 2200 9.9 -9.9 -0.1 0 'I4-J2'

0 2 2840 2280 9.9 -9.9 -0.1 0 'I5-J2'

0 3 832 2300 9.9 -9.9 -0.1 0 'I6-J2'

1 0 515 2200 9.9 -9.9 -0.1 0 'I7-J2'

1 1 2310 2090 9.9 -9.9 -0.1 0 'I8-J2'

1 2 2210 1990 9.9 -9.9 -0.1 0 'I9-J2'

1 3 2260 2120 9.9 -9.9 -0.1 0 'I10-J2'

2 0 2320 2150 9.9 -9.9 -0.1 0 'I11-J2'

2 1 2330 2140 9.9 -9.9 -0.1 0 'I12-J2'

2 2 2080 2080 9.9 -9.9 -0.1 0 'I13-J2'

2 3 2100 1850 9.9 -9.9 -0.1 0 'I14-J2'

3 0 2720 1750 9.9 -9.9 -0.1 0 'I15-J2'

3 1 2970 1590 9.9 -9.9 -0.1 0 'I16-J2'

3 2 2420 1530 9.9 -9.9 -0.1 0 'I17-J2'

3 3 2000 1640 9.9 -9.9 -0.1 0 'I18-J2'

APPENDIX D

FLOW VELOCITY FILE

INSTANTANEOUS HORIZ VELOCITY CM/S

1 0.0001

0 0 0.500000E+02 0.000000E+00 0.500000E+02 0.000000E+00 -0.500000E+02 0.000000E+00

0 0 0.500000E+02 0.000000E+00

0 1 0.000000E+00 0.500000E+02 0.500000E+02 0.000000E+00 -0.500000E+02 0.000000E+00

0 1 0.500000E+02 0.000000E+00

0 2 0.500000E+02 0.000000E+00 0.500000E+02 0.000000E+00 -0.500000E+02 0.000000E+00

0 2 0.500000E+02 0.000000E+00

0 3 0.500000E+02 0.000000E+00 0.500000E+02 0.000000E+00 0.000000E+00 -0.500000E+02

0 3 0.500000E+02 0.000000E+00

1 0 -0.500000E+02 0.000000E+00 0.000000E+00 0.500000E+02 0.500000E+02 0.000000E+00

1 0 0.500000E+02 0.000000E+00

1 1 0.500000E+02 0.000000E+00 0.500000E+02 0.000000E+00 -0.500000E+02 0.000000E+00

1 1 0.500000E+02 0.000000E+00

1 2 0.500000E+02 0.000000E+00 0.000000E+00 0.500000E+02 -0.500000E+02 0.000000E+00

1 2 0.500000E+02 0.000000E+00

1 3 -0.500000E+02 0.000000E+00 0.500000E+02 0.000000E+00 0.500000E+02 0.000000E+00

1 3 0.500000E+02 0.000000E+00

2 0 0.500000E+02 0.000000E+00 0.000000E+00 0.500000E+02 -0.500000E+02 0.000000E+00

2 0 0.500000E+02 0.000000E+00

2 1 0.500000E+02 0.000000E+00 -0.500000E+02 0.000000E+00 0.000000E+00 -0.500000E+02

2 1 0.500000E+02 0.000000E+00

2 2 -0.500000E+02 0.000000E+00 0.500000E+02 0.000000E+00 -0.500000E+02 0.000000E+00

2 2 0.500000E+02 0.000000E+00

2 3 0.500000E+02 0.000000E+00 0.500000E+02 0.000000E+00 -0.500000E+02 0.000000E+00

2 3 0.500000E+02 0.000000E+00

3 0 0.500000E+02 0.000000E+00 0.000000E+00 0.500000E+02 -0.500000E+02 0.000000E+00

3 0 0.500000E+02 0.000000E+00
3 1 0.000000E+00 0.500000E+02 -0.500000E+02 0.000000E+00 0.000000E+00
0.500000E+02
3 1 -0.500000E+02 0.000000E+00
3 2 0.500000E+02 0.000000E+00 0.500000E+02 0.000000E+00 -0.500000E+02
0.000000E+00
3 2 0.500000E+02 0.000000E+00
3 3 0.500000E+02 0.000000E+00 -0.500000E+02 0.000000E+00 0.500000E+02
0.000000E+00
3 3 0.000000E+00 0.500000E+02

APPENDIX E

KL PROGRAM OUTPUT FILE

VELOCITY (CM/S),DEPTH (M),GAS-LIQUID TRANSFER RATE,KL (M/S),GAS-LIQUID TRANSFER RATE,KL2 (M/DAY)

I	J	DX	DY	DEPTH	U1	V1	U2	V2	U3	V3	U4	V4	KL	KL2
0	0	1900	2260	9.900000	0.500000	0.000000	0.500000	0.000000	-0.500000	0.000000	0.500000	0.000000	0.00000272	0.23489287
0	1	2640	2200	9.900000	0.000000	0.500000	0.500000	0.000000	-0.500000	0.000000	0.500000	0.000000	0.00000129	0.11110701
0	2	2840	2280	9.900000	0.500000	0.000000	0.500000	0.000000	-0.500000	0.000000	0.500000	0.000000	0.00000129	0.11110701
0	3	832	2300	9.900000	0.500000	0.000000	0.500000	0.000000	0.000000	-0.500000	0.500000	0.000000	0.00000192	0.16609435
1	0	515	2200	9.900000	-0.500000	0.000000	0.000000	0.500000	0.500000	0.000000	0.500000	0.000000	0.00000425	0.36696330
1	1	2310	2090	9.900000	0.500000	0.000000	0.500000	0.000000	-0.500000	0.000000	0.500000	0.000000	0.00000362	0.31305677
1	2	2210	1990	9.900000	0.500000	0.000000	0.000000	0.500000	-0.500000	0.000000	0.500000	0.000000	0.00000336	0.29068998
1	3	2260	2120	9.900000	-0.500000	0.000000	0.500000	0.000000	0.500000	0.000000	0.500000	0.000000	0.00000752	0.65000254
2	0	2320	2150	9.900000	0.500000	0.000000	0.000000	0.500000	-0.500000	0.000000	0.500000	0.000000	0.00000281	0.24249275
2	1	2330	2140	9.900000	0.500000	0.000000	-0.500000	0.000000	0.000000	-0.500000	0.500000	0.000000	0.00000471	0.40684637

2 2 2080 2080 9.900000 -0.500000 0.000000 0.500000
0.000000 -0.500000 0.000000 0.500000 0.000000 0.00000859
0.74228901
2 3 2100 1850 9.900000 0.500000 0.000000 0.500000
0.000000 -0.500000 0.000000 0.500000 0.000000 0.00000434
0.37527916
3 0 2720 1750 9.900000 0.500000 0.000000 0.000000
0.500000 -0.500000 0.000000 0.500000 0.000000 0.00000100
0.08606311
3 1 2970 1590 9.900000 0.000000 0.500000 -0.500000
0.000000 0.000000 0.500000 -0.500000 0.000000 0.00000389
0.33652207
3 2 2420 1530 9.900000 0.500000 0.000000 0.500000
0.000000 -0.500000 0.000000 0.500000 0.000000 0.00000434
0.37527916
3 3 2000 1640 9.900000 0.500000 0.000000 -0.500000
0.000000 0.500000 0.000000 0.000000 0.500000 0.00000223
0.19244297

APPENDIX F

THREE-DIMENSIONAL FLOW VELOCITY FILE

INSTANTANEOUS HORIZ VELOCITY CM/S

1 0.0001

0 0 0.353600E+02 -0.353600E+02 0.353600E+02 0.353600E+02 0.353600E+02 0.353600E+02 0.353600E+02 0.353600E+02 -0.353600E+02

0 0 -0.353600E+02 0.353600E+02 -0.353600E+02

0 1 0.353600E+02 0.353600E+02 0.353600E+02 0.353600E+02 -0.353600E+02 0.353600E+02 0.353600E+02 0.353600E+02 -0.353600E+02

0 1 0.353600E+02 0.353600E+02 0.353600E+02

0 2 0.353600E+02 0.353600E+02 0.353600E+02 -0.353600E+02 0.353600E+02 -0.353600E+02 -0.353600E+02 -0.353600E+02 0.353600E+02

0 2 0.353600E+02 0.353600E+02 0.353600E+02

0 3 0.353600E+02 -0.353600E+02 0.353600E+02 0.353600E+02 0.353600E+02 0.353600E+02 0.353600E+02 -0.353600E+02 0.353600E+02

0 3 -0.353600E+02 0.353600E+02 0.353600E+02

1 0 0.353600E+02 0.353600E+02 0.353600E+02 -0.353600E+02 0.353600E+02 0.353600E+02 0.353600E+02 0.353600E+02 0.353600E+02

1 0 0.353600E+02 0.353600E+02 -0.353600E+02

1 1 0.353600E+02 -0.353600E+02 -0.353600E+02 0.353600E+02 -0.353600E+02 0.353600E+02 0.353600E+02 0.353600E+02 0.353600E+02

1 1 0.353600E+02 0.353600E+02 0.353600E+02

1 2 0.353600E+02 0.353600E+02 0.353600E+02 -0.353600E+02 0.353600E+02 -0.353600E+02 -0.353600E+02 0.353600E+02 0.353600E+02

1 2 0.353600E+02 0.353600E+02 0.353600E+02

1 3 0.353600E+02 -0.353600E+02 0.353600E+02 0.353600E+02 0.353600E+02 0.353600E+02 0.353600E+02 -0.353600E+02 0.353600E+02

1 3 0.353600E+02 0.353600E+02 0.353600E+02

2 0 0.353600E+02 0.353600E+02 0.353600E+02 0.353600E+02 0.353600E+02 0.353600E+02 -0.353600E+02 0.353600E+02 -0.353600E+02

2 0 0.353600E+02 0.353600E+02 -0.353600E+02

2 1 0.353600E+02 -0.353600E+02 0.353600E+02 0.353600E+02 0.353600E+02 0.353600E+02 0.353600E+02 -0.353600E+02 0.353600E+02

2 1 -0.353600E+02 0.353600E+02 0.353600E+02

2 2 0.353600E+02 0.353600E+02 -0.353600E+02 -0.353600E+02 0.353600E+02 0.353600E+02 0.353600E+02 0.353600E+02 -0.353600E+02

2 2 0.353600E+02 0.353600E+02 0.353600E+02

2 3 0.353600E+02 0.353600E+02 0.353600E+02 -0.353600E+02 -0.353600E+02 -0.353600E+02 0.353600E+02 -0.353600E+02 0.353600E+02

2 3 -0.353600E+02 -0.353600E+02 0.353600E+02

3 0 0.353600E+02 -0.353600E+02 0.353600E+02 0.353600E+02 0.353600E+02 0.353600E+02 0.353600E+02 0.353600E+02 0.353600E+02

3 0 0.353600E+02 0.353600E+02 0.353600E+02
3 1 -0.353600E+02 -0.353600E+02 0.353600E+02 0.353600E+02
-0.353600E+02 0.353600E+02 -0.353600E+02 0.353600E+02 0.353600E+02
3 1 0.353600E+02 0.353600E+02 -0.353600E+02
3 2 0.353600E+02 0.353600E+02 0.353600E+02 0.353600E+02
0.353600E+02 0.353600E+02 0.353600E+02 0.353600E+02 0.353600E+02
3 2 0.353600E+02 0.353600E+02 0.353600E+02
3 3 0.353600E+02 0.353600E+02 0.353600E+02 -0.353600E+02
0.353600E+02 0.353600E+02 0.353600E+02 -0.353600E+02 -0.353600E+02
3 3 -0.353600E+02 0.353600E+02 0.353600E+02

APPENDIX G

DYNAMIC FLOW FIELD FILE

INSTANTANEOUS HORIZ VELOCITY CM/S

0 0.0001

0 0 0.500000E+02 0.000000E+00 0.500000E+02 0.000000E+00 -0.500000E+02 0.000000E+00

0 0 -0.500000E+02 0.000000E+00

0 1 0.500000E+02 0.000000E+00 0.500000E+02 0.000000E+00 -0.500000E+02 0.000000E+00

0 1 -0.500000E+02 0.000000E+00

0 2 0.500000E+02 0.000000E+00 0.500000E+02 0.000000E+00 -0.500000E+02 0.000000E+00

0 2 -0.500000E+02 0.000000E+00

0 3 0.500000E+02 0.000000E+00 0.500000E+02 0.000000E+00 -0.500000E+02 0.000000E+00

0 3 -0.500000E+02 0.000000E+00

1 0 0.500000E+02 0.000000E+00 0.500000E+02 0.000000E+00 -0.500000E+02 0.000000E+00

1 0 -0.500000E+02 0.000000E+00

1 1 0.500000E+02 0.000000E+00 0.500000E+02 0.000000E+00 -0.500000E+02 0.000000E+00

1 1 -0.500000E+02 0.000000E+00

1 2 0.500000E+02 0.000000E+00 0.500000E+02 0.000000E+00 -0.500000E+02 0.000000E+00

1 2 -0.500000E+02 0.000000E+00

1 3 0.500000E+02 0.000000E+00 0.500000E+02 0.000000E+00 -0.500000E+02 0.000000E+00

1 3 -0.500000E+02 0.000000E+00

2 0 0.500000E+02 0.000000E+00 0.500000E+02 0.000000E+00 -0.500000E+02 0.000000E+00

2 0 -0.500000E+02 0.000000E+00

2 1 0.500000E+02 0.000000E+00 0.500000E+02 0.000000E+00 -0.500000E+02 0.000000E+00

2 1 -0.500000E+02 0.000000E+00

2 2 0.500000E+02 0.000000E+00 0.500000E+02 0.000000E+00 -0.500000E+02 0.000000E+00

2 2 -0.500000E+02 0.000000E+00

2 3 0.500000E+02 0.000000E+00 0.500000E+02 0.000000E+00 -0.500000E+02 0.000000E+00

2 3 -0.500000E+02 0.000000E+00

3 0 0.500000E+02 0.000000E+00 0.500000E+02 0.000000E+00 -0.500000E+02 0.000000E+00

3 0 -0.500000E+02 0.000000E+00
3 1 0.500000E+02 0.000000E+00 0.500000E+02 0.000000E+00
-0.500000E+02 0.000000E+00
3 1 -0.500000E+02 0.000000E+00
3 2 0.500000E+02 0.000000E+00 0.500000E+02 0.000000E+00
-0.500000E+02 0.000000E+00
3 2 -0.500000E+02 0.000000E+00
3 3 0.500000E+02 0.000000E+00 0.500000E+02 0.000000E+00
-0.500000E+02 0.000000E+00
3 3 -0.500000E+02 0.000000E+00
3 0.0001
0 0 0.500000E+02 0.000000E+00 -0.500000E+02 0.000000E+00
-0.500000E+02 0.000000E+00
0 0 -0.500000E+02 0.000000E+00
0 1 0.500000E+02 0.000000E+00 -0.500000E+02 0.000000E+00
-0.500000E+02 0.000000E+00
0 1 -0.500000E+02 0.000000E+00
0 2 0.500000E+02 0.000000E+00 -0.500000E+02 0.000000E+00
-0.500000E+02 0.000000E+00
0 2 -0.500000E+02 0.000000E+00
0 3 0.500000E+02 0.000000E+00 -0.500000E+02 0.000000E+00
-0.500000E+02 0.000000E+00
0 3 -0.500000E+02 0.000000E+00
1 0 0.500000E+02 0.000000E+00 -0.500000E+02 0.000000E+00
-0.500000E+02 0.000000E+00
1 0 -0.500000E+02 0.000000E+00
1 1 0.500000E+02 0.000000E+00 -0.500000E+02 0.000000E+00
-0.500000E+02 0.000000E+00
1 1 -0.500000E+02 0.000000E+00
1 2 0.500000E+02 0.000000E+00 -0.500000E+02 0.000000E+00
-0.500000E+02 0.000000E+00
1 2 -0.500000E+02 0.000000E+00
1 3 0.500000E+02 0.000000E+00 -0.500000E+02 0.000000E+00
-0.500000E+02 0.000000E+00
1 3 -0.500000E+02 0.000000E+00
2 0 0.500000E+02 0.000000E+00 -0.500000E+02 0.000000E+00
-0.500000E+02 0.000000E+00
2 0 -0.500000E+02 0.000000E+00
2 1 0.500000E+02 0.000000E+00 -0.500000E+02 0.000000E+00
-0.500000E+02 0.000000E+00

2 1 -0.500000E+02 0.000000E+00
2 2 0.500000E+02 0.000000E+00 -0.500000E+02 0.000000E+00
-0.500000E+02 0.000000E+00
2 2 -0.500000E+02 0.000000E+00
2 3 0.500000E+02 0.000000E+00 -0.500000E+02 0.000000E+00
-0.500000E+02 0.000000E+00
2 3 -0.500000E+02 0.000000E+00
3 0 0.500000E+02 0.000000E+00 -0.500000E+02 0.000000E+00
-0.500000E+02 0.000000E+00
3 0 -0.500000E+02 0.000000E+00
3 1 0.500000E+02 0.000000E+00 -0.500000E+02 0.000000E+00
-0.500000E+02 0.000000E+00
3 1 -0.500000E+02 0.000000E+00
3 2 0.500000E+02 0.000000E+00 -0.500000E+02 0.000000E+00
-0.500000E+02 0.000000E+00
3 2 -0.500000E+02 0.000000E+00
3 3 0.500000E+02 0.000000E+00 -0.500000E+02 0.000000E+00
-0.500000E+02 0.000000E+00
3 3 -0.500000E+02 0.000000E+00
6 0.0001
0 0 0.500000E+02 0.000000E+00 -0.500000E+02 0.000000E+00
-0.500000E+02 0.000000E+00
0 0 -0.500000E+02 0.000000E+00
0 1 0.500000E+02 0.000000E+00 -0.500000E+02 0.000000E+00
-0.500000E+02 0.000000E+00
0 1 -0.500000E+02 0.000000E+00
0 2 0.500000E+02 0.000000E+00 -0.500000E+02 0.000000E+00
-0.500000E+02 0.000000E+00
0 2 -0.500000E+02 0.000000E+00
0 3 0.500000E+02 0.000000E+00 -0.500000E+02 0.000000E+00
-0.500000E+02 0.000000E+00
0 3 -0.500000E+02 0.000000E+00
1 0 0.500000E+02 0.000000E+00 -0.500000E+02 0.000000E+00
-0.500000E+02 0.000000E+00
1 0 -0.500000E+02 0.000000E+00
1 1 0.500000E+02 0.000000E+00 -0.500000E+02 0.000000E+00
-0.500000E+02 0.000000E+00
1 1 -0.500000E+02 0.000000E+00
1 2 0.500000E+02 0.000000E+00 -0.500000E+02 0.000000E+00
-0.500000E+02 0.000000E+00

1 2 -0.500000E+02 0.000000E+00
1 3 0.500000E+02 0.000000E+00 -0.500000E+02 0.000000E+00
-0.500000E+02 0.000000E+00
1 3 -0.500000E+02 0.000000E+00
2 0 0.500000E+02 0.000000E+00 -0.500000E+02 0.000000E+00
-0.500000E+02 0.000000E+00
2 0 -0.500000E+02 0.000000E+00
2 1 0.500000E+02 0.000000E+00 -0.500000E+02 0.000000E+00
-0.500000E+02 0.000000E+00
2 1 -0.500000E+02 0.000000E+00
2 2 0.500000E+02 0.000000E+00 -0.500000E+02 0.000000E+00
-0.500000E+02 0.000000E+00
2 2 -0.500000E+02 0.000000E+00
2 3 0.500000E+02 0.000000E+00 -0.500000E+02 0.000000E+00
-0.500000E+02 0.000000E+00
2 3 -0.500000E+02 0.000000E+00
3 0 0.500000E+02 0.000000E+00 -0.500000E+02 0.000000E+00
-0.500000E+02 0.000000E+00
3 0 -0.500000E+02 0.000000E+00
3 1 0.500000E+02 0.000000E+00 -0.500000E+02 0.000000E+00
-0.500000E+02 0.000000E+00
3 1 -0.500000E+02 0.000000E+00
3 2 0.500000E+02 0.000000E+00 -0.500000E+02 0.000000E+00
-0.500000E+02 0.000000E+00
3 2 -0.500000E+02 0.000000E+00
3 3 0.500000E+02 0.000000E+00 -0.500000E+02 0.000000E+00
-0.500000E+02 0.000000E+00
3 3 -0.500000E+02 0.000000E+00
9 0.0001
0 0 0.500000E+02 0.000000E+00 -0.500000E+02 0.000000E+00
-0.500000E+02 0.000000E+00
0 0 -0.500000E+02 0.000000E+00
0 1 0.500000E+02 0.000000E+00 -0.500000E+02 0.000000E+00
-0.500000E+02 0.000000E+00
0 1 -0.500000E+02 0.000000E+00
0 2 0.500000E+02 0.000000E+00 -0.500000E+02 0.000000E+00
-0.500000E+02 0.000000E+00
0 2 -0.500000E+02 0.000000E+00
0 3 0.500000E+02 0.000000E+00 -0.500000E+02 0.000000E+00
-0.500000E+02 0.000000E+00

0 3 -0.500000E+02 0.000000E+00
1 0 0.500000E+02 0.000000E+00 -0.500000E+02 0.000000E+00
-0.500000E+02 0.000000E+00
1 0 -0.500000E+02 0.000000E+00
1 1 0.500000E+02 0.000000E+00 -0.500000E+02 0.000000E+00
-0.500000E+02 0.000000E+00
1 1 -0.500000E+02 0.000000E+00
1 2 0.500000E+02 0.000000E+00 -0.500000E+02 0.000000E+00
-0.500000E+02 0.000000E+00
1 2 -0.500000E+02 0.000000E+00
1 3 0.500000E+02 0.000000E+00 -0.500000E+02 0.000000E+00
-0.500000E+02 0.000000E+00
1 3 -0.500000E+02 0.000000E+00
2 0 0.500000E+02 0.000000E+00 -0.500000E+02 0.000000E+00
-0.500000E+02 0.000000E+00
2 0 -0.500000E+02 0.000000E+00
2 1 0.500000E+02 0.000000E+00 -0.500000E+02 0.000000E+00
-0.500000E+02 0.000000E+00
2 1 -0.500000E+02 0.000000E+00
2 2 0.500000E+02 0.000000E+00 -0.500000E+02 0.000000E+00
-0.500000E+02 0.000000E+00
2 2 -0.500000E+02 0.000000E+00
2 3 0.500000E+02 0.000000E+00 -0.500000E+02 0.000000E+00
-0.500000E+02 0.000000E+00
2 3 -0.500000E+02 0.000000E+00
3 0 0.500000E+02 0.000000E+00 -0.500000E+02 0.000000E+00
-0.500000E+02 0.000000E+00
3 0 -0.500000E+02 0.000000E+00
3 1 0.500000E+02 0.000000E+00 -0.500000E+02 0.000000E+00
-0.500000E+02 0.000000E+00
3 1 -0.500000E+02 0.000000E+00
3 2 0.500000E+02 0.000000E+00 -0.500000E+02 0.000000E+00
-0.500000E+02 0.000000E+00
3 2 -0.500000E+02 0.000000E+00
3 3 0.500000E+02 0.000000E+00 -0.500000E+02 0.000000E+00
-0.500000E+02 0.000000E+00
3 3 -0.500000E+02 0.000000E+00
12 0.0001
0 0 0.500000E+02 0.000000E+00 -0.500000E+02 0.000000E+00
-0.500000E+02 0.000000E+00

0 0 -0.500000E+02 0.000000E+00
0 1 0.500000E+02 0.000000E+00 -0.500000E+02 0.000000E+00
-0.500000E+02 0.000000E+00
0 1 -0.500000E+02 0.000000E+00
0 2 0.500000E+02 0.000000E+00 -0.500000E+02 0.000000E+00
-0.500000E+02 0.000000E+00
0 2 -0.500000E+02 0.000000E+00
0 3 0.500000E+02 0.000000E+00 -0.500000E+02 0.000000E+00
-0.500000E+02 0.000000E+00
0 3 -0.500000E+02 0.000000E+00
1 0 0.500000E+02 0.000000E+00 -0.500000E+02 0.000000E+00
-0.500000E+02 0.000000E+00
1 0 -0.500000E+02 0.000000E+00
1 1 0.500000E+02 0.000000E+00 -0.500000E+02 0.000000E+00
-0.500000E+02 0.000000E+00
1 1 -0.500000E+02 0.000000E+00
1 2 0.500000E+02 0.000000E+00 -0.500000E+02 0.000000E+00
-0.500000E+02 0.000000E+00
1 2 -0.500000E+02 0.000000E+00
1 3 0.500000E+02 0.000000E+00 -0.500000E+02 0.000000E+00
-0.500000E+02 0.000000E+00
1 3 -0.500000E+02 0.000000E+00
2 0 0.500000E+02 0.000000E+00 -0.500000E+02 0.000000E+00
-0.500000E+02 0.000000E+00
2 0 -0.500000E+02 0.000000E+00
2 1 0.500000E+02 0.000000E+00 -0.500000E+02 0.000000E+00
-0.500000E+02 0.000000E+00
2 1 -0.500000E+02 0.000000E+00
2 2 0.500000E+02 0.000000E+00 -0.500000E+02 0.000000E+00
-0.500000E+02 0.000000E+00
2 2 -0.500000E+02 0.000000E+00
2 3 0.500000E+02 0.000000E+00 -0.500000E+02 0.000000E+00
-0.500000E+02 0.000000E+00
2 3 -0.500000E+02 0.000000E+00
3 0 0.500000E+02 0.000000E+00 -0.500000E+02 0.000000E+00
-0.500000E+02 0.000000E+00
3 0 -0.500000E+02 0.000000E+00
3 1 0.500000E+02 0.000000E+00 -0.500000E+02 0.000000E+00
-0.500000E+02 0.000000E+00
3 1 -0.500000E+02 0.000000E+00

3 2 0.500000E+02 0.000000E+00 -0.500000E+02 0.000000E+00
-0.500000E+02 0.000000E+00
3 2 -0.500000E+02 0.000000E+00
3 3 0.500000E+02 0.000000E+00 -0.500000E+02 0.000000E+00
-0.500000E+02 0.000000E+00
3 3 -0.500000E+02 0.000000E+00
15 0.0001
0 0 0.500000E+02 0.000000E+00 -0.500000E+02 0.000000E+00
-0.500000E+02 0.000000E+00
0 0 -0.500000E+02 0.000000E+00
0 1 0.500000E+02 0.000000E+00 -0.500000E+02 0.000000E+00
-0.500000E+02 0.000000E+00
0 1 -0.500000E+02 0.000000E+00
0 2 0.500000E+02 0.000000E+00 -0.500000E+02 0.000000E+00
-0.500000E+02 0.000000E+00
0 2 -0.500000E+02 0.000000E+00
0 3 0.500000E+02 0.000000E+00 -0.500000E+02 0.000000E+00
-0.500000E+02 0.000000E+00
0 3 -0.500000E+02 0.000000E+00
1 0 0.500000E+02 0.000000E+00 -0.500000E+02 0.000000E+00
-0.500000E+02 0.000000E+00
1 0 -0.500000E+02 0.000000E+00
1 1 0.500000E+02 0.000000E+00 -0.500000E+02 0.000000E+00
-0.500000E+02 0.000000E+00
1 1 -0.500000E+02 0.000000E+00
1 2 0.500000E+02 0.000000E+00 -0.500000E+02 0.000000E+00
-0.500000E+02 0.000000E+00
1 2 -0.500000E+02 0.000000E+00
1 3 0.500000E+02 0.000000E+00 -0.500000E+02 0.000000E+00
-0.500000E+02 0.000000E+00
1 3 -0.500000E+02 0.000000E+00
2 0 0.500000E+02 0.000000E+00 -0.500000E+02 0.000000E+00
-0.500000E+02 0.000000E+00
2 0 -0.500000E+02 0.000000E+00
2 1 0.500000E+02 0.000000E+00 -0.500000E+02 0.000000E+00
-0.500000E+02 0.000000E+00
2 1 -0.500000E+02 0.000000E+00
2 2 0.500000E+02 0.000000E+00 -0.500000E+02 0.000000E+00
-0.500000E+02 0.000000E+00
2 2 -0.500000E+02 0.000000E+00

2 3 0.500000E+02 0.000000E+00 -0.500000E+02 0.000000E+00
-0.500000E+02 0.000000E+00
2 3 -0.500000E+02 0.000000E+00
3 0 0.500000E+02 0.000000E+00 -0.500000E+02 0.000000E+00
-0.500000E+02 0.000000E+00
3 0 -0.500000E+02 0.000000E+00
3 1 0.500000E+02 0.000000E+00 -0.500000E+02 0.000000E+00
-0.500000E+02 0.000000E+00
3 1 -0.500000E+02 0.000000E+00
3 2 0.500000E+02 0.000000E+00 -0.500000E+02 0.000000E+00
-0.500000E+02 0.000000E+00
3 2 -0.500000E+02 0.000000E+00
3 3 0.500000E+02 0.000000E+00 -0.500000E+02 0.000000E+00
-0.500000E+02 0.000000E+00
3 3 -0.500000E+02 0.000000E+00
18 0.0001
0 0 0.500000E+02 0.000000E+00 -0.500000E+02 0.000000E+00
-0.500000E+02 0.000000E+00
0 0 -0.500000E+02 0.000000E+00
0 1 0.500000E+02 0.000000E+00 -0.500000E+02 0.000000E+00
-0.500000E+02 0.000000E+00
0 1 -0.500000E+02 0.000000E+00
0 2 0.500000E+02 0.000000E+00 -0.500000E+02 0.000000E+00
-0.500000E+02 0.000000E+00
0 2 -0.500000E+02 0.000000E+00
0 3 0.500000E+02 0.000000E+00 -0.500000E+02 0.000000E+00
-0.500000E+02 0.000000E+00
0 3 -0.500000E+02 0.000000E+00
1 0 0.500000E+02 0.000000E+00 -0.500000E+02 0.000000E+00
-0.500000E+02 0.000000E+00
1 0 -0.500000E+02 0.000000E+00
1 1 0.500000E+02 0.000000E+00 -0.500000E+02 0.000000E+00
-0.500000E+02 0.000000E+00
1 1 -0.500000E+02 0.000000E+00
1 2 0.500000E+02 0.000000E+00 -0.500000E+02 0.000000E+00
-0.500000E+02 0.000000E+00
1 2 -0.500000E+02 0.000000E+00
1 3 0.500000E+02 0.000000E+00 -0.500000E+02 0.000000E+00
-0.500000E+02 0.000000E+00
1 3 -0.500000E+02 0.000000E+00

2 0 0.500000E+02 0.000000E+00 -0.500000E+02 0.000000E+00
-0.500000E+02 0.000000E+00
2 0 -0.500000E+02 0.000000E+00
2 1 0.500000E+02 0.000000E+00 -0.500000E+02 0.000000E+00
-0.500000E+02 0.000000E+00
2 1 -0.500000E+02 0.000000E+00
2 2 0.500000E+02 0.000000E+00 -0.500000E+02 0.000000E+00
-0.500000E+02 0.000000E+00
2 2 -0.500000E+02 0.000000E+00
2 3 0.500000E+02 0.000000E+00 -0.500000E+02 0.000000E+00
-0.500000E+02 0.000000E+00
2 3 -0.500000E+02 0.000000E+00
3 0 0.500000E+02 0.000000E+00 -0.500000E+02 0.000000E+00
-0.500000E+02 0.000000E+00
3 0 -0.500000E+02 0.000000E+00
3 1 0.500000E+02 0.000000E+00 -0.500000E+02 0.000000E+00
-0.500000E+02 0.000000E+00
3 1 -0.500000E+02 0.000000E+00
3 2 0.500000E+02 0.000000E+00 -0.500000E+02 0.000000E+00
-0.500000E+02 0.000000E+00
3 2 -0.500000E+02 0.000000E+00
3 3 0.500000E+02 0.000000E+00 -0.500000E+02 0.000000E+00
-0.500000E+02 0.000000E+00
3 3 -0.500000E+02 0.000000E+00
21 0.0001
0 0 0.500000E+02 0.000000E+00 -0.500000E+02 0.000000E+00
-0.500000E+02 0.000000E+00
0 0 -0.500000E+02 0.000000E+00
0 1 0.500000E+02 0.000000E+00 -0.500000E+02 0.000000E+00
-0.500000E+02 0.000000E+00
0 1 -0.500000E+02 0.000000E+00
0 2 0.500000E+02 0.000000E+00 -0.500000E+02 0.000000E+00
-0.500000E+02 0.000000E+00
0 2 -0.500000E+02 0.000000E+00
0 3 0.500000E+02 0.000000E+00 -0.500000E+02 0.000000E+00
-0.500000E+02 0.000000E+00
0 3 -0.500000E+02 0.000000E+00
1 0 0.500000E+02 0.000000E+00 -0.500000E+02 0.000000E+00
-0.500000E+02 0.000000E+00
1 0 -0.500000E+02 0.000000E+00

1 1 0.500000E+02 0.000000E+00 -0.500000E+02 0.000000E+00
-0.500000E+02 0.000000E+00
1 1 -0.500000E+02 0.000000E+00
1 2 0.500000E+02 0.000000E+00 -0.500000E+02 0.000000E+00
-0.500000E+02 0.000000E+00
1 2 -0.500000E+02 0.000000E+00
1 3 0.500000E+02 0.000000E+00 -0.500000E+02 0.000000E+00
-0.500000E+02 0.000000E+00
1 3 -0.500000E+02 0.000000E+00
2 0 0.500000E+02 0.000000E+00 -0.500000E+02 0.000000E+00
-0.500000E+02 0.000000E+00
2 0 -0.500000E+02 0.000000E+00
2 1 0.500000E+02 0.000000E+00 -0.500000E+02 0.000000E+00
-0.500000E+02 0.000000E+00
2 1 -0.500000E+02 0.000000E+00
2 2 0.500000E+02 0.000000E+00 -0.500000E+02 0.000000E+00
-0.500000E+02 0.000000E+00
2 2 -0.500000E+02 0.000000E+00
2 3 0.500000E+02 0.000000E+00 -0.500000E+02 0.000000E+00
-0.500000E+02 0.000000E+00
2 3 -0.500000E+02 0.000000E+00
3 0 0.500000E+02 0.000000E+00 -0.500000E+02 0.000000E+00
-0.500000E+02 0.000000E+00
3 0 -0.500000E+02 0.000000E+00
3 1 0.500000E+02 0.000000E+00 -0.500000E+02 0.000000E+00
-0.500000E+02 0.000000E+00
3 1 -0.500000E+02 0.000000E+00
3 2 0.500000E+02 0.000000E+00 -0.500000E+02 0.000000E+00
-0.500000E+02 0.000000E+00
3 2 -0.500000E+02 0.000000E+00
3 3 0.500000E+02 0.000000E+00 -0.500000E+02 0.000000E+00
-0.500000E+02 0.000000E+00
3 3 -0.500000E+02 0.000000E+00
24 0.0001
0 0 0.500000E+02 0.000000E+00 -0.500000E+02 0.000000E+00
-0.500000E+02 0.000000E+00
0 0 -0.500000E+02 0.000000E+00
0 1 0.500000E+02 0.000000E+00 -0.500000E+02 0.000000E+00
-0.500000E+02 0.000000E+00
0 1 -0.500000E+02 0.000000E+00

0 2 0.500000E+02 0.000000E+00 -0.500000E+02 0.000000E+00
-0.500000E+02 0.000000E+00
0 2 -0.500000E+02 0.000000E+00
0 3 0.500000E+02 0.000000E+00 -0.500000E+02 0.000000E+00
-0.500000E+02 0.000000E+00
0 3 -0.500000E+02 0.000000E+00
1 0 0.500000E+02 0.000000E+00 -0.500000E+02 0.000000E+00
-0.500000E+02 0.000000E+00
1 0 -0.500000E+02 0.000000E+00
1 1 0.500000E+02 0.000000E+00 -0.500000E+02 0.000000E+00
-0.500000E+02 0.000000E+00
1 1 -0.500000E+02 0.000000E+00
1 2 0.500000E+02 0.000000E+00 -0.500000E+02 0.000000E+00
-0.500000E+02 0.000000E+00
1 2 -0.500000E+02 0.000000E+00
1 3 0.500000E+02 0.000000E+00 -0.500000E+02 0.000000E+00
-0.500000E+02 0.000000E+00
1 3 -0.500000E+02 0.000000E+00
2 0 0.500000E+02 0.000000E+00 -0.500000E+02 0.000000E+00
-0.500000E+02 0.000000E+00
2 0 -0.500000E+02 0.000000E+00
2 1 0.500000E+02 0.000000E+00 -0.500000E+02 0.000000E+00
-0.500000E+02 0.000000E+00
2 1 -0.500000E+02 0.000000E+00
2 2 0.500000E+02 0.000000E+00 -0.500000E+02 0.000000E+00
-0.500000E+02 0.000000E+00
2 2 -0.500000E+02 0.000000E+00
2 3 0.500000E+02 0.000000E+00 -0.500000E+02 0.000000E+00
-0.500000E+02 0.000000E+00
2 3 -0.500000E+02 0.000000E+00
3 0 0.500000E+02 0.000000E+00 -0.500000E+02 0.000000E+00
-0.500000E+02 0.000000E+00
3 0 -0.500000E+02 0.000000E+00
3 1 0.500000E+02 0.000000E+00 -0.500000E+02 0.000000E+00
-0.500000E+02 0.000000E+00
3 1 -0.500000E+02 0.000000E+00
3 2 0.500000E+02 0.000000E+00 -0.500000E+02 0.000000E+00
-0.500000E+02 0.000000E+00
3 2 -0.500000E+02 0.000000E+00

3 3 0.500000E+02 0.000000E+00 -0.500000E+02 0.000000E+00
-0.500000E+02 0.000000E+00
3 3 -0.500000E+02 0.000000E+00